# CONTROL IMPROVEMENT OF AN ABOVE ELBOW PROSTHETIC LIMB UTILIZING TORQUE COMPENSATION AND REACHING TEST ANALYSIS

by

James Michael Dotterweich

A thesis submitted to the faculty of
The University of Utah
in partial fulfillment of the requirements for the degree of

Master of Science

Department of Mechanical Engineering

The University of Utah

May 2015




The University of Utah Graduate School

# STATEMENT OF THESIS APPROVAL

The following faculty members served as the supervisory committee chair and members for the thesis of James Michael Dotterweich.
Dates at right indicate the members' approval of the thesis.

| | |
|---|---|
| Sanford Meek , Chair | 9/9/2014<br>Date Approved |
| Mark Minor , Member | 9/9/2014<br>Date Approved |
| Andrew Merryweather , Member | 9/9/2014<br>Date Approved |

The thesis has also been approved by Tim Ameel
Chair of the Department/School/College of Mechanical Engineering
and by David B. Kieda, Dean of The Graduate School.

# ABSTRACT

Above elbow prosthesis control has trended toward increasing the number of control channels in the human-prosthetic system, to provide simultaneous joint control. Several methods have had varying success, such as Targeted-Muscle-Reinnervation (TMR) and Electromyograph (EMG) pattern recognition. While the number of control channels is increased, the fundamental control loop is still based on amputees placing the prosthetic end effector through visual feedback. In most clinical uses prosthetic joints are driven with a standard proportional EMG antagonistic muscle controller (S). The S controller can be difficult for the amputee as nonintuitive muscle contractions are needed to overcome internal joint and induced external torques, in particular from gravity. To address these issues, two new controllers, which use gravity and friction compensation techniques, have been developed to share the control of the prosthetic elbow joint and reduce control effort on prosthetic users. The new controllers were tested against the S proportional control by having 10 test subjects reach to 6 targets in their user workspace utilizing a Utah Arm 2 testbed. Motion capture cameras recorded the reaching motions. The controllers were compared using quantitative metrics which define the approach, time to target and smoothness (jerk), and holding, steady state error and variance, stages of a reaching motion. A qualitative metric was also used which surveys a test subject's effort in performing a reach. It was found that when considering the new controllers using the combined data for all test subjects at all targets they outperformed the S

controller, except in smoothness. It was also found that the new controllers statistically performed best over the S controller at target locations where the humerus was in flexion at approximately $45^{o}$, except in smoothness. Smoothness is predicted to be more influenced by the joint friction in the elbow joint. Only one friction compensation method was tested. Further studies on friction affects by varying joint impedance is suggested. Considering these findings, including gravity compensation in the control for active prosthetic elbow joints is found to improve the control over the standard proportional control, as captured in the majority of the physical metrics and in test subject ratings.

This work is dedicated to Mark Steven Dotterweich and to those who “Have not,” may they be the benefactors of the fruits of our labor and contemplation.

TABLE OF CONTENTS

LIST OF TABLES

LIST OF FIGURES

# LIST OF ACRONYMS

| | |
|---|---|
| ADC | Analog to Digital Converter |
| ADL | Activities of Everyday Living |
| ANOVA | Analysis of Variance |
| COM | Center of Mass |
| DC | Direct Current |
| DAC | Digital to Analog Converter |
| DOF | Degree of Freedom |
| EMF | Electromagnetic Force |
| EMG | Electromyograph(y) |
| GC | Gravity Compensation with Torque Feedback |
| GCF | Gravity Compensation without Torque Feedback |
| IR | Infrared |
| PID | Proportional, Integral, Derivative |
| PWM | Pulse Width Modulation |
| S | Standard Proportional EMG Control |
| SHAP | Southampton Hand Assessment Procedure |
| STD | Standard Deviation |
| TD | Terminal Device |
| TMR | Targeted-Muscle-Reinnervation |

| | |
|---|---|
| UI | User Interface |
| UART | Universal Asynchronous Receive Transmit |

# ACKNOWLEDGEMENTS

The Savior and my Savior, Jesus Christ, who without, ‘nothing is possible’. I would like to acknowledge my advisor Dr. Sanford Meek for his tireless effort in instruction and dedication to the education of myself and the Mechanical Engineering students at the University of Utah; also my other committee members Mark A. Minor and Andrew Merryweather. In addition, to my lab partners Dara Scher, Eric McClain, Jeff Naylor and Seth Paul for their kind willingness to participate in so many of the needed trial experiments.

I would further like to acknowledge my faith community at St. Catherine of Siena Catholic Newman center, particularly Fr. Carl Schlichte, Fr. Peter Do, Deacon Gabriel Mosher and Jon Dalton for their loving and kind guidance to inspire the love of God in my heart and to help me see that doing God’s loving will is the path to true wisdom and happiness. Lastly, but never least, I would like to acknowledge my family. Ben, Matt, my Mom, Veronica Dotterweich, and my Dad, Mark Dotterweich. They are the love that inspires and fuels all that I do; I would not be here without their support and help.

# CHAPTER 1

# INTRODUCTION

Powered prostheses for above elbow amputees have been in general use for more than 30 years [1] and [2]. There have been many methods used and explored to control artificial limbs. Simple body-powered prostheses use body movements to pull on cables that actuate the prosthetic joint motions [1]. Switches and force sensors attached to cables amplify body motions similar to the body-powered prostheses. More recently, upper limb prostheses have been integrated with microcontrollers and mobile power supplies to actuate the prosthetic joints using DC motors [3], [4], [5] and [6]. A variety of control methods have been used to command the prosthetic joint motions. Electromyographic, or myoelectric, (EMG) signals have been used in several control modes. Most clinical prostheses use surface EMG electrodes which are placed on remnant muscle sets [3], [4], [5] and [6]. EMGs pick up the electrical signal from muscle contractions to act as the command signal to the prosthetic joints. Simple systems use different amplitude levels of the EMG signal to open and close a hand [7]. These use the EMG signal essentially as a switch. Finer control can be given using the EMG signal proportionally [7]. Typically, the difference of the amplitude of EMGs from a pair of antagonistic muscles is used, producing a proportional control signal for prosthetic joint motion. In standard above elbow prosthesis that use EMGs for the command input, all of

the joints are controlled proportionally with the antagonistic muscles producing the EMG signals. In most clinical prostheses the prosthetic joint motion is accomplished sequentially [8] which is nonnatural. For example, the hand can first be rotated to a correct grip orientation. Then by performing a switch move, typically a quick co-contraction of the antagonistic muscles, the prosthesis will switch control to the elbow joint. The EMG proportional signal can then be used to drive the elbow joint to position the hand in space. All of the control is done with the proportional EMG signal. Current research in prosthetics is attempting to improve prosthetic motion by increasing the number of control channels to control joints simultaneously [2] and [8]. Most research in this area has been towards pattern recognition. There are several difficulties with these methods that have prevented their clinical use. Scheme and Englehart outlined these problems [9]. Other methods such as Targeted Reinervation have begun to realize simultaneous multi-degree-of-freedom control [10]. While this procedure can be a great benefit for the recipients, the surgery is highly invasive and not for the vast majority of amputees [10].

In spite of the advances in prosthesis control methods, there remain fundamental control problems still to be solved. The efferent and afferent communication between the amputee and the prosthesis is a major bottleneck to better upper limb prosthesis use [8]. Prosthesis use by amputees is inhibited by the ability to receive feedback information of the position state of the arm. The arm is mostly positioned and is controlled in a control loop where the prosthetic end effector placement is accomplished by the amputee visually servoing the end effector. The base control type regardless of the prosthetic motion accomplished, sequentially or simultaneously, still involves the use of the EMG signals in a proportional mode to induce motion. The proportional control method requires the

amputee to create a large enough EMG signal through muscle contractions to place the arm in a desired location. With essentially only visual feedback and proportional control for the joints, the muscle contractions an amputee has to produce to perform a desired motion can be difficult to accomplish. The difficulty in producing a desired end effector motion is thought to be the result of the adverse external and internal environmental torques acting on the prosthesis joints that have to be overcome before a desired motion can occur. The lack of a more full "knowledge" of these adverse torques is also thought to unnecessarily increase the perceived control effort by the amputee.

In addition, there are further issues in the evaluation of above elbow prosthetic controllers and whether or not they have actually improved prosthetic end effector placement control in a measureable way. There are multiple tests that measure the kinematics of normal human arm motions [1], [12], [13], [14], [15], and [16] or hand prosthesis [17], [18], and [19] which measure the extents of joint motion and object manipulation. However, there are not as many that evaluate above elbow prosthetics limbs in their primary use, concerning the elbow and shoulder joints, which is reaching. This gives a lack of quantitative understanding of how the above elbow prosthetic limbs and controls have helped regain lost motion in a functional evaluation. The focus of this thesis is to implement and test new solutions to these problems in an attempt to improve the control of above elbow prosthetic limbs, over normal clinical EMG proportional control.

To remove the proportional control burden from amputees, a controller has been developed which utilizes joint angle sensors to obtain arm kinematic data to create torque compensation controllers for the elbow joint. These controllers are predicted to aid in the controllability of the arm and improve a prosthesis user's ability to drive the prosthesis in

a desired fashion. Likewise, to evaluate control improvement, a test method using three-dimensional motion capture cameras has been developed. These experiments test the prosthetic controllers using reaching tasks to obtain quantitative measures of control performance which can be used to ascertain control improvement. Both of these areas are addressed in this thesis as a way to improve and begin to classify prosthetic limb control improvement. The new controllers and a control performance test method are further discussed in the subsequent sections.

## 1.1 Prosthetic Torque Compensated Controller

Many prosthesis control methods use EMG signals to actuate individual joints with no coordinated control between the motion of the prostheses and the remnant limb. Problems can occur during such actions as reaching motions. The elbow can become an inverted pendulum at high humeral flexion angles due to the acting gravity field. This is a statically unstable position causing difficulties in the elbow control. This is a result of the external torques placed on the elbow both in motion and by gravity. The effects of external torques on multijoint human motion including the elbow is well studied [20], [21], and [22]. The biomechanics of the muscles of the human arm are design to create torques about the elbow joint, which include the effects of the external torques [21]. Concerning joint torques as induced by muscle contractions, EMG signals which pick up the muscle contractions have been shown to be equated to muscle forces and thus joint torques [23] and [24]. Torque control and compensation of torques about the elbow have been done previously in prosthetics in various forms. Using EMGs as a torque command, torque controllers about the elbow have been developed [23] and [24]. Some have looked at the full system of torques acting at the elbow due to mass and weights to predict the

torque amount at the elbow and apply the correct EMG signal to correct for this adverse torque. This form of torque EMG signal work has been done by S. Meek et al. [24]. Other prosthetic arm controllers, focused at the elbow, work to change the elbow joint impedance by modifying the predicted inertia or varying joint stiffness to create more fluid motion and allow for better environment interaction [25] and [26]. Others take the approach of designing a full elbow based on a torsion spring which changes the impedance in the elbow joint over the joint range of motion [27]. The goals of this research are to map an impedance gain at the elbow to a position, to better model human motion. Some prosthesis are designed to overcome the effect of their own weight over a certain joint range. In the Utah Artificial Arm (Motion Control, SLC UT), the torque transfer between the motor and the elbow is nonlinear in a way that provides the highest torque when the elbow is at 90°. This is a result of the four-bar linkage present in the arm that transfers rotational motion of the motor to the elbow [5]. This works well if the humerus is vertical, by a person's side. If the humerus is not vertical, then the transfer is not optimal concerning external forces. In addition, the EMG signal gains are usually adjusted to give good control when the humerus is vertical, when the prosthesis is fit to an amputee. Again, if the humerus is not vertical, the gain adjustment is not optimal. While these methods have been fielded and torque controllers equated to muscle force have been equated to the joint control, the controllers do not appear to compensate for external torques across the full ranges of motion.

A method utilizing the knowledge of the arm kinematics and dynamics to predict the external forces imparting torques about the elbow joint is suggested to be used to compensate for adverse torques across the full range of elbow motion. Feedback compensation methods to account for adverse torques in a multilink joint system is a

method that is well studied and is classically used in the robotics field [29]. The human arm in its motion and in conjunction with the prosthesis can be similarly modelled as a multilink system such as a robot arm and use these same techniques of torque compensation about a mechanical joint. With known adverse torques compensated for, it leaves the remainder of the control input to the amputee's muscle contractions and the elbow joint will only move for user desired muscle contractions instead of having to fight adverse joint torques throughout the range of motion. This method of active compensation of external torque at the prosthetic elbow joint is the contribution of this thesis and to the best knowledge of the author, though used in classical robotics, has not explicitly been accomplished in above elbow prosthetic limbs.

In order to implement the torque compensation controller, measurements of the positions of the remnant limb must be made to measure the joint angles of the arm. For the primary motions of the arm these are shoulder rotations and elbow flexion. In previous work [30], a drift-free inclinometer that uses two, 3-axis accelerometers and a rate gyro to determine the direction of the gravity vector was designed. It can accurately calculate the gravity vector in the presence of other accelerations. There is no integration so there is no drift. The details of the design are given in [30]. The original use was to measure leg positions for gait studies. The inclinometer is adapted in this research to measure the humeral position. The inclinometer will be mounted on the amputee's socket. Without bending of the torso, the direction of the gravity vector would indicate the angle of the humerus with respect to the shoulder, both in rotation and abduction. The angle of the elbow is measured by a potentiometer in the artificial arm, so the complete kinematic state of the prosthesis and remnant limb relative to the gravity field as translated to the human body frame can be known.

As a result of these findings, the focus of the shared controller in this thesis will be to implement a gravity torque compensation controller about the elbow joint with the goal to reduce the control effort of a user over the standard EMG proportional control. The prosthetic arm instrumentation and the design of the gravity compensation controls are discussed in Chapters 2 and 3.

## 1.2 Control Improvement Testing

A survey of prosthesis evaluation tests was conducted to better understand how to measure prosthesis motion and if a previously developed test could be used to test the newly developed controllers. As found in this survey one of the primary issues in determining the effect of a controller, on above elbow prosthetic arm performance, is the lack of meaningful quantitative control measurements. Various tests have been developed for prostheses that require an amputee to pick up objects with their prosthesis and move them to different defined spaces while being timed. These include tests such as the Southampton Hand Assessment Procedure (SHAP) [18] and [19]. The test evaluates prosthetic hands in a range of motion that is close to the body with a varying range of objects. The tasks are scored against time to complete and a designed metric of statistical performance. A controller would show improvement if the object being manipulated has moved from its starting configuration to its targeted end configuration with a reduced time and accuracy. While this does provide a time quality to the task, the overall motion of the arm moving through the test workspace is not captured and there is not a quantitative way to link the actual hand motion to the time measurement obtained. Other tests have been adapted to test prostheses from occupational therapy tests for humans with disabilities, such as the Box and Block test [16] . The box and blocks test has been

used to test prosthesis experiments and has been modified to include motion capture cameras to better understand joint motion during the task [31]. In a similar metric to the SHAP test, a time metric and score are given based on how many blocks are moved from one area of a box to another in a minute time frame. In the normal box and blocks test, the test evaluates the dexterity of the lateral motions of the arm. It does not have the ability to measure how the hand or arm is actually moving during the test. How the arm is actually moving is needed to understand the controllability of prosthesis. The lack of these data is addressed by J. S. Hebert et al. [31] where motion capture cameras are used to find the motion of the joints and times of motion of the joints during the tasks. This appears to be a more full method, as two control types, both EMG and body powered tests were compared using joint range and time to move a specific set of 16 blocks. However, these measurements do not gather quantitative metrics that link back to control performance beyond time and joint range, concerning the mechanics of the motion actually being conducted. They also do not look at the full range of elbow motion. Other tests that specifically focus on above elbow prosthetic joint motion over an unconstrained range have also been run to track how prostheses perform [32], [33], [34], and [35]. Some of the tests use optical tracking techniques using IR cameras to obtain information about joint motions and arm kinematics [32] and [34]. The tasks presented to the user of the above elbow prosthesis are based on activities of everyday living (ADL). Grasping tests, using different sized objects, were performed by Bouwsema et al. at different discrete distances to understand the control of a prosthesis [32]. This test captured kinematic data using IR markers and IR cameras to understand how above elbow amputee motion performance compares to below elbow amputees during a reaching grasp. The primary reaching data used to evaluate the prosthesis are movement reach

time and peak velocity. These metrics are good but a more in depth set of metrics linked to the mechanics of the motion being performed are desired. In addition, most of the reaching tests are object specific and involve the direct manipulation of an object. In many cases, the locations of these objects are not generalized, in the sense of starting from a rest position and moving a specific target distance to touch a location in a tests subject's workspace. A test that presents a more general reaching task, to test joint motion, with set target distances in the workspace would be required to quantitatively test prosthetic control improvements. A test that includes repeatable generic reaching motions, which are nonobject specific and the ability to measure the prosthesis position over time is necessary in order to understand the aspects of the prosthesis control. In the evaluated studies the measurement of time to target, or time to complete, is a metric that links to the mechanics of an upper arm and its performance. Other studies show that the upper arm movements can be characterized by the trajectory smoothness or how smooth a "reach" motion is conducted [13]. This is another viable measurement that could be used in evaluating an above elbow prosthesis as trajectory smoothness links to a test subject's ability to move the arm in a desired motion which links to the control implemented. In addition, as found in some studies, the use of a set of IR cameras as a method to track the motion of a prosthesis over time is done to determine how the prosthesis is actually moving during the task. This method can be used to find how a controller is actually working. These techniques can be adapted to fit a more comprehensive form of functional reaching tests that can then evaluate an above elbow prosthesis in a normal upper limb use case.

Using aspects of the work cited above, a method has been developed that tests above elbow prosthetic limbs using reaching tasks, as this is the primary use case for the upper

limb and involves both the elbow and shoulder joint motions which characterize the arm mechanics. A three-degree-of-freedom robotic arm is used to present targets in a test subject's reaching workspace, to simulate generalized distances to objects a person might experience in everyday life. Due to the use of the target robot, the targets are repeatable and can be scaled to fit individual test subjects. A test subject will begin at rest and reach to the target presented in space using a specific prosthetic control type. The motion of the reaching task is captured by IR cameras as set by IR markers on both the target robot and the prosthetic limb. This provides the ability to track time, distance to target, velocities, and accelerations of the reaching path taken to the target. Using the reaching tests, performance measurements related to the mechanics of a reaching motion and thus the controls can be obtained from the recorded motion data. The physical metrics related to a reaching motion can then be used to better understand control improvements to an above elbow prosthesis.

## 1.3 Thesis Overview

Applied methods of gravity compensation control and a new reaching based test to measure prosthetic limb control performance are addressed in this thesis as a way to improve and begin to classify above elbow prosthetic limb control. These methods will help lead to a better understanding of prosthetic limb control by providing quantitative control measurements. The overall goal is to return prosthetic limb motion to a more natural limb motion, while reducing amputee control effort. The content of this thesis is organized as follows:

1. Chapter 2 contains the description of the system architecture and sensor package upgrades to the prosthetic limb used to obtain kinematic joint data. It also

includes the hardware control interfaces used to run the prosthesis.

2. Chapter 3 describes the human-prosthetic arm kinematics and dynamics. This chapter also includes the design and description of the newly developed gravity torque compensation controllers.
3. Chapter 4 details the experimental setup and methods used to test the prosthetic controllers. It also includes the description of the equipment setup and control improvement metrics used with the experimental data.
4. Chapter 5 contains the description of the results of the tests performed as well as the discussions of the results to understand prosthetic control improvement. This section includes the description of the discussion of the statistical analysis used to interpret the data.
5. Chapter 6 details the conclusions and future work that provides areas of further study.

# CHAPTER 2

## PROTHESIS INSTRUMENTATION

To design a gravity torque compensated controller for an above elbow prosthesis, kinematic state knowledge must be used. This requires that the joint angular data be obtained for the full human-prosthetic system, specifically the joint angle data from the shoulder and elbow. These angles are elbow flexion, humeral abduction, and humeral flexion. The reset of the degrees of freedom such as humeral rotation or wrist flexion are not considered, as the primary function of interest is the positioning of the upper limb. The humeral rotation, though part of the larger upper limb motions, is not included as the Utah Arm 2, in use, does not have this degree of freedom (DOF) as a mechanized or controllable joint. Therefore the primary joints of interest are the elbow and shoulder joints. To acquire the kinematic joint data the position sensors on the prosthesis must be repurposed. The data for the elbow joint use sensors already present in the forearm of the prosthesis. A potentiometer is used to obtain the elbow angle and a strain gauge load cell is used to obtain the torque about the elbow. As the prosthesis and human arm are coupled, the shoulder joint angles must also be measured. This is accomplished by measuring the shoulder joint angles relative to the gravity vector with a previously developed but modified inclinometer sensor [30]. The joint sensor data in conjunction with the mass, inertia, and lengths of the combined human-prosthetic system can be used

to modify the control of the prosthesis.

## 2.1 System Architecture

Due to the need to modify and study new controllers and include new sensors on the Utah Arm, the test bed for the prosthetic limb is built around a dSpace® 1104 control board (Paderborn, Germany). This real-time embedded controller connects to the hardware of the prosthetic limb. The other components are the DC power supply, which supplies power to the prosthesis as well as the supporting analog circuitry. The general system architecture is displayed in Figure 1, with the supporting sensor data in the subsequent sections.

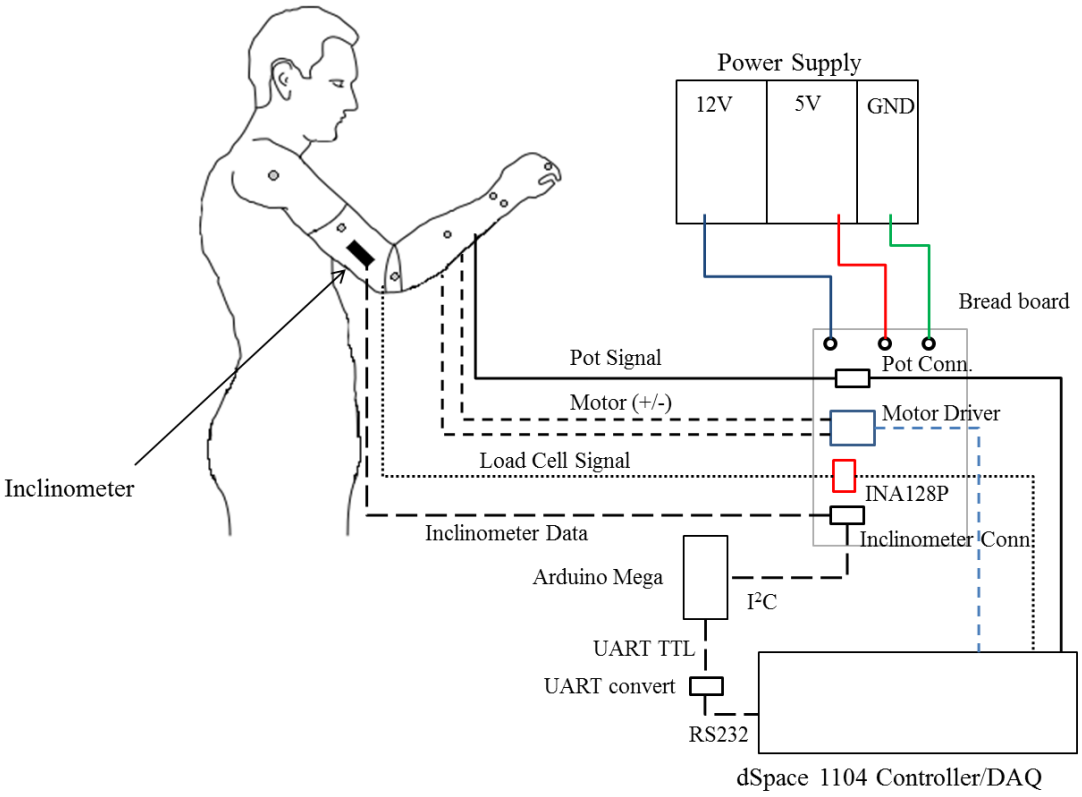


Figure 1: System Architecture

2.1.1 dSpace 1104 Controller

In order to read new sensor data and provide control channels, a real-time controller board is used. It is necessary for the controller to integrate analog sensor data, read UART communications, and send PWM motor controller signals. For this reason, and based on availability, a dSpace 1104 controller is used. This controller's key specifications can be seen in the dSpace manual [36]. The pin out diagram and how each component connects to the dSpace break out panel is in Figure 2 and Table 1. In Figure 2, the ports that are highlighted in black are used for the prosthetic arm connections. The ones in blue are used with the target robot arm for the reaching tests, covered further in Chapter 4.

The dSpace board is programmed using Simulink® in the MATLAB® 7.0.1 (Mathworks, Natick MA) software. This is where the control algorithms for both the testing robot and the prosthetic limb are written. When the code is deployed it runs natively on the 1104 card and is only accessible by the interface software developed by dSpace called Control Desktop® (Paderborn, Germany). Control Desktop is the user interface used to manipulate gains and obtain feedback of sensor outputs in real-time.

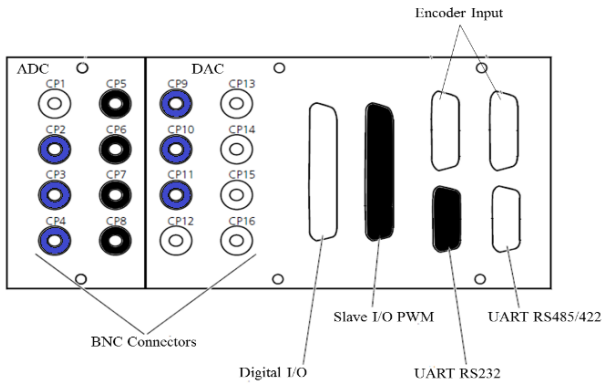


Figure 2: dSpace CLP1104 Breakout Panel

Table 1: dSpace Pin-out Table

| dSpace 1104CLP Break out Panel Connections | |
|---|---|
| **dSpace Channel** | **Connection** |
| **ADC** | |
| CP2 | Target Robot Base Pot (Joint 1) |
| CP3 | Target Robot Joint 2 pot |
| CP4 | Target Robot Joint 3 Pot |
| CP5 | Utah Arm Load Cell |
| CP6 | EMG Ch. A |
| CP7 | EMG Ch. B |
| CP8 | Utah Arm Forearm pot |
| **DAC** | |
| CP9 | Target Robot Base Motor Amp Vin (+/-) |
| CP10 | Target Robot Joint 2 Motor Amp Vin (+/-) |
| CP11 | Target Robot Joint 3 Motor Amp Vin (+/-) |
| **SLAVE I/O PWM** | |
| Pin 2 (SCAP1 Dig. I/O) | Motor Driver M2INA |
| Pin 11 (SPWM9) | Motor Driver M2PWM |
| Pin 21 (SCAP2 Dig. I/O) | Motor Driver M2INB |
| **UART RS232** | |
| Pin 2 (RXD) | Arduino Mega Pin16 TX2 |
| Pin 3 (TXD) | Arduino Mega Pin17 RX2 |
| Pin 5 (GND) | Arduino Mega GND |

## 2.2 Prosthetic Limb

The Utah Arm 2 is an advanced prosthetic limb with on board microcontrollers and a DC motor circuitry to read in EMG signals and convert them to elbow and terminal device motion. While the arm has circuity to run individual sensor and motor components, these circuits are specialized and do not allow for the customization of advanced controllers. Therefore, none of the on board circuitry was used and all control and sensor reading was accomplished through the dSpace controller. The sensors used on the limb are the potentiometer and the load cell inside and inherent in the arm. The external inclinometer was added as an additional sensor. These sensors are discussed in the following sections of this chapter. A picture of the Utah Arm 2 is in Figure 3.

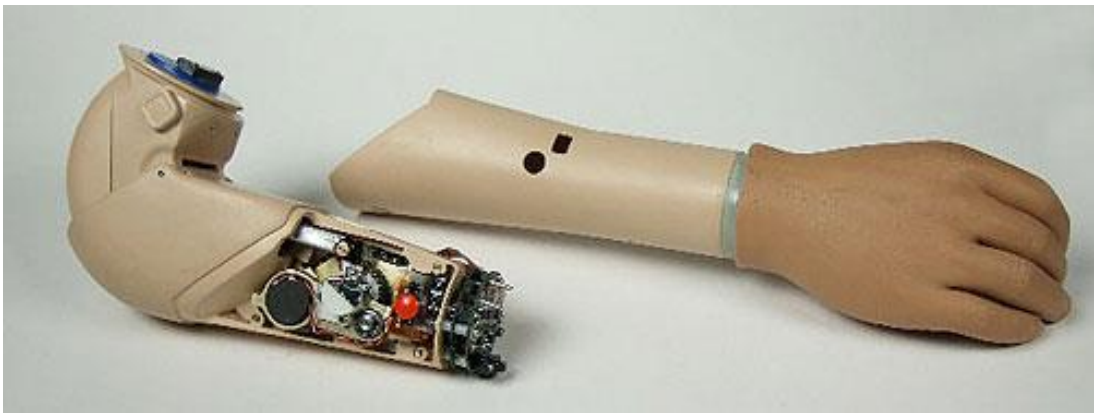

Figure 3: Utah Arm 2 (Curts. Motion Control, SLC, UT)

2.2.1 Internal Sensors

2.2.1.1 Load Cell

The load cell consists of two strain gauges set together in a full bridge configuration located in the back of the humeral portion of the prosthetic limb. Normally the load cell is used to determine when to run the free-swing mode on the prosthesis. For this research, it has been repurposed to sense the torque about the elbow joint and is used in the control loops. This load cell is in line with the elbow joint such that it can be linearized to read the "torque" on the elbow pin. The load cell is paired with an INA128P instrumentation amplifier to provide a gain that will send the voltage range from 0 to 12V and is balanced at approximately 6.38 volts for the nominal no load voltage. This load cell reads the force in only one axis and has a "mechanical stop" or state at which the strain can no longer be detected, to protect the load cell. The load cell axis is in line with the elbow pin in a $90^{o}$ orientation. This can be seen in Figure 4. The load cell construction can be seen in Figure 5. Due to the fixed position, the load cell reading can be equated to the elbow torque, through linearization of the voltage vs. force applied at the load cell divided by the set distance to the elbow pin. Due to the mechanical stop the load cell has a limit.

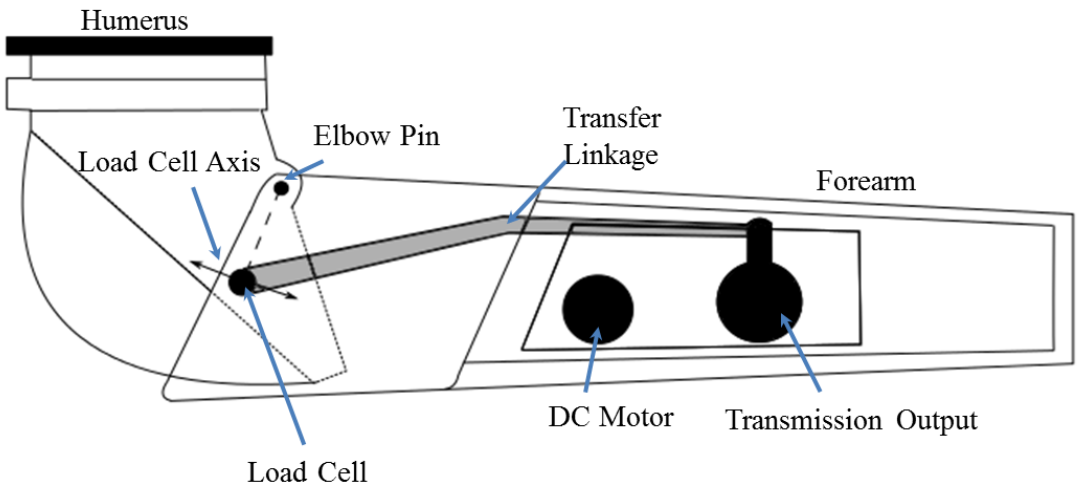


Figure 4: Internal Connections of the Utah Arm and Load Cell Axis Orientation

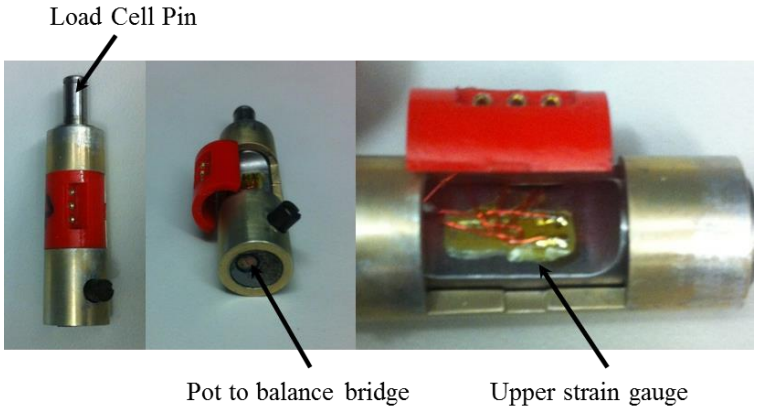


Figure 5: Load Cell Construction

This limit was at approximately -54N of force in one direction and approximately 43N in the other, Figure 6. Though this limit is undesirable, it is considered within a usable limit for the research tests conducted. However, it is suggested that a strain gauge setup that has a larger ranged of sensing (above 75N which is the highest weight of the arm at the load cell) be obtained if future testing is to occur. The voltage to force linearization curve for the load cell is in Figure 6.

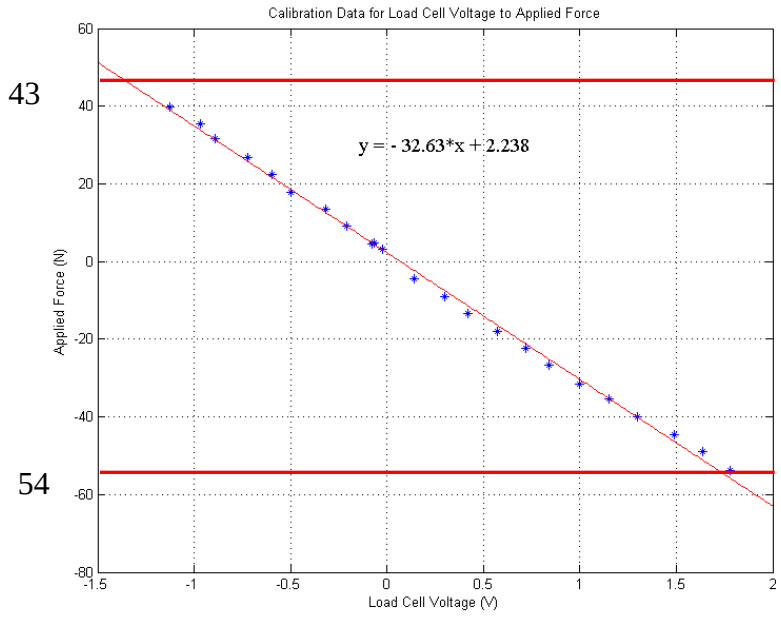


Figure 6: Load Cell Calibration

2.2.1.2 Potentiometer

The potentiometer (pot) is located in the center of the forearm and is attached by a plastic linkage to the output of the gear box to the crossed four-bar input linkage. This can be seen in Figure 7. The pot is modified to have a regulated supply of 5V and is calibrated to the external elbow angle as well as the transmission angle of the input linkage of the cross four-bar linkage. Both the external angle of the actual elbow position and the internal angle of the output of the transmission are needed. The external angle is needed to know the actual state of the arm's position in space. The internal angle of the transmission linkage output is needed to know the correct torque to apply from the motor and how the force through the linkage is being transferred to the load cell pin. These plots can be seen in Figure 8 and Figure 9 along with the relationship used to obtain the angle data from pot output voltage.

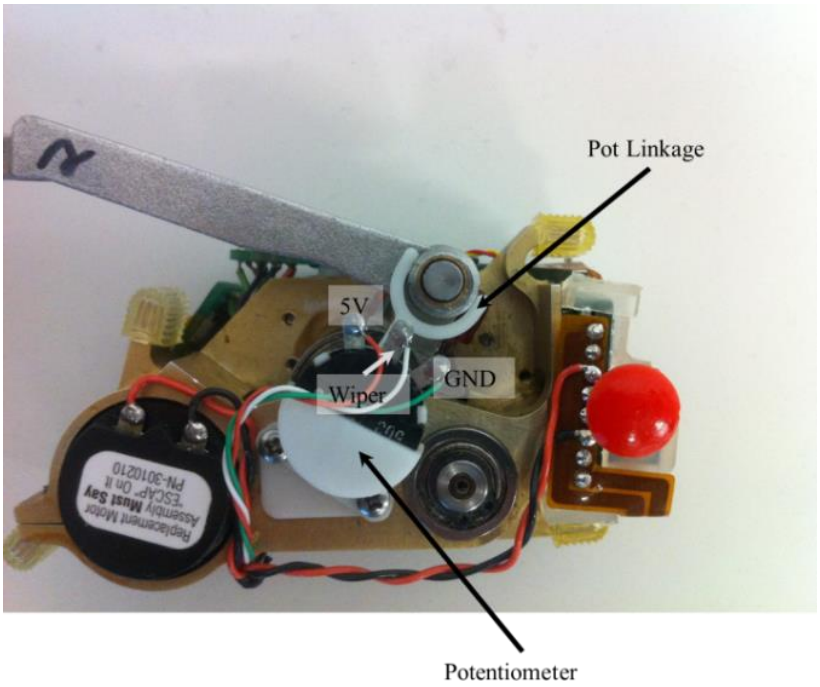


Figure 7: Potentiometer in Utah Arm 2

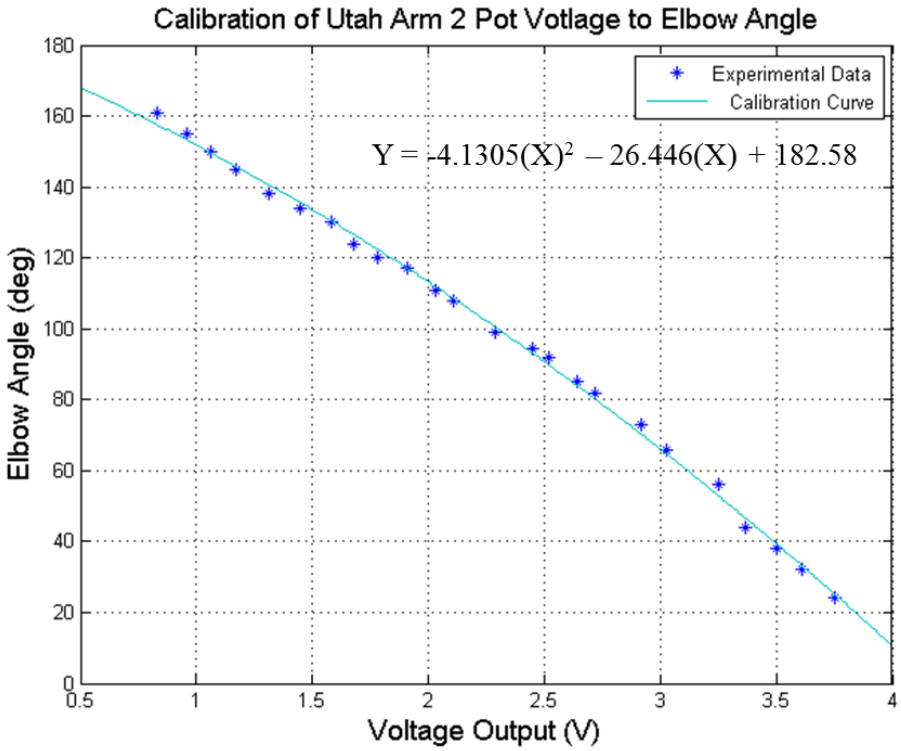


Figure 8: Elbow Angle vs. Pot Voltage

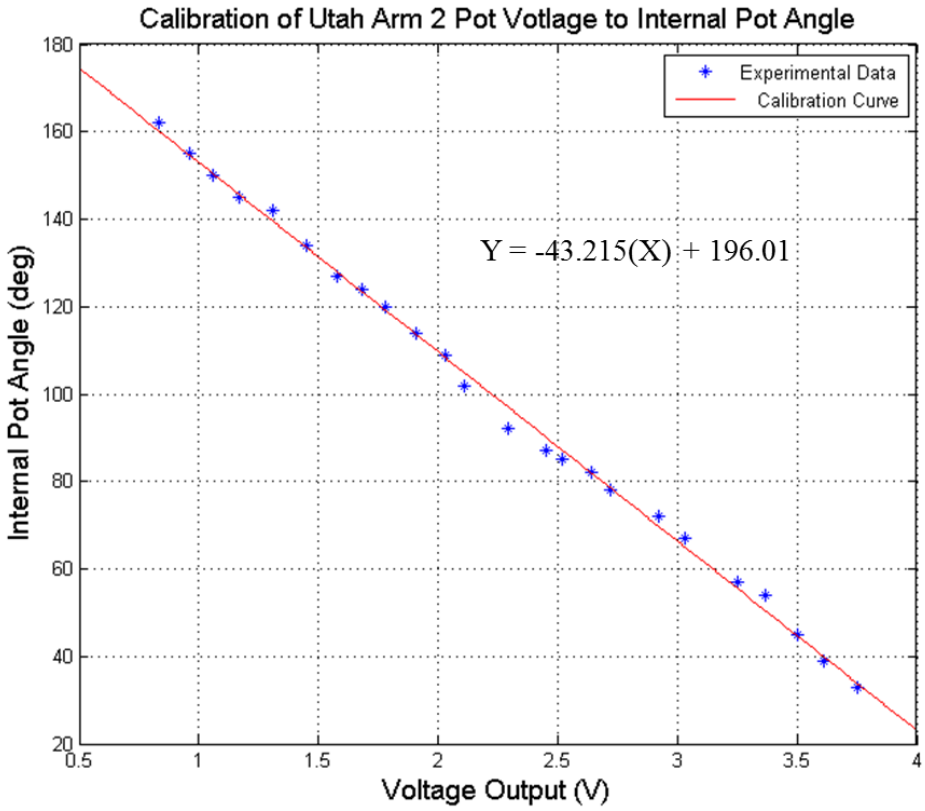


Figure 9: Internal Pot Angle vs. Pot Voltage

2.2.1.3 Inclinometer

The inclinometer, as developed by Petruska and Meek [30], is redesigned to use new digital sensors but packaged in a similar configuration as the original design. The sensors onboard are: two ADXL345 accelerometers and one ITG3200 rate gyro, Figure 10, connected to an Arduino Mega using an $I^2C$ bus for communication. These data are sent from the Arduino every 10ms to a RS-232 converter and then read into the dSpace 1104 controller. At this stage, the angle calculations are done in Simulink. Simulink was chosen to do the angle calculations over the Arduino due to processing speed and the ability to manipulate/display the data in the user interface in Control Desk.

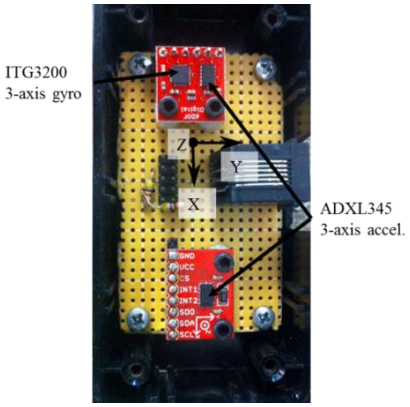


Figure 10: Inclinometer Components and Layout

The inclinometer code currently does not account for high velocity changes in rotation as the design implemented by Petruska and Meek. High angular velocity code was thought not to be needed, as the rate at which a person reaches, concerning rotations of the humerus, are low and would not impact the sensor. This is further verified by unit testing in the sections below. Thus the acting equation to obtain abduction and flexion are merely based on the tangent equations concerning accelerometer readings of the gravity field Equation (1) and (2). The sensor value of ay, ax, and az are the averaged values read from both sensors in the corresponding direction where $\theta_1$ is humeral abduction and$\theta_2$ is humeral flexion as seen in Chapter 3.

$$\theta_1 = \text{atan2}(ay,ax) \quad (1)$$

$$\theta_2 = \text{atan2}(az,ax) \quad (2)$$

The data collected in Figure 11, Figure 12, and Figure 13 show the inclinometer output as tested on a Quanser® SRV-02 (Quanser, Toronto CN) [37] to better understand the error in both the static and dynamic readings. The error over the range of desired

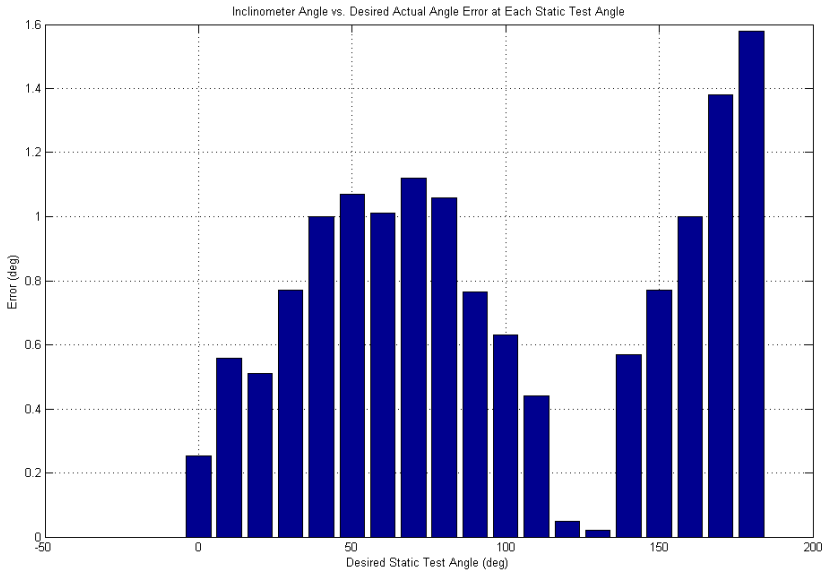


Figure 11: Inclinometer Error vs. Desired Static Angle in Degrees

angles is displayed in Figure 11. Overall the error is fairly minimal for the range of angles approximately $\pm$ 1$^{o}$ on average. Most of the error seen is due to sensor alignment in the inclinometer itself as the two accelerometers are not exactly in-line with each other, which will cause each one to read a different value from the gravity field at each axis. The manufacturing of the sensor package or better calibration to account for misalignment as implemented in software, such that the accelerometers and gyro are better aligned with each other, can be accomplished in future designs. Considering these factors, the design implemented contributes an error that is thought to be within reason, as measured by its affect to the developed controllers. A sensitivity of shoulder angle error on the gravity compensation models is discussed further in Chapter 3. The inclinometer was also tested for tracking speed. The inclinometer tracked the angle from the Quanser SRV-02 well, up to about 2Hz of rotational speed. From the results obtained from the inclinometer during rotation the sensor output is considered acceptable.

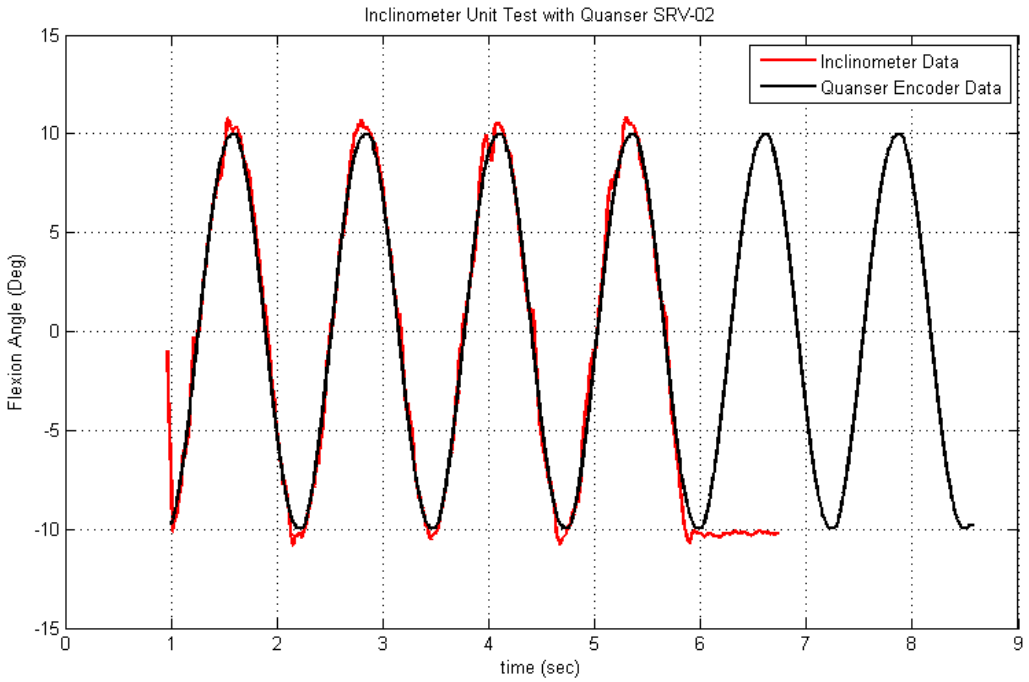


Figure 12: Inclinometer Test at 10 Degrees Amplitude at 0.5Hz in Flexion Direction

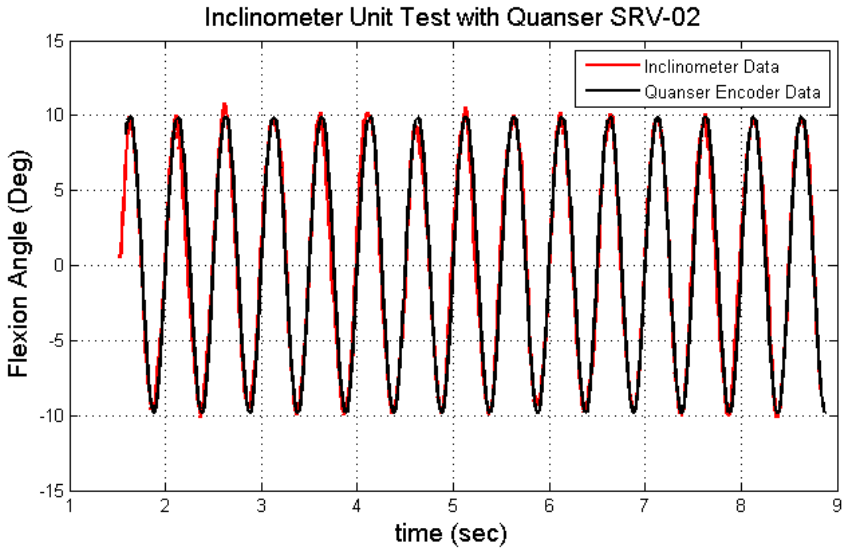


Figure 13: Inclinometer Test at 10 Degrees Amplitude at 2 Hz in Flexion Direction

The inclinometer is located on the external part of the socket, which is worn by the test subject. This allows for the detection of the desired angles of shoulder abduction and flexion through the reading of the changes in the gravity vector as detected in the local x, y, and z-axes of the accelerometer. Figure 14 shows its placement along the external socket to detect the shoulder angles as relative to the gravity vector and thus the human torso. This site was originally chosen as the location for the inclinometer as it is the direct location of the joint axis of interest. However, if the combined limb kinematics are known, the inclinometer can actually be placed anywhere in the combined human-prosthetic system and still obtain the joint angles from the reading of the gravity vector. This can be considered future work and was not taken into design consideration for this thesis.

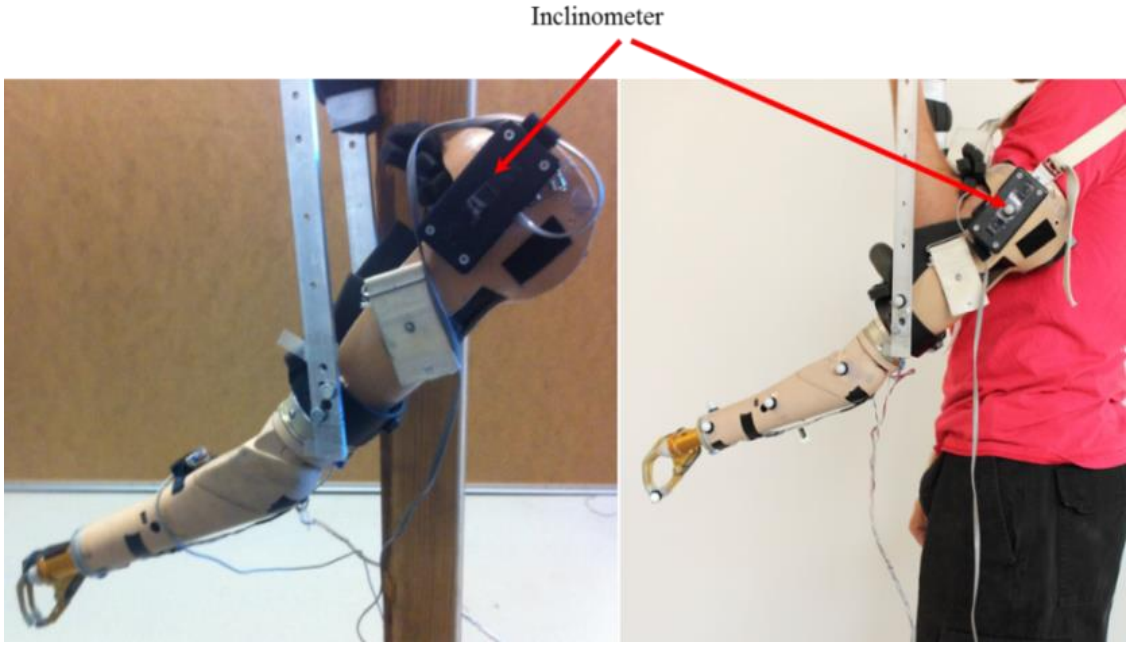


Figure 14: Inclinometer Location on Prosthetic Limb

### 2.2.2 Mechanical

There are three primary mechanical components internal to the prosthetic limb that are necessary to account for in order to perform control improvements on the arm. These components are all related to force transfer from the DC motor to cause the arm to move. To design a controller the parameters of the DC motor, the transmission, and the crossed four-bar linkage are required. This also includes the electronics for the motor driver and the necessary pin out connections as this is considered to be part of the DC motor system.

#### 2.2.2.1 DC Motor

The DC motor used in the series of arm that was set for the testing bed was an ESCAP 23LT12-216E. Its specification can be seen in Table 2. This motor was modified for testing by disconnecting the original leads form the onboard PWM module and connecting it to an external motor driver driven by PWM. The motor is powered when on the arm by the 12V battery, so the same limit was set for the motor externally. The external motor driver is a Pololu VNH5019 Motor Driver shield which can take up to 24V and supply at most 12A continuously, Figure 15. The motor itself is suggested to be limited to about 0.92 (A) continuous current. However, for the configuration built there was no protective circuitry to ensure this limit. The only precaution was set by observing the output current of the external power supply powering the motor driver and cutting power if the current went too high for too long.

Table 2: ESCAP Motor Characteristics

| ESCAP 23LT12-216E Motor Data | |
|---|---|
| **Characteristic** | **Value** |
| Measuring Voltage (V) | 12 |
| Stall Torque (mNm) | 22 |
| Avg. No-load current (mA) | 90 |
| Max continuous current (A) | 0.92 |
| Max cont. torque (mNm) | 10.3 |
| Max. angular accel. (10^3rad/s^2) | 109 |
| Back-EMF const. (V/1000rpm) | 1.3 |
| Torque Const. (mNm/A) | 12.4 |
| Terminal Resistance (ohm) | 6.9 |
| Rotor Inductance (mH) | 0.4 |
| Rotor Inertia (kgm^210^-7) | 4.7 |
| Mech. Time const. (ms) | 21 |

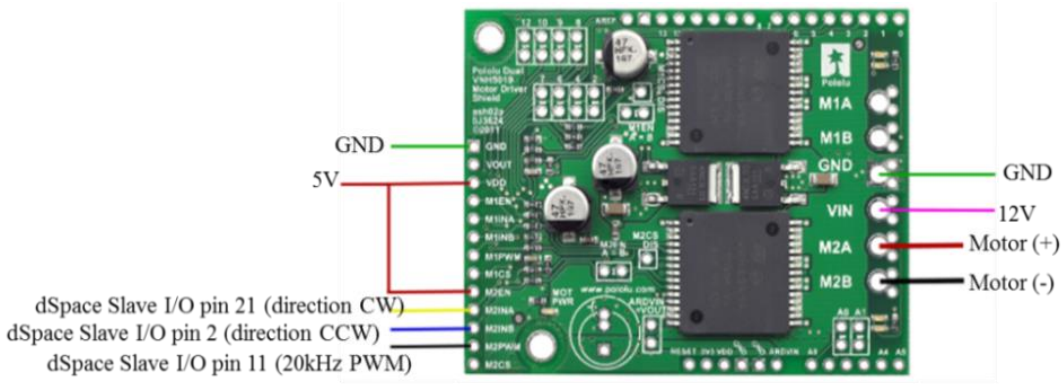


Figure 15: Pololu VNH5019 Motor Driver and Pin-out

#### 2.2.2.2 Transmission

The transmission in the arm is a series of belt drives and Evoloid gears that have a degree of back drivability, seen in Figure 16. This allows the arm to move both directions with some effort under external load. The transmission ratio is 323:1 from the motor input to the output of the transmission [5]. With this higher gear ratio the internal torque effect from the motor can affect the prosthetic control system but in this thesis only external torques are considered.

#### 2.2.2.3 Crossed Four-bar Linkage

The crossed four-bar linkage is connected from the output of the transmission and is linked back to the humerus part of the prosthetic limb where it connects to the load cell pin. The linkage can be seen as highlighted in Figure 17. The linkage itself has been designed to have high torque at elbow angles around $90^o$ (forearm parallel to the ground) to fight the force of gravity when there is a maximum moment due to arm position [5]. However, this assumes that the humeral position is at $0^o$ and is hanging by the side. If the total arm is in a different position, the linkage due to design, fights a force that isn't necessarily present and can causes too high a sensitivity in rotation using the same EMG signal levels as if the humerus is at $0^o$. Outside of the elbow being around the $90^o$ range the transmission angles of the linkage become extreme and the force transferred is very poor as the linkage transfer angles are small. Due mostly to the crossed four bar linkage, the range of useable motion as measured, in the prosthesis, is about $28^o$ elbow flexion, with the forearm up against the humerus, to about $155^o$ where the forearm is fully extended. This is the convention used in tracking the arm angle. By analyzing the force the linkage transfers through its structure, the amount of force the DC motor can transfer

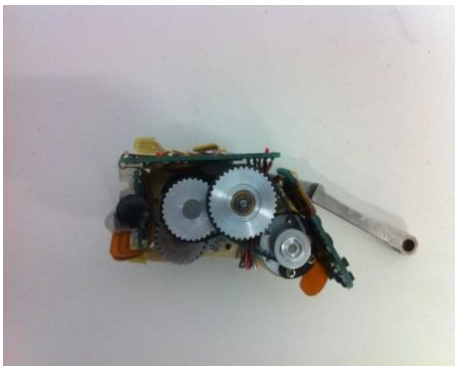

Figure 16: Utah Arm 2 Transmission

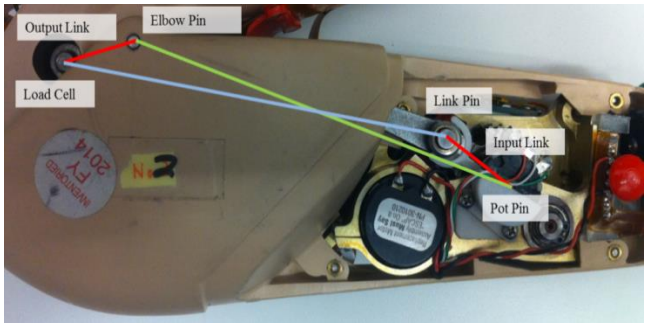


Figure 17: Crossed Four-bar Linkage in the Utah Arm 2

to the load cell pin to rotate the arm about the elbow pin can be determined. This force transfer knowledge is used in the control loop to set the PWM signal to the correct level such that the torque from the motor is sufficient to rotate the forearm about the elbow pin, regardless of arm position. The torque transfer analysis of the crossed four-bar linkage is located in Appendix A.

## 2.3 Chapter Summary

The Utah Arm 2 above elbow prosthetic limb system has been analyzed to understand the mechanical and sensor capabilities such that the human-prosthetic limb kinematics might be obtained to build gravity compensated controllers. There are three

primary angles to obtain for the limb kinematics: the humeral flexion, the humeral abduction, and the elbow flexion. To obtain these angles it requires the modification and the repurposing of data from angular position and torque sensors already present on the Utah Arm 2, which is the prosthesis used in testing. The potentiometer in the elbow joint of the Utah Arm was calibrated to obtain the angular position of the forearm and the internal angles of the Utah Arm crossed four-bar linkage. The load cell in the elbow joint of the Utah Arm was calibrated to obtain torque data as measured about the elbow joint, to be used in the control schemes. Obtaining kinematic data of the human-prosthetic system also requires joint knowledge of the shoulder. This is accomplished through the inclusion of an inclinometer sensor, which measures angular position relative to the gravity vector, to obtain the joint angles of humeral abduction and flexion. The inclinometer was tested to find the error it would induce in the system. The error is small, around 1 degree difference, for static positions. The inclinometer also tracked input signals well for rotations up to $40^{o}$/s. This is sufficient for testing of general human reaching tasks. The overall human-prosthetic system architecture is built on the dSpace 1104 series controller. The combined prosthetic sensor systems and control are all integrated through Simulink programming which interfaces to the dSpace controller for real-time control of the prosthetic limb. From the sum of these modifications, the prosthetic limb kinematic data as well as control feedback channels have been increased. Utilizing the kinematic knowledge of the arm system, the effect of the external forces can be modeled and a gravity torque compensation method can be developed.

# CHAPTER 3

## COUPLED DYNAMICS AND COMPENSATION CONTROL

This chapter presents the coupled dynamics of the human and above elbow prosthetic system as well as two new gravity torque compensation controls for the prosthetic elbow joint. The kinematic equations that describe the combined human-prosthetic system are based on robotic system coordinates as found in J. Craig [29]. The kinematics describe the combined human-prosthetic system as a multilink manipulator. The known physical parameters of the multilink human prosthetic system, such as mass and length, are used in conjunction with the kinematics to determine the predicted torque at the prosthetic elbow joint. Similar work has been done by S. Meek et al. [24] as mentioned in Chapter 1. Using robot controller techniques for multilink systems a controller can be built on top of the standard prosthetic controller but include torque compensation techniques to account for nonlinarites. The actual adverse environmental or induced torque experienced in real motion can be accounted for by using the theoretical models. By programming the predicted torque into the control, the adverse effects of actual environmental torques that impede desired motion of the joints can be nullified, causing the only torque about the joint to be the desired driving torque. This method is hypothesized to improve the physical performance of the prosthesis as well as reduce control effort. As such, a user would be able to apply muscle contractions that more easily yield desired motion.

## 3.1 Coupled Human andProsthesis Dynamics

### 3.1.1 Human Arm Coordinate System

The above elbow amputee's remnant limb (shoulder and humerus) and the prosthetic limb are dynamically coupled. For the focus of this research only three primary degrees of freedom (DOF) of the human-prosthetic arm system are considered. The DOF considered are shoulder abduction, shoulder flexion, and elbow flexion. Humeral rotation is not included as this is not a DOF that is mechanized in the prosthesis used in testing. The 3-DOF multilink coordinate system is developed such that the joint rotations are all done about a local z-axis and all of the local joint x-axis point in-line with the next linkage. This convention was chosen to be consistent with DH-parameters used in robotics. The coordinate system is based on an initial global frame (frame 0) as seen in Figure 18; this is the person's torso. This frame is positioned at the top of the shoulder and is assumed to be in-line with the gravitational field during limb joint motion, i.e., the dynamics assume that the torso of the individual is not bent but straight up and down. In Figure 18, $\theta_1$ is shoulder abduction, $\theta_2$ is shoulder flexion, and $\theta_3$ is elbow flexion. There are two linkages in this system as labeled L1 and L2. The humerus, labeled L1, is the length between the rotation center of the shoulder to the elbow joint; the forearm, labeled L2, is the length between the elbow joint and the tip of the fingers. These parameters can vary between persons and are necessary to measure on a per subject basis.

### 3.1.2 Joint Dynamics

Using the developed coordinate system the dynamics of the arm can be introduced. The shoulder movements are directly controlled by the amputee, as these are the remnant limb sections. For control improvement, the only dynamics that need to be

considered are about the prosthetic elbow joint. This is the only joint that is mechanized in the identified 3-DOF coupled system. However, the shoulder joints and the mechanical elbow both need to be considered in the full arm system dynamics to improve control about the elbow. The diagram of torque about the elbow is in Figure 19, where $L_{COM\ X}$ is the horizontal distance along the x-axis to the center of mass, $L_{COM\ Y}$ is the vertical distance along the y-axis to the center of mass, Fg is the force due to gravity, COM is the center of mass, $\tau_{motor}$ is the torque at the elbow from the motor, $\tau_{int}$ is the internal adverse torque to overcome due to friction, and $\tau_{ext}$ is the external torque due to the forces of gravity and motion affects. The model uses a Center of Mass (COM) for the acting location of the gravity force. Each primary component of the arm is measured for mass, distance in x, and distance in y in frame 4 as shown in Figure 18 and Table 3. The distance in z, which is out of the page according to Figure 19, is not taken into account as the components of the arm are all in plane with the arm and do not deviate out of the z-plane to a significant degree. The three primary torques present at the elbow joint are the external torque ($\tau_{ext}$) which is due to gravity G, inertia M, and Coriolis/centripetal affects V; the internal torque ($\tau_{int}$) due to friction terms N; and the torque applied by the motor ($\tau_{motor}$) or Motor(V). The combined torques are written in Equation (3). The external torque terms that are present have their primary impact about the elbow joint when all of the joints are being rotated in actions such as reaching.

$$\tau_{elbow} = \tau_{external} + \tau_{internal} + \tau_{motor} = \overbrace{\underbrace{M(\theta)\ddot{\theta} + V(\theta,\dot{\theta})}_{\tau_m} + G(\theta)}^{\tau_{ext}} + \overbrace{N(\dot{\theta})}^{\tau_{int}} + Motor(V) \quad (3)$$

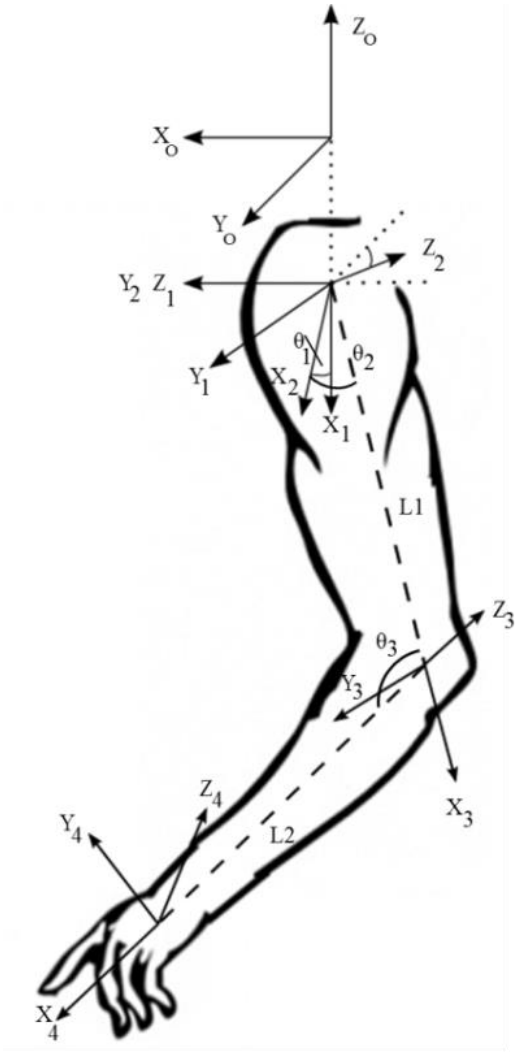


Figure 18: Arm Coordinate System

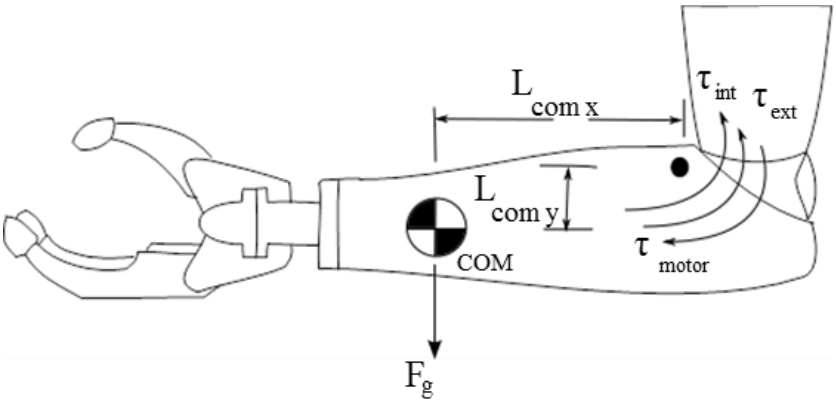


Figure 19: Elbow Joint FDB

Table 3: Utah Arm 2 Primary Components and Characteristics

| **Forearm Components** | | | |
|---|---|---|---|
| **Component** | **Mass(kg)** | **X(cm)** | **Y(cm)** |
| Forearm Housing | 0.11 | 6 | -4 |
| Motor and Trans. | 0.21 | 8 | -4 |
| Forearm Cover | 0.105 | 14.7 | -3 |
| Forearm wrist connector | 0.032 | 13.5 | -3 |
| Wrist Motor | 0.11 | 19 | -3 |
| Prosthetic Gripper | 0.34 | 28 | -3 |
| **Totals** | **Mass(kg)** | **COM X(cm)** | **COM Y(cm)** |
| | 0.907 | 17.56 | -3.35 |

3.1.2.1 Torque Due to Motion

The motion induced torque for the coupled system includes the inertia (M) and centripetal/Coriolis terms (V). These terms are only analyzed about the elbow joint. The equations concerning the motion torque terms are below in the final equation, Equation (4). The more complete derivation of this torque is in Appendix B. Where $I_{axis}$ is the inertia about the specified axis, $C_{angle}$ and $S_{angle}$ are the sine and cosine about the angle number indicated, $l_{COM\ Y}$ and $l_{COM\ X}$ are the center of mass distances in the local forearm frame (frame 4), and $l_{hy}$ $l_{hx}$ are the distances in the local humerus frame (frame 3).

$$\tilde{\tau}_{motion} = z_3.(n_4 + \vec{r}_{14} x f_{12})$$

$$t_1 = \left[(\ddot{\theta}_2 + \ddot{\theta}_3) l_{COM\ X} + ((\dot{\theta}_2 + \dot{\theta}_3)^2 l_{COM\ Y} + \dot{\theta}_1(\dot{\theta}_2 + \dot{\theta}_3) l_{hx})\right]$$

$$t_2 = \ddot{\theta}_2 l_{hx}$$

$$t_3 = \left[\left((\ddot{\theta}_2 + \ddot{\theta}_3) l_{COM\ Y} + \ddot{\theta}_2 l_{hy}\right) - (\dot{\theta}_2 + \dot{\theta}_3)^2 l_{COM\ X}\right]$$

$$t_4 = \dot{\theta}_1^2 l_{hx}$$

$$t_5 = \dot{\theta}_1^2(-C_{23} l_{COM\ X} + S_{23} l_{COM\ Y} - C_2 l_{hx} + S_2 l_{hy})$$

$$A = (l_{COM\,X} + l_{hx}C_3 + l_{hy}S_3)$$

$$B = (l_{COM\,Y} - l_{hx}S_3 + l_{hy}C_3)$$

$$C = t_1 + t_2C_3 + t_2S_3 - t_5S_{23})$$

$$D = (t_3 - t_4C_3 + t_2S_3 + t_5C_{23})$$

$$\tilde{\tau}_{motion} = \left(\ddot{\theta}_2 + \ddot{\theta}_3\right)I_z + \left(\dot{\theta}_1^2 C_{23}S_{23}I_y - \dot{\theta}_1^2 C_{23}S_{23}I_x\right) + m_{forearm}(AC - BD) \quad (4)$$

3.1.2.2 Torque Due to Gravity

The other external torque in $\tau_{ext}$ is induced by the presence of gravity G(θ). The predicted gravity torque term for the arm is as follows: The gravity force acting on the arm is written in terms of the local forearm coordinates, frame 4 in Figure 18, shown by superscript in the equation. Rotations utilizing Euler angles, which are the effective joint angles as previously listed, are necessary to move the gravity acceleration term to the correct local frame, frame 4. The cross product with the COM vector, in frame 4, then yields the theoretical solution in Equation (5), expressed in frame 4. This theoretical term is denoted with the tilde script to denote an approximation. The torque due to gravity is only dependent upon the joint position of the arm and does not depend upon the joint velocities. The term is also dependent upon all three joint states, both shoulder joints and the elbow joint. Its accurate evaluation is dependent upon having accurate measurements of the joints angles and COM parameters. The prediction of the gravity torque computed at the elbow and the actual calibrated torque readings from the load cell are compared in section 3.2.3.

3.1.2.3 Internal Torque Due to Friction Terms

The internal torque due to friction is mostly due to the meshed gears in the transmission. There are both stiction terms and dynamic friction terms that need to be overcome in order to move the arm in a fluid motion. However, these terms are not well known, as the combined gear system causes difficulty in obtaining the friction models during motion. The stiction torque in the gear box to overcome is approximately 1.2 Nm as obtained from experiments. As a result of these adverse friction forces, an adverse torque to overcome is present about the elbow joint. This torque can be handled by using a torque feedback loop at the elbow joint using the load cell. This method is further discussed in the controls section of this chapter.

$$R_0^4 = R_3^4 R_2^3 R_1^2 R_0^1 = R_z(180 - \theta_3) R_z(\theta_2) R_x(90) R_z(\theta_1) R_y(90)$$

$$[R_0^4] \begin{bmatrix} 0 \\ 0 \\ -g \end{bmatrix}^0 = \begin{bmatrix} -mg(-C\theta_2 C\theta_1 C(180 - \theta_3) + C\theta_1 S\theta_2 S(180 - \theta_3)) \\ -mg(C\theta_2 C\theta_1 S(180 - \theta_3) - C\theta_1 S\theta_2 C(180 - \theta_3)) \\ mgS(180 - \theta_3) \end{bmatrix}^4 = G^4$$

$$\tilde{\tau}_{gravity} =$$

$$(mgC\theta_2 C\theta_1 C(180 - \theta_3) - mgC\theta_1 S\theta_2 S(180 - \theta_3))L_{com\,y} + (-mgC\theta_2 C\theta_1 S(180 -$$

$$\theta_3) - mgC\theta_1 S\theta_2 C(180 - \theta_3))L_{com\,x} \quad (5)$$

3.1.2.4 Simplifications from Assumptions

In this thesis several assumptions are made concerning the system dynamics of the combine human-prosthetic system so as to test the validity of the developed theories in

the simplest cases of motion before more complex motions are introduced. These are presented in the sections below.

*3.1.2.4.1 Coordinate System*

The assumption made concerning the coordinate system is that all testing of developed elbow control types will only be done in the flexion plane. This restriction is made to reduce the number of degrees of freedom the humerus is moving to better isolate the control of the elbow function while still presenting a standard use case of the human arm in motion. The flexion plane only concerns the elbow ($\theta_3$) and the humeral flexion ($\theta_2$) angles. Therefore, the shoulder abduction angle is not considered ($\theta_1$). This affects the developed full dynamics presented in the previous sections by simplifying the affect the predicted gravity and motion torques will have about the elbow joint. The gravity term, when not considering humeral abduction, is simplified to Equation (6). The motion torque can be further simplified from the above form in Equation (4), if the motion about $\theta_1$ is zero (no humeral abduction), causing motion only in the flexion plane which yields Equation (7). This effectively drops the motion torque from the out of plane terms.

*3.1.2.4.2 External Torques*

Though the dynamics for the inertial and velocity induced torques about the prosthetic joint have been developed, initial research in this thesis focuses on the stationary external induced torque from gravity to see its effect. Future work will be contributed to assessing these torques and their effect on the joints. Any inertial or rotational velocity induced torque by motion in the flexion plane is not considered and is dropped. This leaves the primary acting torque on the arm to be the effective torque due

to gravity G(θ), the internal friction torque N($\dot{\theta}$), and the torque from the DC motor. With the motion torques dropped, the resultant torque about the elbow is in Equation (8). The motion torques will be considered in future research. Therefore the only adverse torques that needed to be compensated for are the gravity and friction terms, given the assumptions.

$$\tilde{\tau}_{gravity} = (mgC\theta_2 C(180-\theta_3) - mgS\theta_2 S(180-\theta_3))L_{com\,y} + (-mgC\theta_2 S(180-\theta_3) - mgS\theta_2 C(180-\theta_3))L_{com\,x} \quad (6)$$

$$t_1 = \left[\left(\ddot{\theta}_2 + \ddot{\theta}_3\right)l_{COM\,X} + \left(\left(\dot{\theta}_2 + \dot{\theta}_3\right)^2 l_{COM\,Y}\right)\right]$$

$$t_2 = \ddot{\theta}_2 l_{hx}$$

$$t_3 = \left[\left(\left(\ddot{\theta}_2 + \ddot{\theta}_3\right)l_{COM\,Y} + \ddot{\theta}_2 l_{hy}\right) - (\dot{\theta}_2 + \dot{\theta}_3)^2 l_{COM\,X}\right]$$

$$t_4 = 0$$

$$t_5 = 0$$

$$A = (l_{COM\,X} + l_{hx}C_3 + l_{hy}S_3)$$

$$B = (l_{COM\,Y} - l_{hx}S_3 + l_{hy}C_3)$$

$$C = t_1 + t_2C_3 + t_2S_3 - t_5S_{23})$$

$$D = (t_3 - t_4C_3 + t_2S_3 + t_5C_{23})$$

$$\tilde{\tau}_{motion} = \left(\ddot{\theta}_2 + \ddot{\theta}_3\right)I_z + m_{forearm}(AC - BD) \quad (7)$$

$$\tau_{elbow} = G(\theta) + N\left(\dot{\theta}\right) + Motor(V) \quad (8)$$

## 3.2 Prosthetic Control

### 3.2.1 Utah Arm Standard Control

The Utah Arm 2 as described above in Chapter 2 is the prosthesis that was utilized in control testing about the prosthetic elbow. The standard controller that comes with the Utah Arm is a proportional EMG based control which classically targets the Bicep and Triceps as the antagonistic muscle pair to drive the elbow [5]. The standard controller for the Utah Arm 2 also has a secondary mode which is activated after the EMG levels drop below a certain preset level typically designated by the prosthetic technician. This mode is called free-swing and causes the elbow to drive freely "out-of-the-way" so as to act limp by a person's side [5]. This mode is intended to assist in walking so as to mimic the free swing of a natural human arm in this motion. Both of these modes combined make up the standard controller of the Utah Arm 2. This controller is used in testing later to act as the baseline of current performance to compare to the newly developed gravity compensation controllers. This standard controller based on the actions captured in [5] is the foundation for the newly developed control types.

#### 3.2.1.1 Proportional EMG

The standard control of the Utah Arm, at the elbow joint, is accomplished through proportional antagonistic muscle control using EMGs [5] and [6]. For above elbow amputations, the muscle pair is typically the remnant bicep and triceps. The contractions are detected by surface EMGs located at these muscle sites. The captured EMG signals, after being rectified and then low-pass filtered ($t_c$ = 150ms) externally in the Myolab II unit [37], are internally filtered in the dSpace controller ($t_c$ = 20ms median filter) and then multiplied by a gain to amplify the signal, which also effectively sets the sensitivity of the

bicep and triceps contractions. In the proportional controller the difference between the bicep and triceps signals is used as the command signal to directly set the command voltage for the motor PWM. The generated signal to move the prosthesis about the elbow follows similar biomechanics of the natural arm. If the bicep signal is higher than the triceps, the forearm will move up. If the triceps signal is higher than the bicep, the forearm will move down. The control loop is "closed" through the visual feedback of the prosthetic user to control the position of the terminal device (TD), as this is a human-in-the-loop system. In this case, the contractions of the arm muscles provide the full control input and must overcome the adverse torques both externally and internally in order for the arm to move. In order to compensate between users, the proportional constant used for the EMG signals to amplify the command voltage to the motor, can be adjusted. This changes the amplitude at which an amputee would have to provide a muscle contraction but also changes the sensitivity of how the forearm moves in different positions set by user preference.

#### 3.2.1.2 Free-swing Mode

Free-swing, in a sound human arm is the natural motion where the natural arm swings freely by a person's side. For example, when a person is walking the natural forearm swings freely. The standard controller in the Utah Arm 2 mimics this natural motion to make the arm appear more natural when walking [5]. The free-swing mode is activated after the EMG signal levels, as a result of muscle contractions, drop below a preset level. The free-swing mode in the prosthesis uses the load cell readings and essentially drives the DC motor such that the readings as detected by the load cell are zero. Free-swing is

controlled by a gain labeled “Free-swing Gain” as seen in Figure 20. This gain effectively changes the impedance about the elbow joint when it is active. If a force on the prosthetic forearm can be detected through transfer to the load cell, the force will be compensated for by driving the arm in the direction to reduce the induced torque and thus the load cell output voltage. As an example, the arm due to its own weight will fall in the gravity field and act limp due to the torque servo which attempts to drive the load cell to a zero reading. Another example would be the forearm being forcibly moved back and forth from an external source. In this case, the rotation about the elbow offers little resistance to the external motion and the forearm moves effortlessly in the forced direction. The block diagram of the standard controller can be seen in Figure 20.

### 3.2.2 Gravity Compensated Control

As indicated in Section 3.1, there are adverse external and internal torque effects that the user of the prosthetic limb has to overcome in different limb configurations in order to drive the prosthesis in a desired fashion. Initial research for this thesis only considers gravity compensation, in conjunction with internal torque compensation, for the compensated control schemes for testing of control improvements.

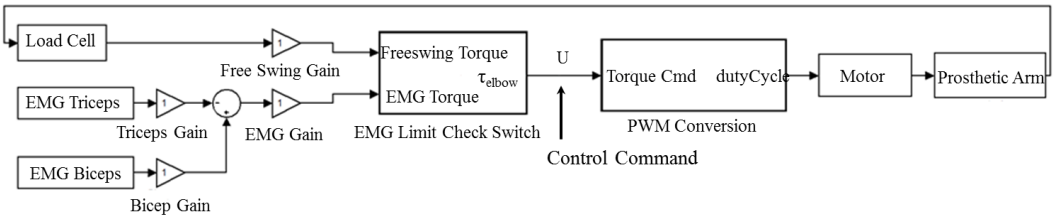


Figure 20: Copy of the Utah Arm Controller

The Utah Arm standard control architecture [5] and [6] of the elbow joint is the foundation for the new compensated control schemes. The prosthetic elbow is driven by proportional EMG signals and free-swing is still active. The intention of gravity compensation is to nullify the adverse nondriving gravity torque that acts about the elbow by applying predictions of this torque value in the control law command. With compensation methods applied to the control of the forearm, the forearm will only move under user desired torque commands sent by the EMG signals. This essentially turns the control of the elbow into a torque controller. As mentioned in the Introduction, Chapter 1, torque control of prosthetic joints has been done in previous work [24] though the method taken in this thesis is slightly different in its approach as it fits more with robotic techniques which use feedback compensation utilizing a theoretical model of adverse torques. With the torque controller, it is thought that control of the prosthesis will be done in a less exhaustive way, as primary external torques such as gravity are being compensated for in the controls. The torque compensation in the prosthesis application is accomplished by using the kinematic and dynamic models of the combined human-prosthetic system to predict the torque. The predicted torque value is added to the control inputs thus compensating for their effect on the arm dynamics.

Two forms of gravity compensated control are developed. One controller named (GC) uses the EMG signals to command a torque about the elbow joint with the load cell providing feedback. The GC controller compensates for both the friction torque as well as the gravity torque. The other controller, called GCF, is built on the standard controller and only compensates for the gravity torque and does not account for friction. The design of these controllers and the control block diagrams are located in the subsequent sections. The controllers are presented in block diagram form and have the corresponding control

command listed below the block diagram for the new controllers.

3.2.2.1 Gravity Compensation with Torque Servo

*3.2.2.1.1 Controller Design*

This control type addresses the adverse torques of both the gravity term $G(\theta) = \tau_g$ and the friction term $N(\dot{\theta})$ through compensation methods. The control of the arm is changed such that the control command is in terms of torque and is compared to the load cell torque to create a torque servo, while also including compensation for the gravity torque in the control loop. For this control type the EMG signals command a torque to be set at the elbow, which is compared to the load cell reading to create the control command. This effectively turns the arm into an impedance based control about the elbow. The sensitivity of the impedance is set by a proportional gain "Torque Servo Gain" as seen in the block diagram in Figure 21.

*3.2.2.1.1.1 Friction Compensation Using Impedance Change from Torque Servo*

Consequently, by using the load cell to read any adverse torques and by including the load cell reading into the control command the adverse torque due to friction effects is detected by the load cell, once the effect of gravity torques are removed. Using this load cell reading in the control command as an input the control loop will drive the motor such that this detected resistance force, static or dynamic friction terms, will essentially be close to "zeroed" thus making the elbow joint, depending upon the impedance gain set by the Torque Servo Gain in Figure 21, "frictionless".

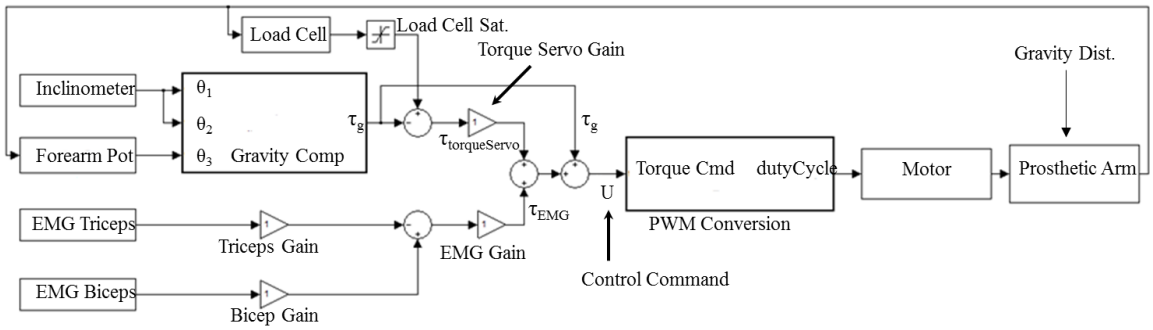


Figure 21: Gravity Compensated Control Block Diagram

$$U_{ctrlCMD} = EMG\ Gain(\tau_{EMG}) + TorqueServoGain(\tau_{torqueServo}) + \tau_g \quad (9)$$

Compensating for friction enters in the control loop with the $\tau_{torqueServo}$ term. With this mode, the arm, given any other force than gravity will drive itself out of the way of a disturbance force in a smooth fashion. It is thought that the implementation of this control design will allow for more fluid forearm motion. The control block diagrams and the control commands are in the following sections.

*3.2.2.1.1.2 Gravity Compensation*

In conjunction with the torque servo based control, the external force of gravity is compensated for by use of a theoretical approximation. This is a method that is classically used in the robotics field to remove nonlinear effects or to linearize a system through feedback [29]. The implementation of this method in the Utah Arm requires that the theoretical value, as displayed in Equation (6), first be subtracted from the load cell signal to remove the detected torque induced by gravity. By subtracting the gravity load from the load cell reading in software, the torque servo mode is not activated by the gravity force. The gravity torque is then added back into the control command (U) such that the motor is always outputting the necessary torque to hold the arm up under its own

weight. Figure 21 shows the control block diagram and Equation (9) is the control command.

*3.2.2.1.2 Static Characteristics*

Under static states when an amputee or test subject is not sending an EMG signal to move the forearm, the arm should be stationary in terms of its rotation about the elbow joint. This is due to the gravity compensation signal sending the needed control input to have the DC motor support the arm's weight. If an external disturbance is present on the forearm and the force is high enough to be detected, the arm will move out of the way of the disturbance due to the torque servo function mode.

An instability state is present around configurations were the full coupled system has the humerus and elbow joint close to $90^{o}$ in flexion. At these states the forearm acts like an inverted pendulum. With gravity compensation on, the effect of the arm falling should be much reduced causing the arm only to move with user intended driving contractions in these locations. Statically the arm should be much more stable as no continuous control signal needs to be sent from the user to the arm to keep it in place.

*3.2.2.1.3 Dynamic Characteristics*

For this control scheme the gravity compensation mode is always on and the torque servo is used to command position. This means that during forearm rotation motion the motor is producing a torque necessary to support the arm weight as it moves through the range of motion as well as the force necessary to drive past any adverse internal torque detected by the load cell. This is designed to help smooth the arm motion and make it less sensitive to gravity effects. However, because of the torque servo, the control might have

a tendency to cause overshoot of targets as there is little internal resistance to offer any damping effect during rotation. Using gravity compensation in conjunction with a torque servo control is only one variation possible in the elbow controller, and multiple other control types can be used. This mode was specifically chosen so as to model the natural motion of the human arm which naturally compensates for internal and gravity torques.

3.2.2.2 Gravity Compensation without Friction Compensation

*3.2.2.2.1 Controller Design*

This control method is implemented by modifying the standard control scheme, Figure 20, to include gravity compensation. This control type only compensates for the gravity term $G(\theta) = \tau_g$ and does not account for friction. This method permits the friction in the elbow joint to be present in the system, unlike the GC control type. The test subject will need to provide an EMG signal to compensate for this adverse force. Thus, like the standard controller, the EMG signal directly sets the signal to the motor. The control block diagram and the corresponding control command are in Figure 22 and Equation (10).

$$U_{ctrlCMD} = EMG\ Gain(\tau_{EMG}) + \tau_g \tag{10}$$

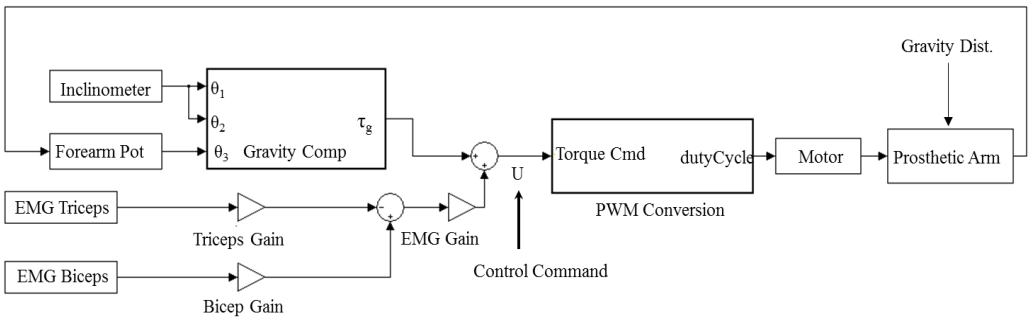


Figure 22: Gravity Compensation Added to Standard Controller

*3.2.2.2.1.1 Gravity Compensation*

The gravity compensation in this control scheme changes the controller by adding in the gravity term to the EMG signal to command the duty cycle. The free-swing mode normally present on the standard controller is not effectively active in this control design as a result of the gravity compensation.

*3.2.2.2.2 Static Characteristics*

In the instability states as described in the section on the GC controller, with gravity compensation on, the effect of the arm falling should be much reduced causing the arm only to move with user intended driving contractions in these locations.

*3.2.2.2.3 Dynamic Characteristics*

With this controller active and the arm in motion due to EMG signal inputs over the set limits, the free-swing mode is off but the gravity compensation mode is on. The free-swing mode in dynamic motion is meant to smooth the arm's movement by not having the internal friction forces acting on the arm. However, with no free-swing or really without a reduced impedance about the elbow joint, in motion an amputee has to provide a larger EMG signal to overcome this force. In addition, since the impedance is higher, the smoothness of the trajectory in both start and stop conditions might not be as good as compared to the gravity compensation with free-swing. However, with the EMG limit presets it will also not be as sensitive to slight muscle contractions which can yield more stable control around instability points.

### 3.2.3 Unit Testing of Gravity Compensation

To verify the gravity compensation algorithms, a static test was developed to compare the theoretical gravity torque predicted by the load cell at the elbow to the actual load cell readings. This test was accomplished by setting the shoulder flexion angle at discreet angles and taking load cell readings at various elbow angles through the entire elbow range of motion. The compared relationship is displayed in the following plotted results. As noted previously, the load cell reaches a point where an increase in actual applied force no longer is registered on the load cell. This does not mean that the torque required to lift the forearm is this value; it is just that the load cell can read no higher. The actual torque necessary to apply to the arm is still larger which is seen as the second curve in all of the plots.

As can be seen, the theoretical follows the actual load cell data to a close degree, Figure 23 to Figure 27. However, areas close to the ends of the data curves show the experimental data vastly deviating from the theoretical and diving to lower than predicted values. This can particularly be seen in Figure 23 and Figure 24, with the last data point. In these areas it was observed that on the prosthesis, the forearm's external plastic housing was beginning to rest on the humerus's housing, causing a different distribution of force across the elbow joint which could not be predicted. These occurrences only happen at the extreme elbow angles of the prosthesis near the extents of motion of the arm. This was around elbow angles greater than $145^{o}$ and less than $35^{o}$ (out of the approx. $155^{o}$ to $28^{o}$ joint range), so this was not as much of a concern when considering the primary range of motion. The error overall in all cases was never greater than 0.2 Nm in magnitude, excluding areas where the load cell could no longer accurately track the applied torque.

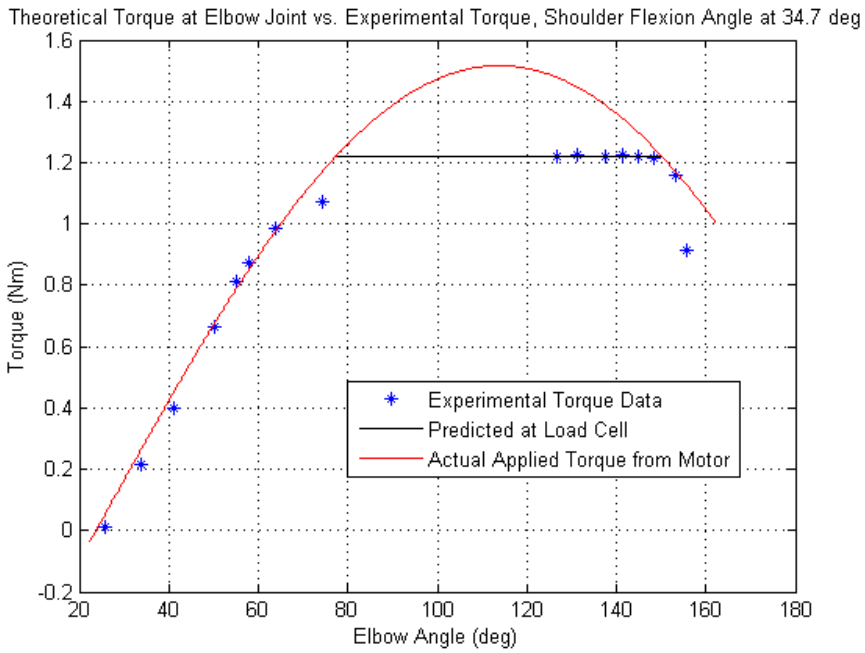


Figure 23: Theoretical Gravity Compensation Torque vs. Measured Torque at the Elbow Joint (humerus at 34.7$^{o}$ in flexion)

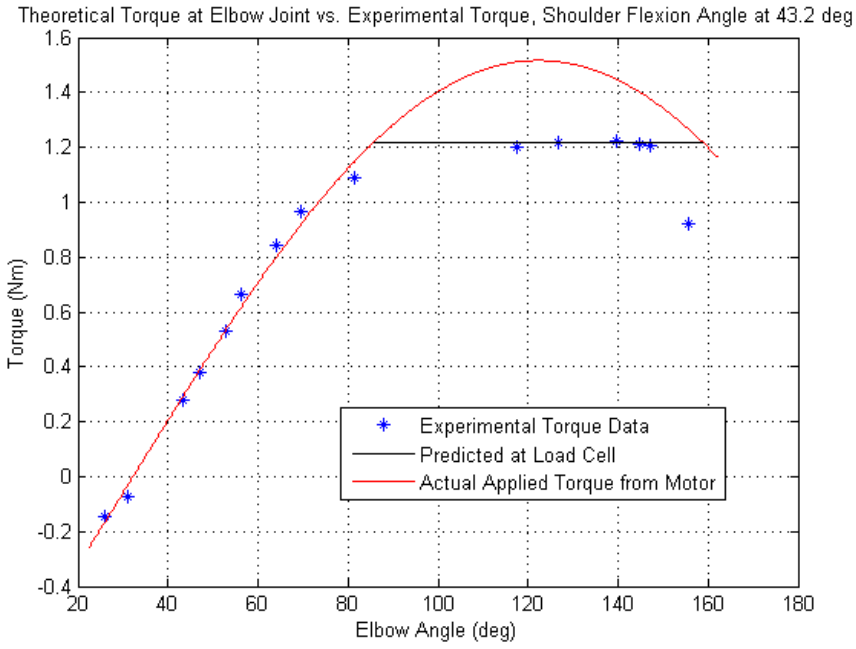


Figure 24: Theoretical Gravity Compensation Torque vs. Measured Torque at the Elbow Joint (humerus at 43.2$^{o}$ in flexion)

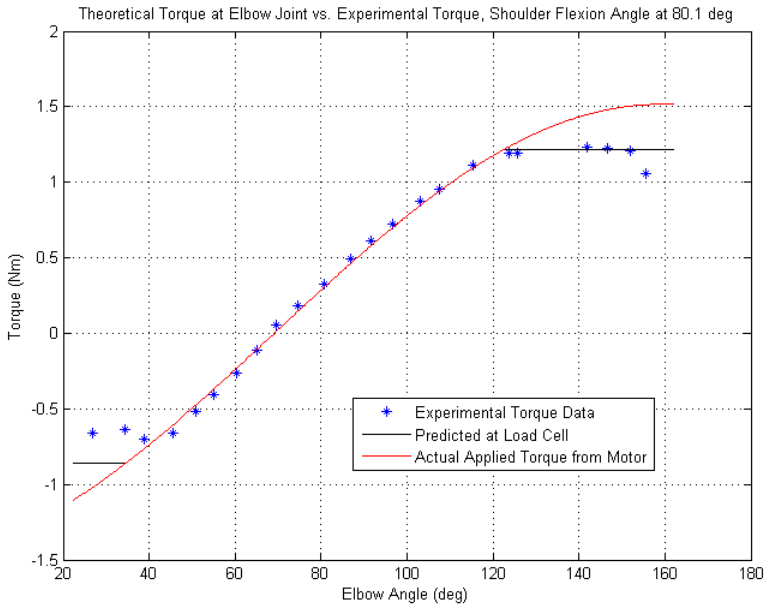


Figure 25: Theoretical Gravity Compensation Torque vs. Measured Torque at the Elbow Joint (humerus at 80.1$^{o}$ in flexion)

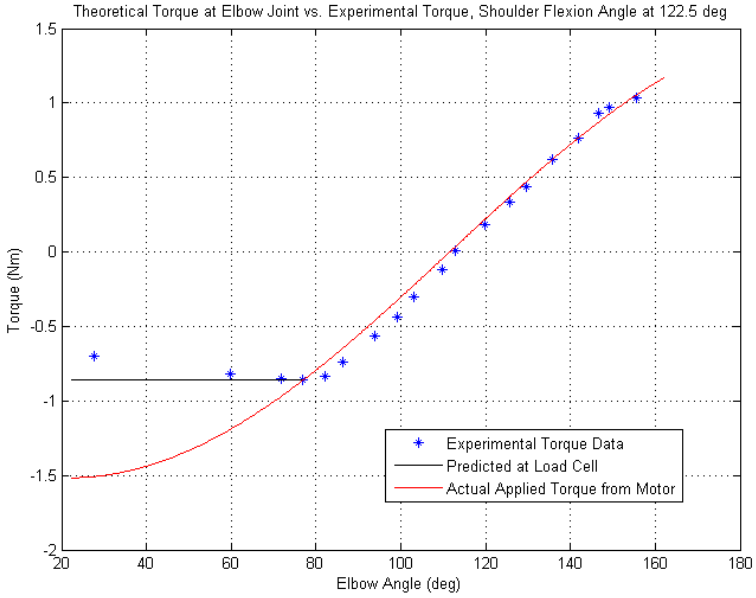


Figure 26: Theoretical Gravity Compensation Torque vs. Measured Torque at the Elbow Joint (humerus at 122.5$^{o}$ in flexion)

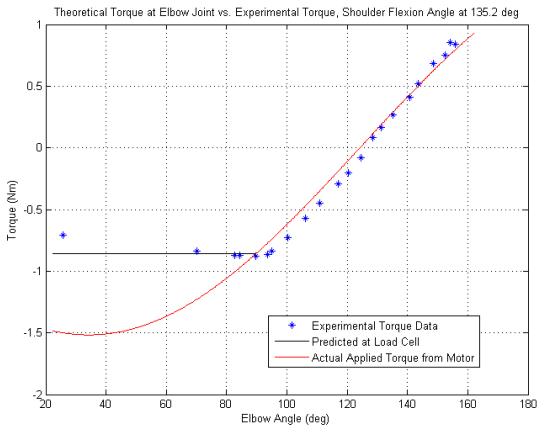


Figure 27: Theoretical Gravity Compensation Torque vs. Measured Torque at the Elbow Joint (humerus at 135.2$^{o}$ in flexion)

In the areas where the theoretical tracked the measured torque to a close degree, the difference between theoretical and experimental values was not enough to cause the arm to fall under its own weight.

3.2.3.1 Inclinometer Sensitivity

Inclinometer sensitivity was also studied as the effects of this developed sensor showed possible error during unit testing as seen in Chapter 2. This was only tested in the shoulder flexion range as it is the tested motion in the designed reaching experiments. Three static shoulder angles were chosen to see the effects, one angle below 90$^{o}$ (humerus at 34.7$^{o}$), one angle close to 90$^{o}$ (humerus at 80$^{o}$), and one above 90$^{o}$ (humerus at 122.5$^{o}$). In each case the error was set to be $\pm$ 2$^{o}$ flexion, as this is just larger than the maximum error found, displayed in Chapter 2 Section 2.2.1.3. Overall, the error due to influence of the inclinometer does not greatly affect the predicted values for torque from gravity compensation as seen in Figure 28 to Figure 30. The inclinometer error in the 2$^{o}$ range would still yield acceptable theoretical gravity torque values to use in all cases.

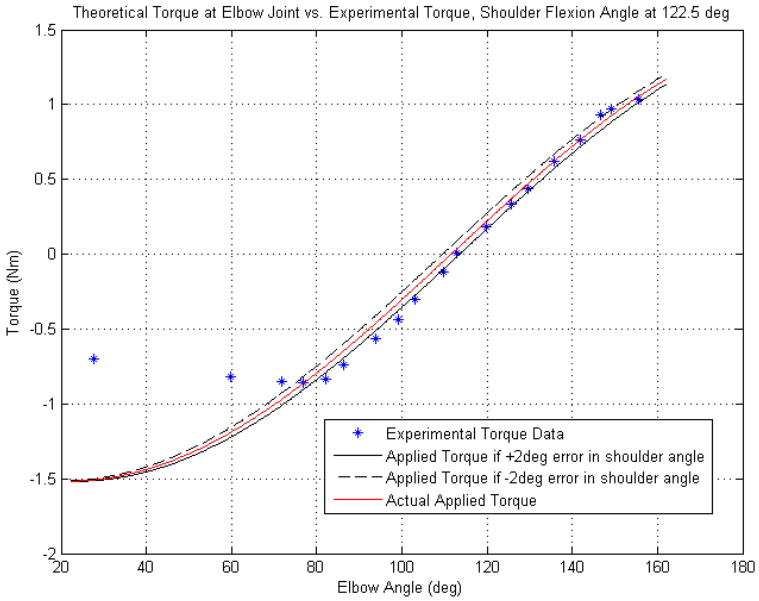


Figure 28: Theoretical Gravity Torque with Inclinometer Error Bounds (humerus at $122.5^{o}$ of flexion)

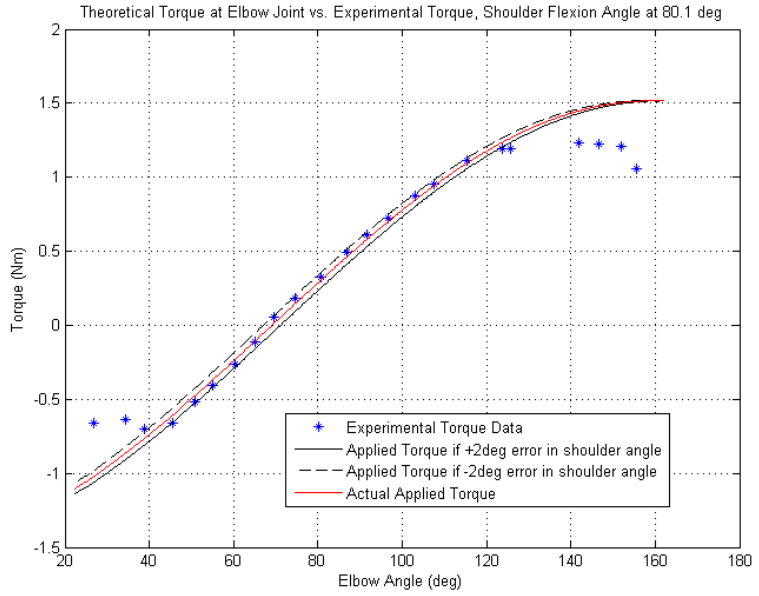


Figure 29: Theoretical Gravity Torque with Inclinometer Error Bounds (humerus at $80.1^{o}$ of flexion)

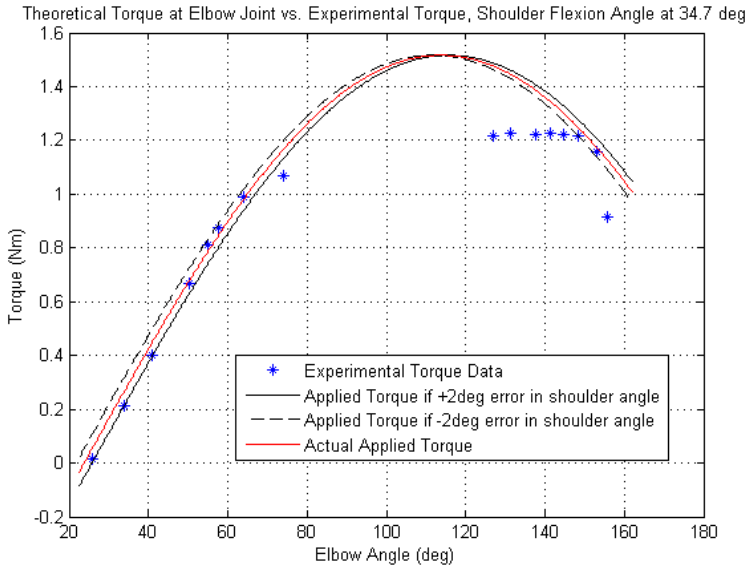


Figure 30: Theoretical Gravity Torque with Inclinometer Error Bounds (humerus at $34.7^{o}$ of flexion)

## 3.3 Chapter Summary

This chapter presented the human-prosthetic dynamically coupled system kinematics and the resultant gravity torque compensation controllers that can be derived from this knowledge. The techniques used for torque compensation are based on well-established principles used in robotics where theoretical dynamics of the system are used in a feedback loop to remove nonlinear torque effects. A coordinate system was developed to describe the human-prosthetic system which is based on a 3-DOF concerning the humeral abduction, humeral flexion, and humeral elbow. The system was reduced to the flexion plane to simplify the system dynamics for the experiments to study the initial controller effects on the elbow. Using a prediction of the gravity torque by accounting for the mass and lengths of the prosthesis and natural arm, torque compensation methods were developed to include into the EMG proportional control of the elbow joint. The first controller compensates for both gravity and the internal friction in the elbow, while the second controller only accounts for the gravity term and only adds the gravity

compensation to the standard controller. The gravity compensation theoretical model was compared to the actual readings coming from the load cell in flexion angles only. In all humerus test cases where the elbow was placed, the theoretical model matched the experimental data very well only deviating by 0.2Nm at max difference across the whole range of motion. There were areas where the load cell no longer read the correct value and flattened out to a constant reading. In these cases the theoretical is set to that constant to match the saturated output. The inclinometer was also analyzed. In the cases where the inclinometer might have error in its flexion angle readings around $\pm 2^{o}$ there was not a large effect at any humerus angle prediction of gravity torque and the error bound was acceptable in all cases. With the verification of the gravity compensation theoretical model and the development of two controllers the control schemes can be tested to see which performs the best in comparison to the natural human arm and to the standard controller. The testing methods and metrics are presented in Chapter 4 and the results of testing, including the discussion of the obtained data, are presented in Chapter 5.

# CHAPTER 4

## EXPERIMENTAL SETUP AND METHODS

This chapter presents the experimental setup and methods used to obtain measurements from the prosthetic limb to understand control improvements. The experiments to obtain data about prosthetic controller performance are built around reaching tests where a test subject starts at rest with the prosthesis at their side and then goes to reach for a target presented in their workspace. Reaching tests were chosen as this is the primary daily use case of the combined shoulder and elbow joint system. These reaching tests are designed to induce both the shoulder and elbow joint motions such that the entire human-prosthetic system is evaluated using each controller type, all of which are presented in Chapter 3. The new controllers are compared to each other to find if there is control improvement over the standard control. There are two forms of data used for evaluating the control improvement of the prosthetic controllers, one quantitative and the other qualitative. The quantitative data are data concerning the measurements of the physical performance of a prosthetic controller when performing a reaching task. The quantitative data are comprised of four designed measurements called metrics. The first two metrics are measures of the prosthetic motion from rest to a presented target; this stage of the reach is called the approach. The metrics are the time to target and trajectory smoothness or jerk. The second two metrics are measurements of the controller's

capability to hold at a target, this stage of the reach is called the hold. The metrics are the steady state error and the variance of the prosthetic end effector at the target. The qualitative data are a measure of a test subject's personal feel of how "controllable" the prosthesis is with a certain controller. Controllability is the measure comparing a control type to the natural limb in terms of control effort on a scale where 0 is worst and10 is best or exactly comparable to the natural limb effort. The metrics are defined in depth in Section 4.3.

As mentioned, these metrics are obtained through a series of reaching tests to targets presented in a user's normal workspace. The targets are set by a 3-DOF robot arm. The target robot arm and the user's natural arm or prosthesis, has IR markers placed at discreet points along their structure. Three-dimensional motion capture cameras track these points in time and record their position. The position data of the markers relative to each other is the foundation of the quantitative data. A series of reaching tests are conducted for six targets with three trials per target for all three types of prosthetic controllers. The targets are randomized per test subject. All of the control types are tested on one target before the next target is presented. The first controller for a target is used to conduct a reach from rest at the side of the test subject's body to the target. The control type is then switched to one of the remaining two controllers, and reaches are repeated until all control types have been tested. The test subject does not know what controller, by its formal name, is being used but is told it is controller A, B, or C. All controllers are assigned a different letter at each target and are not consistently labeled between targets. This is to prevent test subjects determining the control types. After the test sequence is run for a target the test subject is asked to evaluate controllers A, B, and C in a survey to obtain information concerning test subject rated control effort during the test, as

mentioned previously. A total of 10 users were tested and the performance data for each controller between individuals and between target positions are processed using the controller metrics.

Several design restrictions have also impacted the experimental test setup. The restrictions can impact the tests and are as follows: Nonamputees were tested instead of amputees as part of the preliminary evaluation of the controllers; only a left-sided socket was used, and the EMG site for prosthetic activation was switched from the normal bicep and triceps site on an amputee to the right side forearm flexor muscles. All of these influences can impact testing. However, the data between control types are being compared relatively and the overall trend of improvement, which is being captured, should not be affected. The following sections of this chapter discuss the details of the equipment, setup and methods used to evaluate control performance.

## 4.1 Experimental Setup

The experimental setup includes both equipment and initial test subject preparation. The primary testing equipment is the 3-DOF target robot, the three-dimensional motion capture cameras by Vicon® (Oxford U.K.), and the dSpace controller. These systems allow for the presentation of targets in the user workspace as well as the capture of limb motion as a test subject moves toward a target. The test environment requires that the test subject and robot be placed such that the test subject can reach the end effector of the target robot and the reach motion can be recorded. This is the primary goal of the test preparation.

4.1.1 Testing Equipment

The test equipment consists of two independent systems, the target robot and the motion capture camera system. The target robot system is used to present reaching targets to a test subject, and the Vicon camera system is used to record the motion of a reaching task. The testing equipment architecture can be seen in Figure 31 and Figure 32. Each system is presented in detail in the following sections. The target robot system runs independently from the Vicon system and does not need to be synchronized for obtaining the experimental results in this thesis, as only the video recordings of the IR markers are needed.

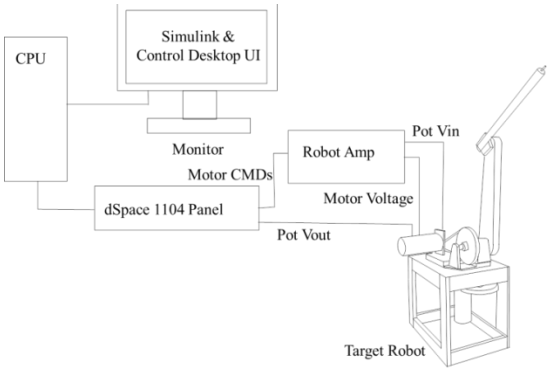


Figure 31: Target Robot System Architecture

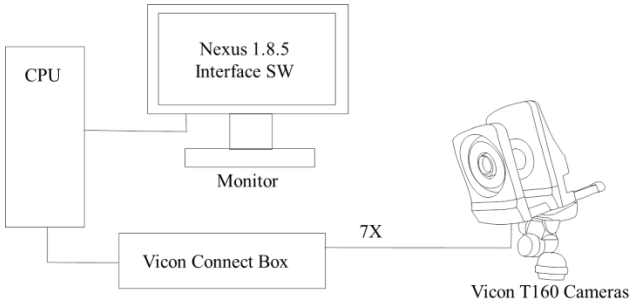


Figure 32: Motion Capture (Vicon) System

#### 4.1.1.1 Target Robot System

##### *4.1.1.1.1 dSpace Controller and User Interface*

The dSpace controller system acts as the hub for the target robot controller as well as the controller for the prosthesis which is covered in Chapter 2. It uses a user interface (UI) to act as the control board for both the robot and the prosthesis called Control Desktop. During testing this interface is where the test proctor sets the control type being used on the prosthesis as well as the target position to go to, for the target robot. The dSpace controller interfaces, as previously discussed, through Simulink which acts as the programming environment. Once the program is built it is pushed to the dSpace control board and acts as an embedded program running in "real-time". The testing interface can be seen in Figure 33, with the key components listed in Table 4. The connections for the dSpace system to the target robot are located in Chapter 2. There are six connections that are present for the robot which are the driving voltage signals to the robot amplifier that runs the target robots motor, and the three robot joint potentiometers.

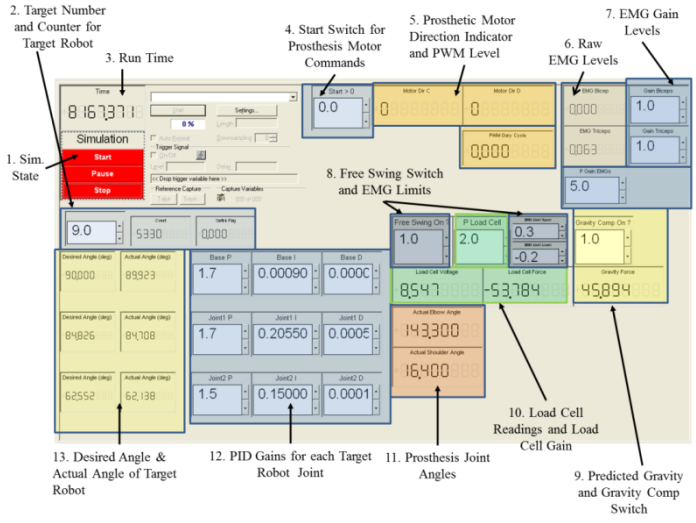


Figure 33: Control Desktop Testing and Operations Interface

Table 4: Control Desktop UI Functions

| **Control Desktop Interface Descriptions** | |
|---|---|
| 1. Sim State | This UI element controls the running of the dSpace card and starts, pauses, or stops a simulation from running. |
| 2. Target Number and Counter for Target Robot | This interface allows for the entry of the desired target number. The counter and switch flag boxes indicate how much time there is to complete a trajectory and when the next target can be entered. |
| 3. Run Time | This is the current run time of the simulation |
| 4. Start Switch | This is the start switch flag which activates the PWM module on the dSpace to control the Prosthesis |
| 5. Prosthetic Motor Dir. Indicator and PWM level | These box display which direction the motor is spinning and what the PWM duty cycle is |
| 6. Raw EMG Levels | These are the raw EMG signal levels read by the dSpace ADC |
| 7. EMG Gain Levels | These are where the individual gain for each muscle group is set as well as the overall EMG gain |
| 8. Free Swing Switch and EMG Limits | These interfaces turn the free-swing mode on or to a state where it is only active after EMG activity drops below the set EMG limits. |
| 9. Predicted Gravity and Gravity Comp Switch | This turns the gravity compensation control on or off. It also displays the theoretical force due to gravity at the load cell |
| 10. Load Cell Readings and Load Cell Gain | These boxes display the actual load cell output voltage as well as the calculated force on the load cell. The gain of the load cell is also set. |
| 11. Prosthesis Joint Angles | These boxes display the joint angles of the elbow and shoulder flexion |
| 12. PID Gains for each Target Robot Joint | These interfaces set the PID gains of the target robot joints |
| 13. Desired Angle and Actual Angle of Target Robot | The left boxes display the desired angle as set by the trajectory planner. The left boxes display the actual angle as read by the dSpace controller from the pots. |

*4.1.1.1.2 Target Robot*

The target robot is a 3-DOF robot that presents reaching targets to the test subject(s). The robot has three primary joints that allow for the placement of the robot end effector in space. These joints are each actuated with brushed DC motors which drive each robot joint with a set of belts. Each joint has a potentiometer directly attached to the link joint and each has been linearized to read the joint angle in degrees. The potentiometers of the robot are connected to the ADC channels of the dSpace system as indicated in Chapter 2. A figure of the target robot can be seen in Figure 34 along with the IR markers on the robot links. The actual target presented to the test subject is in Figure 35. It is the point of a black post sticking out of the end of the robot. This post is approximately 2cm in length. As discussed in the control improvement metrics in Section 4.3, the test subject needs to place their end effector marker within ± 7.8mm of the target as this is the radius of the IR Marker. The markers are labeled in the Vicon software to accurately record the position data of each robot marker location. The marker names are listed in Figure 34.

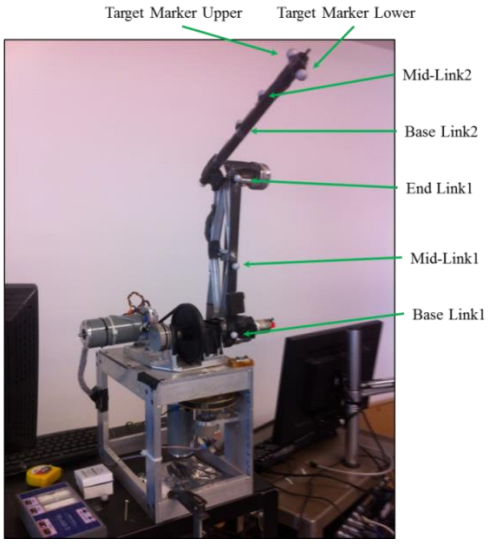


Figure 34: Target Robot with IR Markers

Figure 35: Robot Target

*4.1.1.1.2.1 Target Robot Kinematics*

In order to place the robot end effector in space both forward and inverse kinematics for the target robot are used. The dimensions of the target robot that were used for the kinematics of the system are displayed in Table 5. For testing, the robot was placed on a cart which raised its base above the ground. The cart had to be accounted for to find the overall global placement of the robot end effector. A figure with the robot on the testing cart andcorresponding dimensions to the zero plane of the robot are in Figure 36. The use of the kinematic joint data from the robot arm was used in the Simulink code to place the robot end effector at desired target locations.

Table 5: Target Robot Dimensions

| Robot Dimensions andJoint Ranges | |
|---|---|
| Link 1 (in) | 12 (304.8 mm) |
| Link 2 (in) | 10 10/16 (269.8mm) |
| Joint 0 (Base) | $0^o – 180^o$ |
| Joint 1 | $0^o – 180^o$ |
| Joint 2 | $-180^o – 180^o$ |

*4.1.1.1.2.2 Target Robot Trajectory Planning and Controls*

The robot arm is programmed to present up to six different targets to the test subject at locations in Cartesian space based on the robot zero-plane. The robot moves between targets in a short time frame in order to reduce the time of testing. This requires the use of both a trajectory planning algorithm as well as a PID control loop which uses the potentiometers at each robot joint for feedback to place the end effector of the robot accurately. There is no set trajectory the robot must follow from point to point but rather the path between targets is computed in real-time using the desired end target location and the beginning target location with a cubic trajectory planner. The trajectory itself does not matter but only that the robot can get to and present the next end point target location. In practice, the error at each joint, once the robot has settled, is approximately less than 0.2 degrees, which can yield up to an error in the x and z direction (target robot zero plane as shown in Figure 36) of 1.5% of the desired end location. This permits the robot to move from one target to another with a repeatable target location each time. The target coordinates are stored in a list set in Simulink by a set number (one through six) for each particular test subject. The robot is set to move from one target to another by entering in a desired target number in the Control Desktop UI, Figure 33 label # 2.

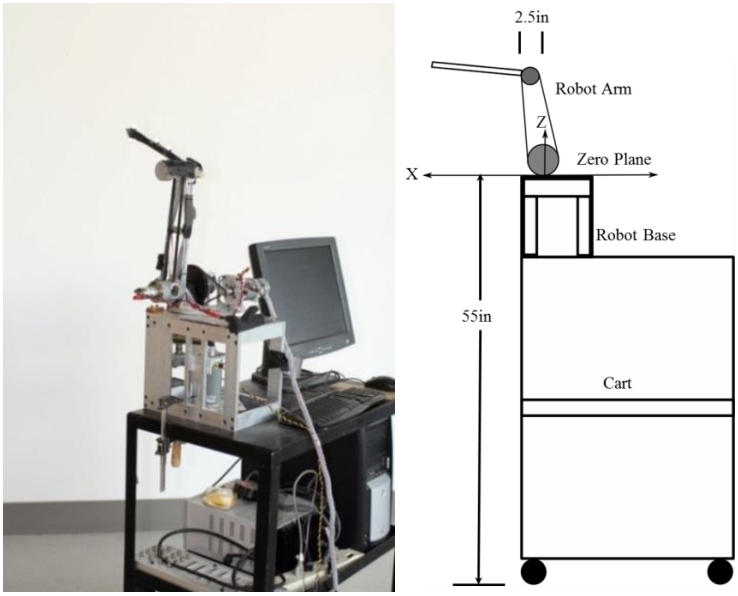


Figure 36: Target Robot on Cart and Sketch with Zero Plane Dimensions

4.1.1.3 Three-dimensional Motion Capture Cameras (Vicon) System

In order to capture the target robot, the prosthesis, or the natural limb motion, a 3D motion capture camera system is used. The camera system is made by Vicon and works in conjunction with the Nexus 1.8.5 software. The camera system is set up and calibrated before a recording. In addition, subject models are built in the Nexus software which links sets of IR markers together to form the subject model. There are three subject models that are created: the target robot, the prosthesis, and the natural limb. The marker placements may vary slightly between test subjects but are for the most part the same. Marker placement is discussed further in Test Subject Preparation, section 4.1.2. The cameras track and record all motion of the placed IR markers. There are seven T160 cameras used for recording. They are placed around the target robot reaching space in a circle with the test subject's left side having five cameras and the right side having two cameras. This allows for more viewing angles of the test subject's left side, as this is the

side capable of being tested with the prosthesis. The approximate location of the test cameras is in Figure 37 in a top down view. An image of the T160 camera is in Figure 38. For each test, 3D position data of the IR markers along with a time stamp are saved in a .csv file. The three-dimensional position data for each labeled marker are in millimeters as referenced to the camera ground plane, which is set in calibration. The average image error in pixels given the calibration used for the experiments is 0.8 pixels which equates to 0.21mm in camera back plane residual error. To characterize the average error in the x-z plane in the testing volume used for reach tests, the position data from the target markers on the robot and prosthesis were taken and compared to other target markers positions which remained static relative to each other. In this case three trials were used from each of, 2 targets from all 10 test subjects. The markers on the target robot called target upper and target lower were used as well as the end forearm and pointer markers on the prosthesis. These had known distances of 4cm and 37.59cm from each other as measured on each object, respectively. The average resultant variance of the markers was 0.32 mm in the combined x-z plane. This variance was used in later post analysis to help in smoothing the marker positions to real world motion as from captured motion. The marker position data is post processed in MATLAB to obtain the desired quantitative testing metrics, as described in detail in Section 4.3.

### 4.1.2 Test Subject Preparation

Test subject preparation involves instruction as to the tests that are conducted, placement of the IR markers on the natural limb and the prosthetic limb, placement of the EMG electrodes, and initial EMG tuning. The reaching space of each test subject is different and this requires the fitting of their general reaching workspace to the

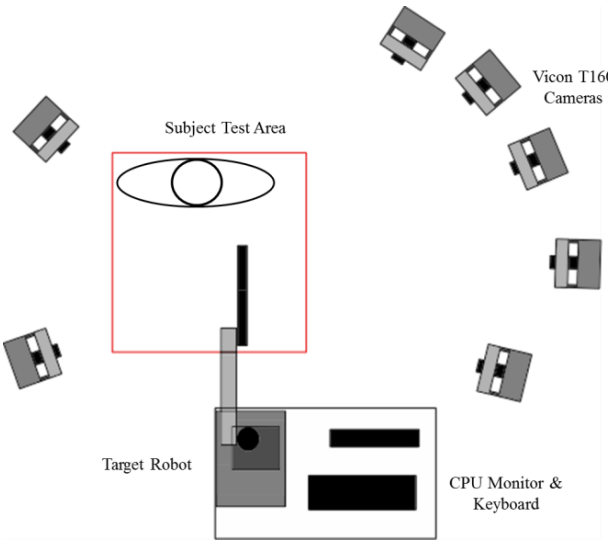


Figure 37: Vicon Camera Setup (Top-Down View)

Figure 38: Vicon T160 Camera

workspace of the target robot such that the robot presents targets that overlap with the test subject's space. There are three humeral flexion angles. These are humerus angles of 0, 45, and 90 degrees. The target points are selected in space such that the test subject will be inclined to have the humerus at these approximate angles when reaching for a target. These locations are calculated using the overlay of the human reaching workspace and the target robot workspace and selecting points along a curve that represents the extents of a test subjects reach, with their humerus set in flexion at one of the discreet angles. A plot of this overlay can be seen in Figure 39. This assumes that the individual is

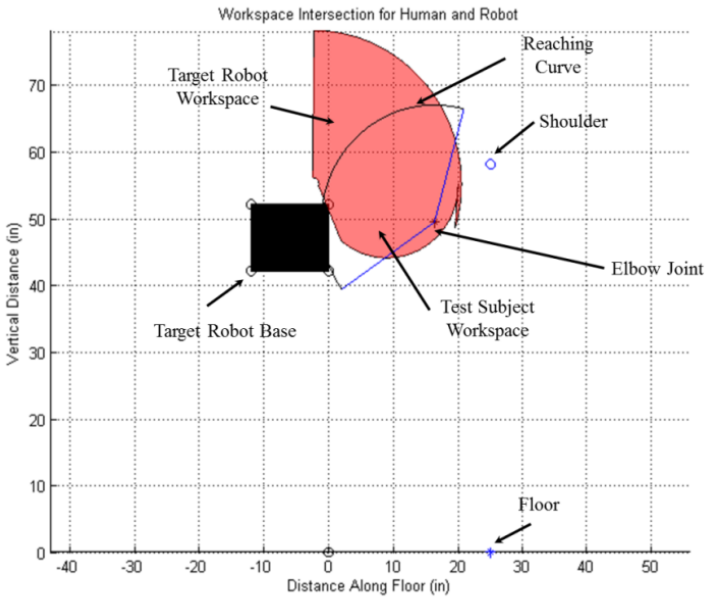


Figure 39: Target Robot and Test Subject Workspace Overlay

standing at a set distance from the robot, which in practice is approximately 25in (635mm) away from the cart for all tests. It also requires the measurement of the test subject's shoulder height, humerus length, and forearm length to the pointer marker. Further details of the relative target locations for a test are covered in Section 4.2. The target locations selected along the reaching curve are entered into the dSpace system for the target robot to reach too.

#### 4.1.2.1 IR Marker Placement

The markers are placed in set configurations both on a natural limb and the prosthesis, depending on which is being tested. The markers are used with the Vicon camera system to record their motion during reaching tasks. The markers might have slight variability in their placement from subject to subject but their pattern and placement, given a test subjects dimensions, are approximately the same. The placement

locations including the labels of each marker as listed in the Nexus software are in Figure 40 for the natural limb and Figure 41 for the prosthesis. The key marker used in the experimental analysis of the reaching tasks is the pointer marker. This is the marker located on the finger of the prosthetic hand in the prosthetic figure, Figure 41, and the metal grip in the natural limb figure, Figure 40. A metal grip was used in the natural limb reaching tasks to reduce the possibility of camera occlusion. If held normally between the fingers, the cameras along the left side could not sufficiently see the pointer marker. To change this, the metal grip is used which is held by the user allowing for better viewing angles from the cameras. The grip was set such that it would be approximately the same length as if the fingers were extended to pinch grasp the marker, thus not affecting the overall distance to the target to a significant degree. The subject was instructed not use their wrist or fingers during reaching, but to keep the marker in-line with their forearm.

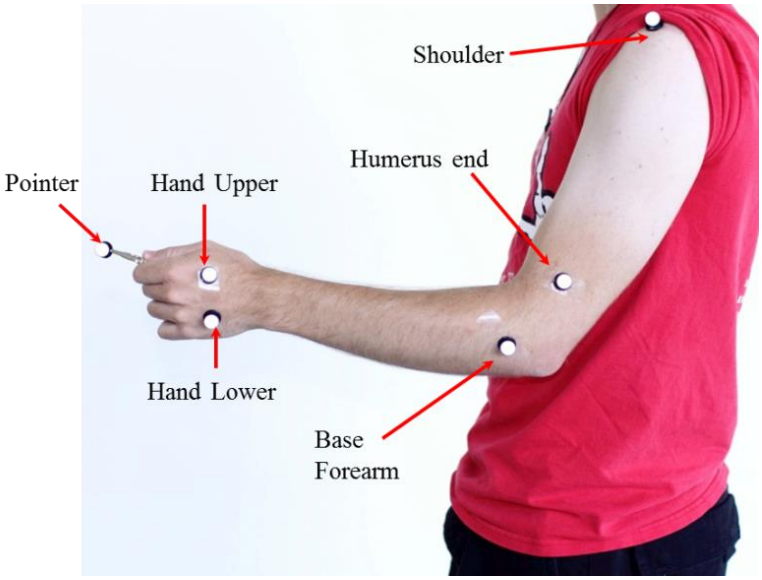


Figure 40: Natural Arm with IR Markers

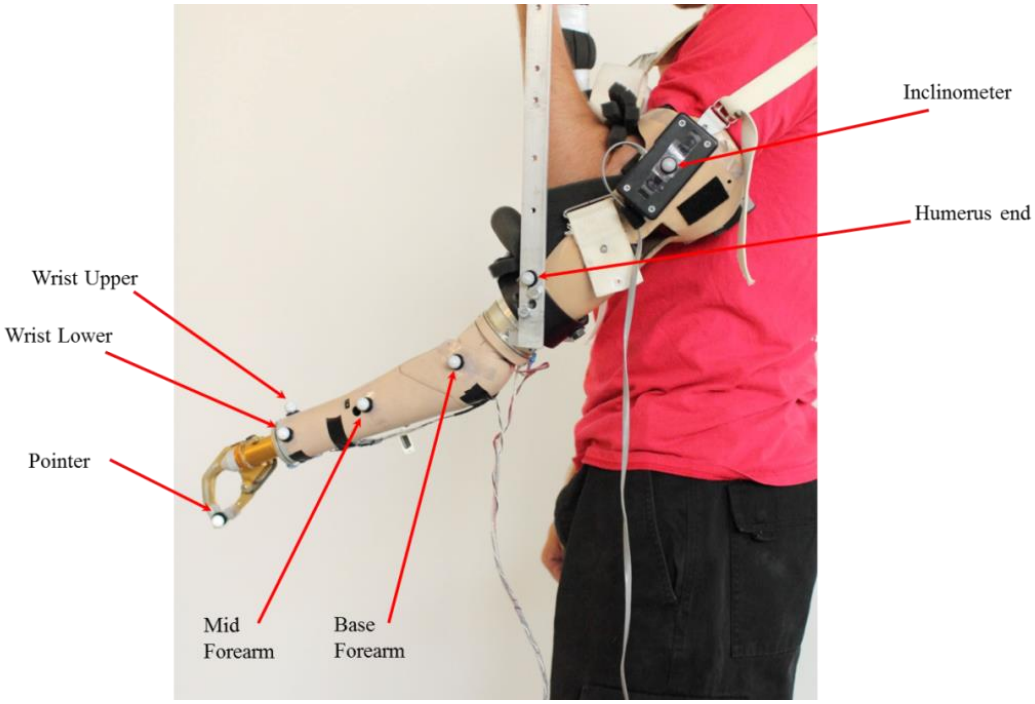


Figure 41: Prosthetic Limb with IR Markers

4.1.2.2 Prosthesis Operation and Bypass Socket

Before amputees are used in testing the controllers, normal human test subjects are used to verify their control validity such that amputee time is spent prudently. Therefore normal human subjects with sound motion in both their right and left arms are the first selected test pool. The use of test subjects with sound upper limb motion requires the use of a bypass socket. The bypass socket is manufactured from a normal socket with the front side wall cut out and a lift support bar attached. The test subject slips their arm through the top of the socket and then through the cut out front side wall of the bypass socket. This places the test subject's elbow in the socket cup at the bottom of the socket. The test subject bends their elbow such that their forearm is in position for their hand to grab onto the lift support bar. Foam is then added to the socket cup between the socket

sidewall and the test subject's humerus so that it is a snug fit. A shoulder harness is also strapped to the test subject such that the load of the full prosthetic test system is supported on the shoulder as well as the lift support bar. The harness is the exact same as an amputee would use with their socket. This is designed to reduce fatigue. Figure 42 shows a test subject with the bypass socket and shoulder harness being worn in the proper configuration.

There was only a left sided bypass socket available, so only the left side of a test subject could be evaluated in these tests. It is not thought to impact the controllers in reaching as each controller is tested on the left side to show only a relative comparative change.

EMG signals for prosthesis operation are captured by a Myolab II EMG signal capture unit (Motion Control, SLC Utah). This system takes in the muscle contraction signals as captured by two preamp electrodes. It then rectifies and low-pass filters ($t_c$ = 150ms) the signal such that the EMG signal output is smooth. The filtered EMG signals are fed into the ADC of the dSpace controller as listed in Chapter 2. The Myolab II picture is in Figure 43.

In the initial test setup it was found that the bicep and triceps of the test subjects had difficulty in producing a desired EMG signal to activate the arm with the bypass socket present. They were not capable of contracting their muscles to produce a sufficient signal because the muscles were used to hold the weight of the prosthesis. This would not be an issue with an amputee. For this reason the EMG sites for control of the elbow joint are repositioned to the forearm of the right side. The EMG signals are pulled from the wrist flexor muscles.

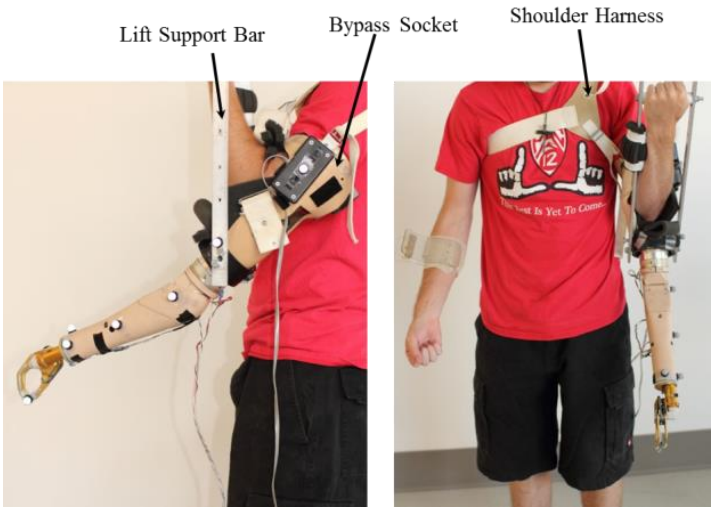


Figure 42: Bypass Socket and Harness

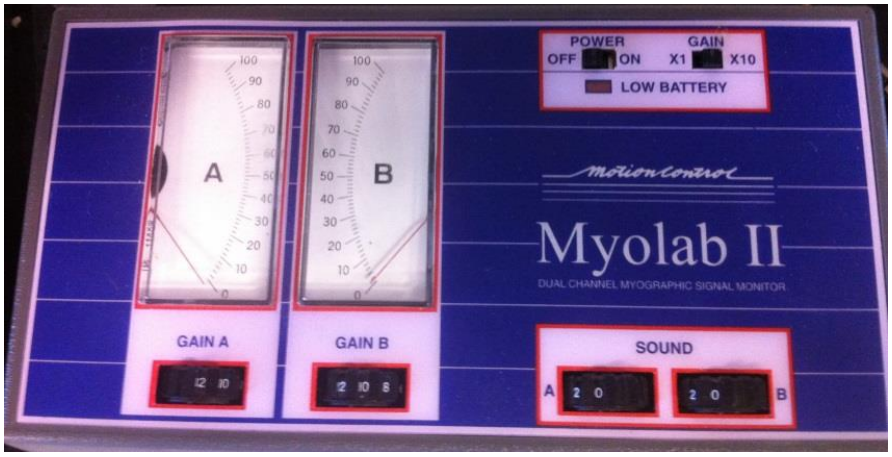


Figure 43: Myolab II EMG Signal Capture System

The EMG electrode to lift the prosthetic forearm up is placed on the upper side of the test subject's right forearm. The EMG preamp electrode to move the prosthetic forearm down is placed on the lower side of the right forearm. The electrode placement can be seen in Figure 44. The electrodes are kept in place with medical wrap and a plastic clip, such that they do not slide. There is no skin preparation in this test to place the electrodes. This is the same as the amputee electrode setup where no skin preparation is needed.

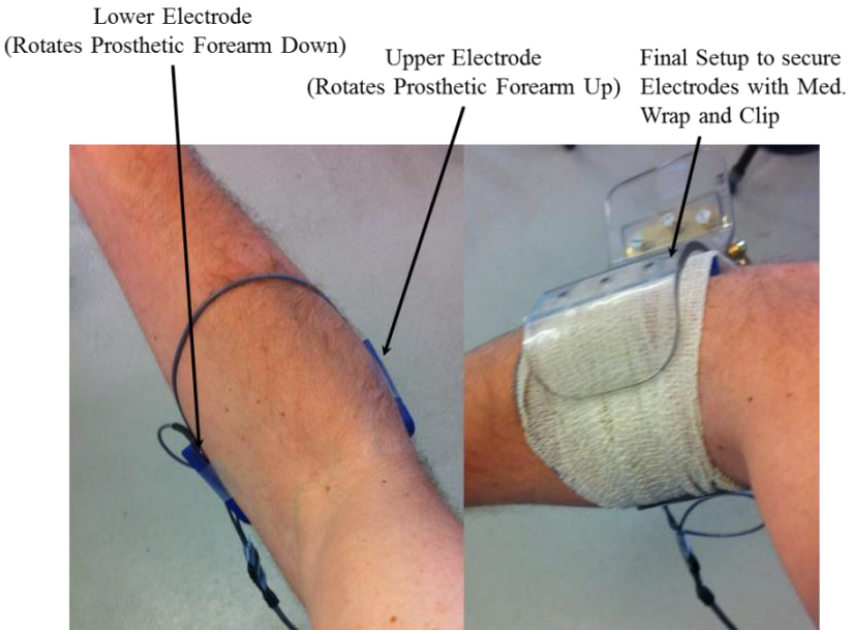


Figure 44: EMG Electrode Setup

## 4.2 Experimental Method

The experimental method includes the reaching test procedures necessary to conduct a full series of subject reaching tests. Each test subject is tested with their own set of targets that are predetermined before the testing sequences begin. This requires that the subject's natural arm dimensions are known. This also requires that the test subject be of able body and capable of lifting the prosthesis. All of the tests were conducted in accordance with IRB approval and test subject consent as set in IRB Approval #: 66441. A copy of the consent form is in Appendix C.

### 4.2.1 Reaching Test

In the case of this thesis, though the mechanics for shoulder abduction are known, targets are only presented in a location where shoulder flexion and elbow flexion are necessary. This simplifies the test results to better understand how the newly developed

controls work firstly in plane. Future tests will expand to out of flexion plane motion. The reaching tests are set such that the targets presented are at distances that would be present in a user's daily workspace, such as a cup in a cabinet or a button on an elevator. The tests are not designed to be object specific, in the sense that a button or a cup is actually in use, but that the distance to such objects is presented in a similar analog. The reaching targets are repeatable in space and are not subject to direct human placement error as each target is presented to the test subject by the target robot arm. The target itself is the end effector of the robotic arm which moves in the test subject's flexion plane as covered in the previous sections. There are six targets presented to the test subject as calculated through the robot and human workspace overlay as seen in Figure 39. The six targets are presented at similar locations between test subjects, based on the humerus angle. Though each test subject is different, the range of each test subject's motion, to reach similarly spaced targets considering arm length dimensions, is the same. For this reason, the targets are categorized into regions based on the humerus flexion angle. Two targets at each humerus angle are presented where the humerus is close to $0^o$, $45^o$, and $90^o$ in flexion. One target is presented where the elbow is set more in flexion and the other where the elbow is set more in extension, along the reaching curve. This allows the test subject to attempt reaching targets across the range of motion of the elbow at that humerus angle. These site locations are displayed in Figure 45, low targets, Figure 46, mid targets, and Figure 47, for high targets. These targets are labeled 1 to 6, in the respective order, going from lowest point to highest. Each one of these targets is reached to three different times, by each test subject, each with one of the three controllers or the natural limb.

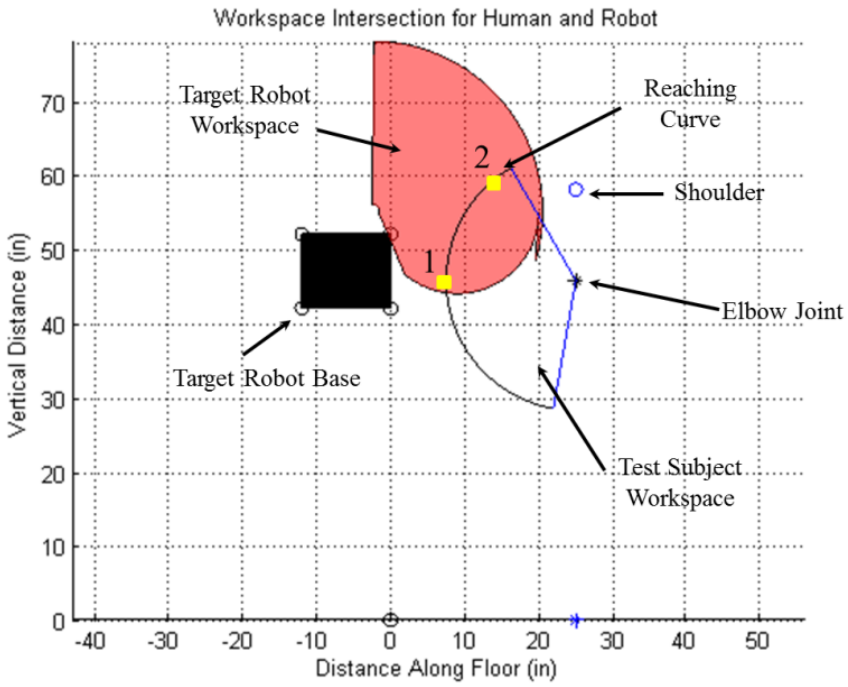


Figure 45: Target Locations for Lower Targets (Humerus = 0$^{o}$) in Workspace Overlay

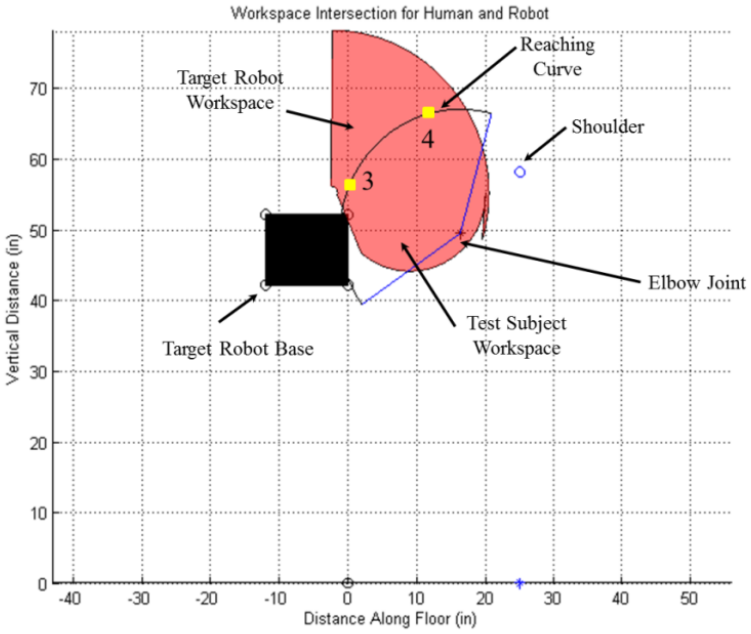


Figure 46: Target Locations for Mid Targets (Humerus = 45$^{o}$) in Workspace Overlay

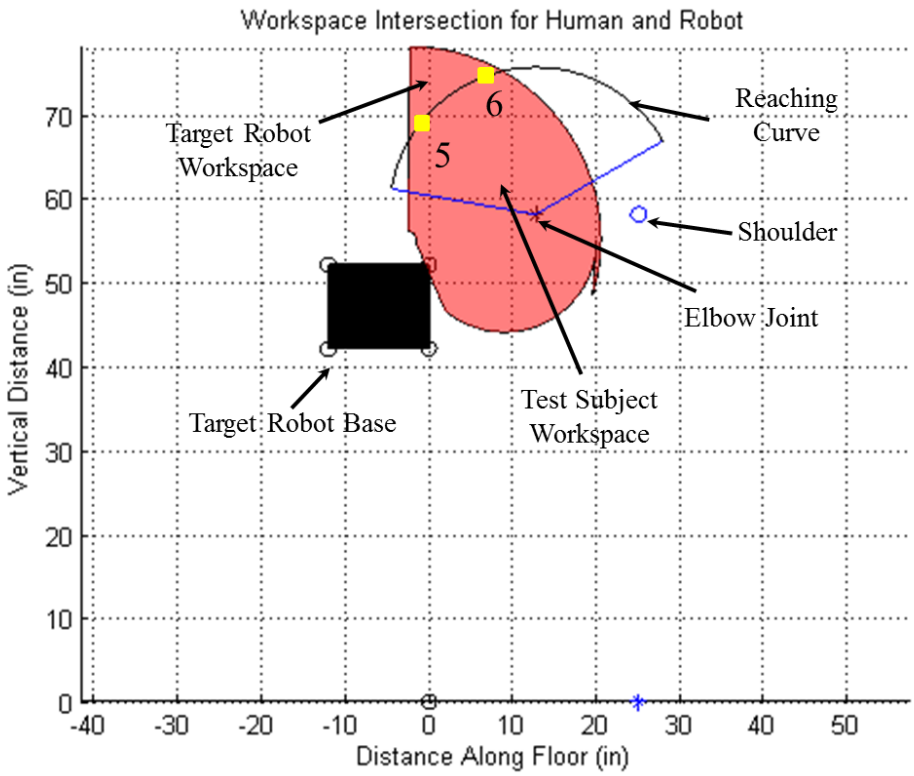


Figure 47: Target Locations for High Targets (Humerus = 90$^{o}$) in Workspace Overlay

At six targets with three reaches each at four different reach types the number of reaches is 72 if completed without fault in a test. This combination was chosen as a result of both preliminary reaching data and user reported fatigue. In preliminary tests 10 data points were tested at 5 times each. The data proved to be too tedious and there were areas of repeated coverage. In addition, the number of test points caused a large amount of test subject fatigue which started to cause data degradation as they no longer were capable of lifting the whole arm assembly in an unstressed manner toward the end of the test. Thus it was decided to divide the testing into regions across the range of motion capable of the prosthesis. The number of trials at each point was then reduced to three reaches to reduce fatigue effects.

#### 4.2.1.1 Reaching Test Sequence

There are two sets of tests to be run for each test subject: one set of tests with the natural arm and the other with the prosthesis. Each test reaches to the same targets and follows a similar sequence. The test is run such that the natural limb is tested first, which is then followed by the prosthetic limb. The testing sequence starts with the robot arm presenting a target location to the test subject. The test subject starts at rest with the limb or prosthesis at their side. The test subject is positioned relative to the robot such that they are approximately 25 inches (635 mm) away from the robot base. This location is marked on the floor by tape such that it is a repeatable point of reference should the test subject move between tests. The test proctor then selects record on the Vicon camera computer. He then indicates verbally to the test subject that they can now go and reach for the target at a self-selected comfortable pace. They then reach forward, toward the robot end effector (target), and hold the end effector at the target for approximately three seconds before returning to rest. A target is considered engaged or "reached" when the test subject places the limb end effector at the end of the robot effector, or the end effector reaches a point where the test subject can go no further and is at a steady state.

The figures of what an engaged state looks like are in Figure 48, for the natural limb, and Figure 49, for the prosthetic limb. In the three-second time frame from initial contact with the target the test subject does their best to stay in engaged with the target, holding the limb end effector steady. After the three seconds, which is counted by the test proctor, the test subject returns to rest and the recording of the motion is stopped. At this point the next controller out of the three is loaded. The test subject is given time to try the control type and is told it is the next controller to be tested for this target location.

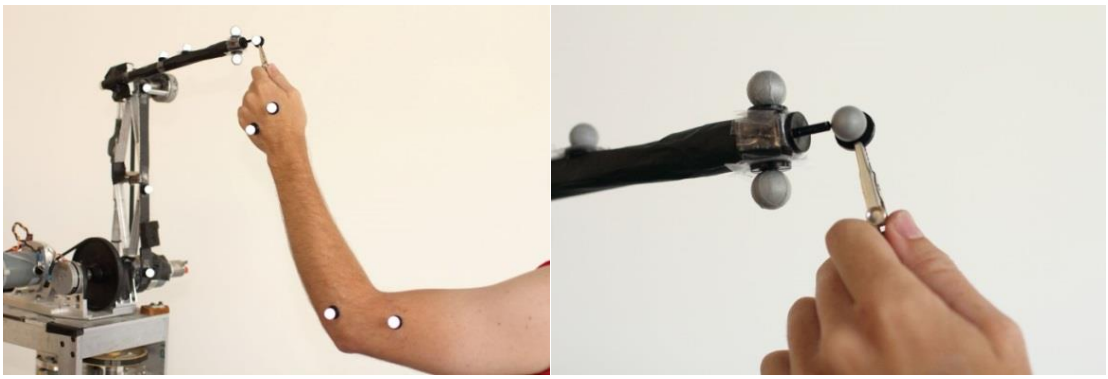

Figure 48: Natural Arm Engaging Target

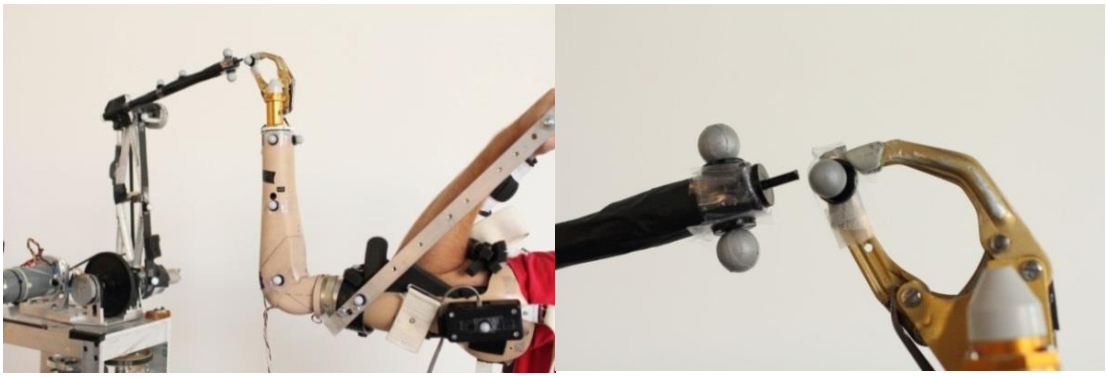

Figure 49: Prosthetic Arm Engaging Target

Once all three controllers have been tested at a single target the test subject is asked to rate the controller on its “controllability” or how mentally straining it was to perform the reaching task for each controller. The controllers are not rated vs. each other but rather vs. the natural limb motion where 10 is the best case, i.e., natural limb and0 is the worst case or uncontrollable. This is covered in more detail in Section 4.3.

The testing sequence follows Table 6 in sequence to test all of the target locations with all of the controllers three different times. In the cells, S is the standard controller, GCF is the gravity compensated controller without free-swing active, and GC is the gravity compensated controller with free-swing,

Table 6: Prosthesis Controller Test Sequences

| **Controllers and Trials** | | | | |
|---|---|---|---|---|
| **Targets** | | **Trials** | | |
| **Angle Series** | **Target Number** | **1** | **2** | **3** |
| 0,low | 1 | S,GCF,GC | GC,GCF,S | GCF,S,GC |
| 45,high | 4 | S,GC,GCF | GC,S,GCF | GCF,GC,S |
| 90,low | 5 | S,GC,GCF | GC,GCF,S | S,GC,GCF |
| 0,high | 2 | S,GCF,GC | S,GCF,GC | GCF,S,GC |
| 90,high | 6 | GC,S,GCF | S,GCF,GC | GC,GCF,S |
| 45,low | 3 | GCF,S,GC | S,GCF,GC | GC,S,GCF |

these controllers are discussed in detail in Chapter 3. The test starts with Target number 1 on trial 1. The three controllers in the listed sequence of S, GCF, and GC are tested by the test subject. The test subject then rates the controllers on the controllability scale. The next target is then set by the target robot, target 4, and the listed controllers in trial 1 for target 4 are tested. This sequence repeats until all of the targets are tested under the trial 1 column. The trial is then switched to trial 2 and the targets are retested with the listed sequence of controllers. This sequence of tests is run completely in this pattern with the last test being target 3 on trial 3, with the controllers GC, S, GCF. This is the same sequence used for all test subjects. This completes the testing sequence for the prosthesis. The process of this testing sequence can be seen in Figure 50. If the natural limb is being tested the test subject after reaching to the first target location will go back to rest and then repeat the reach to each target location the remaining two times. The target robot arm is then moved to the next target in the sequence and the test subject reaches to the next target three times. This process is continued for all targets, three separate times. The process is in Figure 51.

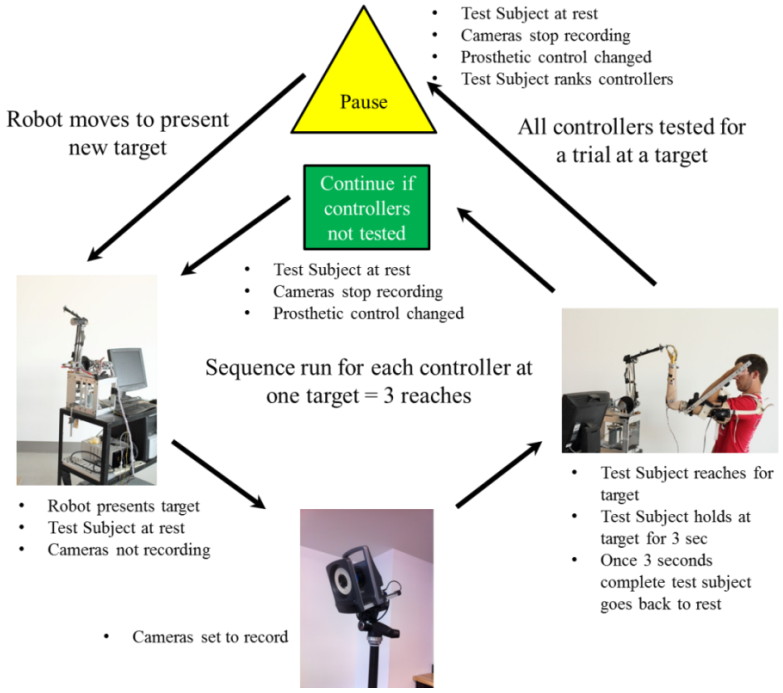


Figure 50: Reaching Test Sequence for Prosthesis

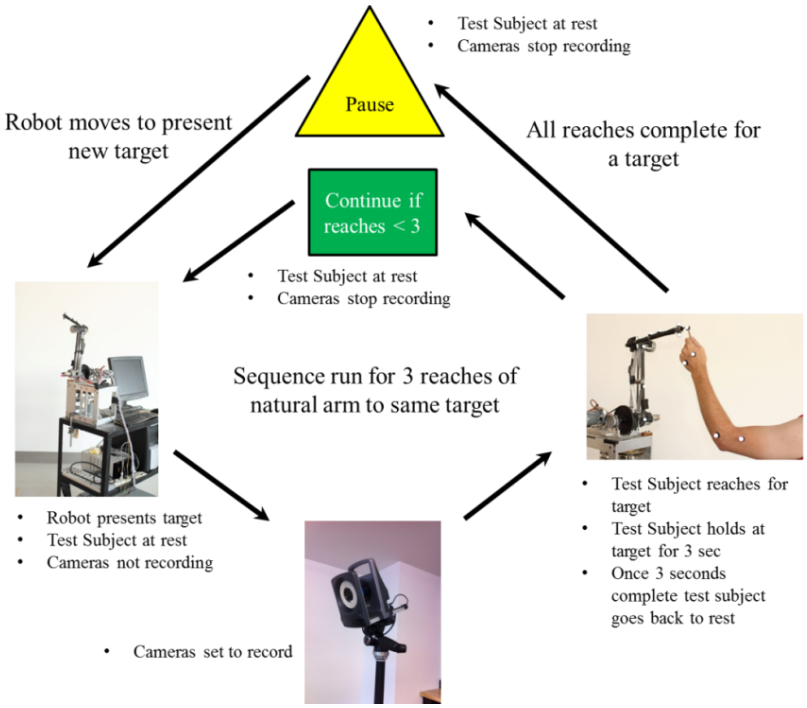


Figure 51: Reaching Test Sequence for Natural Arm

## 4.3 Control Improvement Testing Metrics

There are five metrics that are captured during the reaching tests that provide measurements to determine controller performance, one qualitative and four quantitative. Quantitative data are pulled from the motion capture recordings concerning the three-dimensional position and time stamp of each of the IR markers recorded over a reaching time period. These data are reduced to quantitative metrics that describe the control performance of the prosthesis in reaching to and holding at a target. These are time to target, trajectory smoothness, steady state error at the target, and variance of the pointer marker held at the target. The qualitative data are a measurement given by each test subject on a scale which ranks how "controllable" or how much effort it takes to move the arm as desired. These measurements are covered in the subsequent sections.

### 4.3.1 Quantitative Data

The quantitative data are a measure of the physical performance of the prosthetic controllers during a reaching task. These metrics are measurements that are linked to the mechanics of a reach and describe how physically a reach was performed. A reaching motion can be split into roughly two stages as concerned in this research, the approach and the hold. The approach is the measurement of the performance of the limb moving from rest to the target. To characterize this region, similar metrics are used as in previous research as mentioned in Chapter 1. The main concern in this region is how long it takes the pointer marker to move from rest, to a target and how smoothly that motion is performed. The developed metrics are the time to the target and the trajectory smoothness which is the time normalized sum of the jerk, which is defined similarly to work done by Hogan et al. [13] in human reaching tasks. Once at the target the second part of a reach

that characterizes its performance is taken as the ability to hold or stay at a target within a particular range. The hold, in this research, is defined as the measurement of performance of the limb holding the pointer marker on target in a steady fashion. The metrics that define this area are similar to the measurements used in robotic manipulators in analyzing control performance, which is the ability of the mutlilink system to hold the end effector at a desired point in space. The metrics are the average steady state error and the variance of the pointer marker relative to the desired target, over a period of time. These metrics are thought to best characterize the reaching task and can be used to evaluate how the controllers perform relative to each other. The subsequent sections describe each metric.

#### 4.3.1.1 Time to Target

The time to target is the time it takes to move the pointer marker (prosthesis or natural) from rest, the arm by the test subject's side, to the presented target at the self-selected comfortable pace.

#### 4.3.1.2 Trajectory Smoothness (Jerk)

The trajectory smoothness is how smoothly the arm moves from rest, by the test subject's side, to the target. This measurement is originally taken from work by Neville Hogan on human reaching motions [13]. It is used to better understand the ability to move in a fluid motion from one point to another without any hard accelerations or direction changes that would indicate a difficulty in control. This is important in reaching tasks as it is desired to move from one point to a desired target without wild or jerky motion. This value is a measure of how steady the controller performance is over a range

of approach motion.

#### 4.3.1.3 Steady State Error

The steady state error is taken as the average distance, in the flexion plane, of the pointer marker to the target over the attempted holding period. This period begins after the prosthesis end effector or natural limb has come to the closest point of rest at the target and then attempts to hold at the target for a period of three seconds. This distance is measured in mm from the target. This value is a measure of how accurately the controller can be piloted to reach and hold at a target.

#### 4.3.1.4 Variance

The variance or average standard deviation is the measurement of how steady the holding period around the target is. It is a measurement of average shakiness around the target. It is measured over the time period after target engagement, in reference to the steady state error. This value is in mm and measures how well the test subject is capable of controlling the prosthesis to remain steady at a target.

### 4.3.2 Qualitative Data

The qualitative measurements are based on a test subject's opinion of each controller. The controllers by actual name are not known by the test subject but are just known by designated letter A, B, or C which is changed between targets to which controller they represent. By this means, the test subject is ranking the controller on a blind "feel" and performance basis relative to the natural limb without bias. This makes a single blind test. The test subject gives each controller tested a number based on a scale relative to the

natural arm. The ranking is given on a 0 (worst) to 10 (best) scale, where 10 is the natural arm effort and0 is uncontrollable. The data on a per-subject level are compared between all test subjects to best understand the control preferences. This analysis is covered in Chapter 5.

## 4.4 Chapter Summary

This chapter covered the experimental setup and test methods for the prosthetic limb controllers. The experimental setup is comprised of two different independent systems. The Target Robot System presents reaching targets. The Motion Capture System records the reaching motion of a test subject over time to a presented target. Reaching tasks are chosen as this is the best motion to capture controller performance about the elbow. Only reaching in the humerus and elbow flexion plane are initially considered to understand controller performance. There are six reaching targets presented to a test subject which are coordinated to be at set humerus locations corresponding to their reaching workspace at shoulder flexion zones where the humerus is at $0^o$, $45^o$, and$90^o$ from the torso. These six targets are reached to three different times to capture an average of reaching performance while accounting for test subject fatigue. Two test sequences are run, one testing the natural limb and the other testing the three prosthetic controllers. The natural limb reaching is performed such that each target is reached to three times before switching to the next target. In the prosthetic controller tests, each target is reached to with each controller for three different trials in an order unknown to the test subject. At the end of a reaching set to a target with the three controllers the test subject rates the controllers on a scale from 0 (worst) to 10 (best) in comparison to their natural arm controllability effort. Once the test subject is done reaching to all of the targets, both with

their natural limb and the prosthesis, the full test sequence is completed. The quantitative data recorded by the cameras and the qualitative data obtained by the test subject controllability survey are analyzed to best understand control improvement and performance. Chapter 5 continues with data analysis of the reaching test data to deduce the impacts of the new controllers and the control improvements from their implementation.

# CHAPTER 5

# RESULTS AND DISCUSSION

This chapter presents the collected results of the reaching tests for each tested controller and the natural arm. Ten test subjects were tested for a full set of reaching tests with the natural limb and all three control types as presented in Chapter 4. The test data were recorded by the Vicon camera system and stored in a .csv file which contains the IR marker's three-dimensional position and a time stamp. These data were analyzed using MATLAB 2011a and the Statistical Analysis toolbox to find statistical significance in the quantitative measurements and qualitative ratings to determine control improvement. These methods are described in the following section which lists both the methods and the results obtained in testing.

## 5.1 Data and Statistical Analysis Techniques

For all test subjects, the primary data that were used to analyze the controllers was the distance between the target and the pointer marker. This distance was plotted over time in the flexion plane designated as the x-z plane using the target robot zero plane coordinate system convention presented in Chapter 4, in Figure 35. The distance was taken using the linear distance formula. The distance to the target is taken as the distance to the actual tip of the target post. The target can be seen in Chapter 4. The target post location was

calculated by computing the distance from the two target markers on the end of the target robot, assuming a triangle configuration. As each reaching test to the target was started at a different time and the dSpace and Vicon testing systems were not synchronized, the obtained data had to be individually plotted and inspected per reaching test to determine when the reaching motion began, when the target was initially engaged, and when the reaching test ended, as viewed in the x-z plane over time. These points were used to compute the quantitative metrics. In certain scenarios short gaps in data were found over a period of a few hundredths to tenths of a second for the marker coordinate data for the target robot IR markers. As the target robot was static the data points, beyond slight amounts of sensor noise from the cameras, were considered to be in the same location and the last data point was copied over the few missing spots. The location of the target robot markers are averaged over the entire recording time period and the resultant point was taken as the location the target robot was located for the test. In other sections the actual marker for the pointer on the prosthesis would be missing and there would be gaps. In these situations, if the gaps were on the approach the recorded file could be reprocessed to fill in the gaps using the Vicon subject model algorithms. Where this did not work, the data were summed over the gaps as best as possible. This only affected the trajectory smoothness parameter and only occurred on approximately 6 recordings out of the 10 test subjects. If the gaps were on the holding portion, the Vicon software would again reprocess the trajectories to fill in the gaps using the subject tracking algorithms. If this did not work the data were summed as best as possible. This only affected approximately 5 recordings out of the 10 test subjects and the gaps were minimal. The methods used to compute the quantitative data and the statistical methods used to analyze the data are in the following sections.

5.1.1 Quantitative Metrics

The quantitative data were obtained from the x-z plane plot of the pointer marker approaching the target marker over time. The Vicon camera system tracks the center point of the markers as they move through space. However, in the physical world the marker has a significant radius which was taken as approximately 7.8mm given measurements of the IR markers being used for the reaching tests. This required that a window of an acceptable range of what an "engaged" state of the pointer marker resting at the target post meant. This bound is the radius of the marker or the $\pm$ 7.8mm radius distance around the target post. If the pointer marker is recorded in this region, the distance to the target is considered to be zero. In some cases this state was never quite reached. The pointer marker on the prosthesis never quite breaks the 7.8mm boundary but is always a few mm short. In these cases the points were taken where the x-z plane plot has reached its closest resting point. In Figure 52, the reaching task to target number 4 is displayed for the natural arm (1) and the three controllers, which are the Standard prosthetic controller (2), the Gravity Compensated with torque servo (GC) (3) and the Gravity Compensation without torque servo (GCF) (4). The horizontal lines toward the bottom of each plot are the $\pm$ 7.8mm target boundaries where the distance to the target is considered to be zero. The three points marked in each plot are the points used to obtain the four quantitative metrics and delineate the boundaries between the approach stage and the hold stage. The approach to the target is between the first and second points and the hold stage is between the second and third point. As previously mentioned, as each test subject and reach is different, each point on the plots has to be manually picked for all test subjects and all tests. This can introduce human error in selection, as each point needs to be selected through manual inspection.

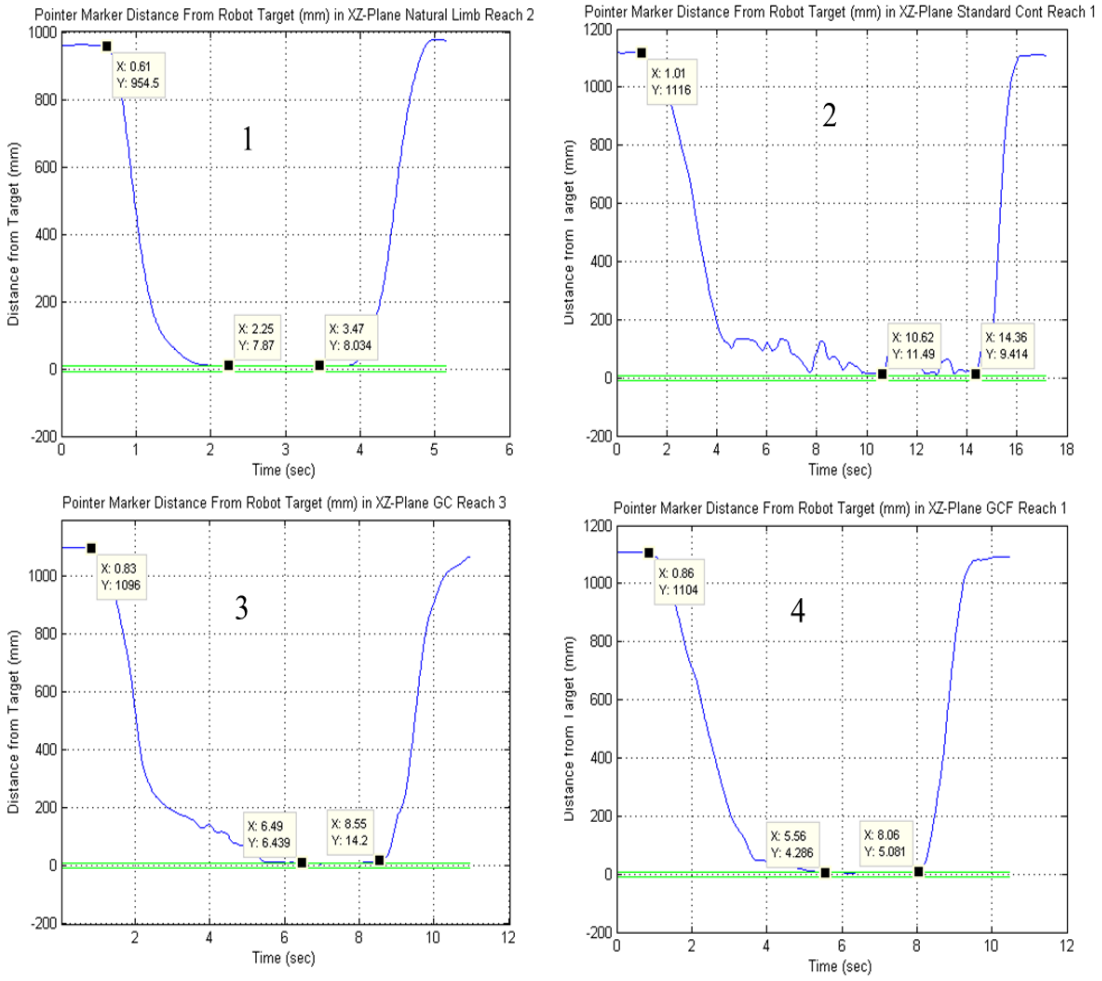


Figure 52: Plot of the Pointer Marker Distance from Target in the Flexion Plane over Time for all Reach Types (Note the differences in the time scale)

In practice, if data points needed to be reset they would only vary by a slight amount as the points to select on the plots are defined well. This might cause a slight variance in the quantitative metrics over a few hundredths of seconds or millimeters, which is not thought to impact data trends over the ranges captured to a significant degree as the actual data is on a magnitude of seconds and millimeters. With these points selected the data as stored in an indexed array in MATLAB are used to calculate the desired metrics over these ranges. These calculations are covered in the next section.

5.1.1.1 Approach Metric Calculations

The approach metrics as listed in Chapter 4 in Section 4.3 are the time to target and the trajectory smoothness. These are calculated by analyzing the data array of distance and time between the start of the reach, which is set as point one, and finally reaching the target, which is point 2 on Figure 52.

- Time to Target: This metric is calculated by taking the beginning time of the reach and the time at the second point and subtracting the two. This yields the time it took from the start of the reaching motion to engage the target with a specific controller or the natural arm.
- Trajectory Smoothness: This is a measure of how smooth the reach is from the start of the reach to the point where the target is engaged. The jerk is the third derivative of the position data, in this case the pointer marker as it moves toward the target. However, taking the third derivative of the raw position data resulted in nosy jerk information which, as a result, does not have high fidelity. This was fixed by using a spline estimation curve of the position data which ultimately smoothes the raw position data to fit within a tolerance of acceptable error. This is a method that is well documented as seen in [39] and [40]. To actual compute the spline curve the MATLAB function spaps(time,data,tol) was used. This function works by taking in the time and position data (data) and minimizing the following set of equations such that it returns the smoothest function f that lies within the given tolerance (tol) of the data points [41]; default is to fit a cubic spline. In Equation (11), E(f) is the sum of the distance from the raw data to the spline prediction at the first data point location, where in this case the weight w is set to 1, which assumes there

is only one data point per time division. The predicted f function that produced the distances E(j) has the second derivative taken and summed across min and max of the data sets at the current time in Equation (12) which is the smoothing parameter. These values are then taken and the additive function of Equation (11) and Equation (12) is then set to minimize Equation (13). This process then repeats until Equation (13) is minimized.

$$E(f) = \sum_{j=1}^{n} w(j)|y(:,j) - f(x(j))|^2 \quad (11)$$

$$F(D^m f) = \int_{\min(x)}^{\max(x)} \lambda(t)|D^m f(t)|^2 dt \quad (12)$$

$$Minmize: pE(f) + F(D^m f) \ \ where\ p\ i\ such\ that\ pE(f) = tol \quad (13)$$

Once the position spline is computed the spline derivative is taken using the MATLAB function fntlr(spline,derivative_level,time). The jerk is calculated by taking the 3rd derivative of the spline curve which is then considered absent of the nosy or extreme changes in position over the time frame taken. In this case the tolerance was set to 0.32mm which is the found error of the Vicon camera system and the possible variance on the position data as seen in Chapter 4. Figure 53 shows the resultant spline fit curve over the experimental curve, which practically are on top of each other. Figure 54 shows the resultant jerk calculation from the smoothed spline data vs. the raw experimental data.

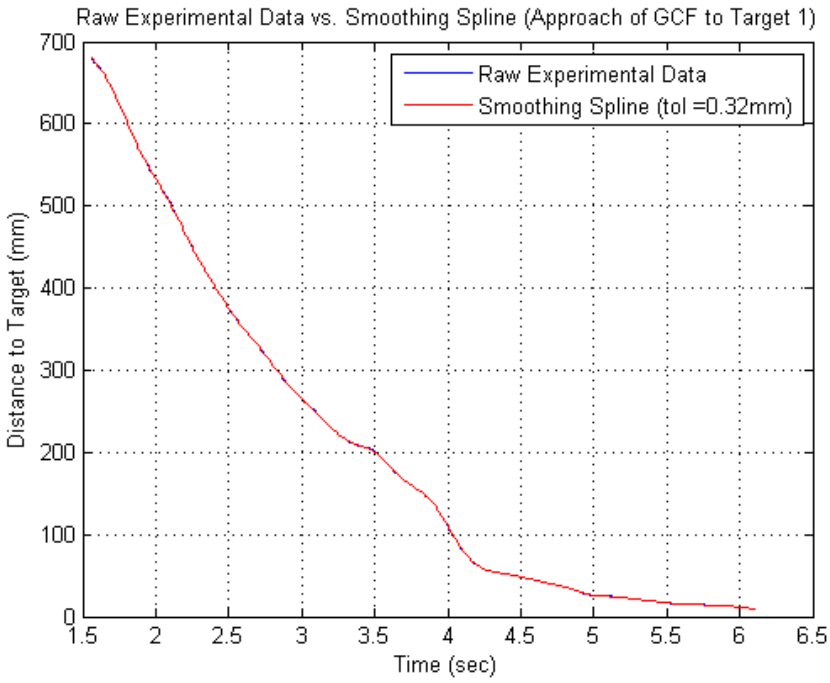


Figure 53: Raw Experimental Position vs. Smoothing Curve

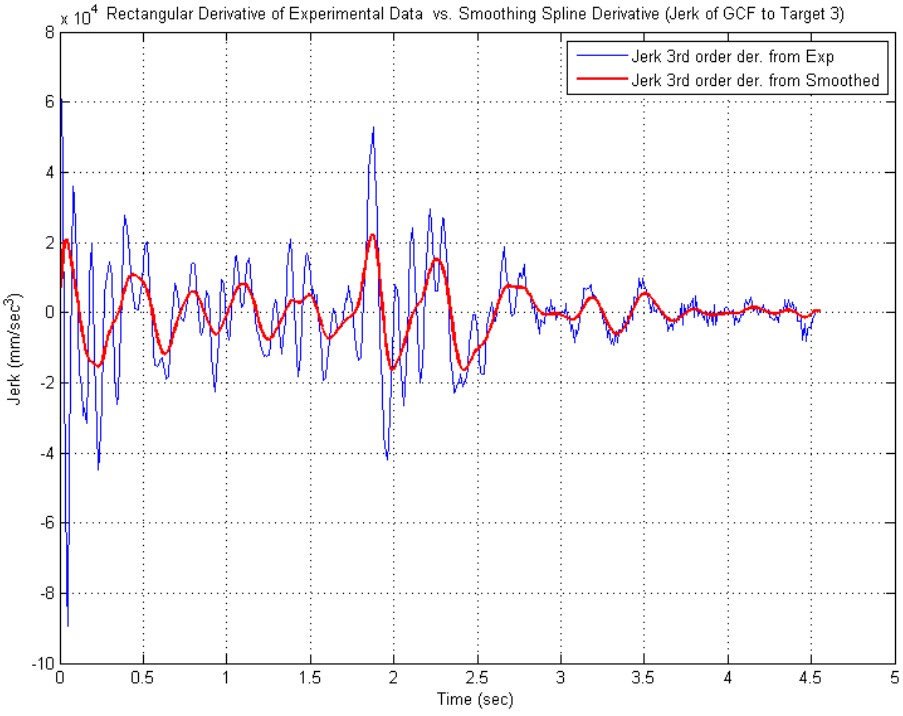


Figure 54: 3rd Order Derivative Using Rectangle Method on Raw Experimental vs. Derivative from the Spline

As can be seen even though the spline position curve follows the experimental data tightly the resultant jerks are different as any noisy artifacts are removed from the smoothing. In order to obtain a nonsigned metric these results were squared and then summed over the whole time to target range. This value was then normalized to the time to target value computed. The resultant units are $m^2/sec^{10}$ which are the readings used for the sum of the jerk squared divided by time to target. The equation used is below in Equation (14).

$$Trajectory\ Smoothness\ Metric = \frac{\sum Jerk^2}{Time\ to\ Target} \quad (14)$$

5.1.1.2 Holding Metric Calculations

The holding metrics as listed in Chapter 4 in Section 4.3 are the steady state error and the variance around the target when attempting to hold in place. These are calculated by analyzing the data array for the average distance from the target and the average standard deviation around the target between the second and third points as marked in Figure 52.

- Steady State Error (SSE): The SSE is measured at the start of target engagement or where the prosthesis is closest in their reach at a steady point in attempting to reach the target. It is then measured until after the period of hold where the prosthesis or natural arm depart from the target to return to rest. Over this hold range the distance to the target is taken as the pointer marker's location minus the 7.8mm boundary range. If the pointer marker is below the 7.5 mm range the error is taken as zero. These values are then averaged over this range to obtain the average error over the holding stage

which is this metric's value.

- Variance: The variance is taken as a measure of the "stability" of the end effector at the holding stage. It is the average standard deviation over the holding range. This helps indicate how "stable" the test subject and thus controller is at holding the prosthesis on target. As with the SSE, if the pointer marker of the prosthesis or natural arm were in the 7.8mm boundary the value error was taken as zero such that the standard deviation in this area is counted only outside of the boundary.

### 5.1.2 Statistical Methods

The statistical methods used in this thesis are implemented to determine if there is any statistical significance between the standard controller and the newly developed controller. These methods are based on an analysis of variance and median comparison between data sets. There is an initial data reduction before performing the statistical analysis. The three reaching trials of each controller at each position are averaged. This reduces the data from counting all of the prosthetic reaches and natural reaches with four metrics each for all three trials, to a set of averaged reaches over the trials with the same four metrics. This gives a set of data for each of the six targets and the four quantitative metrics that describes a controller's ability to reach the targets.

The first statistical tests run are to test if the controller data sets are normally distributed on a per metric basis. The normality condition is necessary to use the ANOVA methods of statistical analysis and the mean comparison Tukey tests. The combined test subject data for each metric are organized into columns of control type. There are four 60 x 3 matrices formed where the rows are the targets and the columns are

the controllers, one matrix set for each metric. There are 10 test subjects which are block sets that are organized in the matrix. The first six rows are test subject 1's, the next six are test subject 2's , etc. The normality tests look for the condition that the data set meets a normal distribution to 5%, within one standard deviation of the mean. The test used was the Jarque-Bera test which looks for this condition [42]. In MATLAB this is called with the jbtest function which returns a h = 0 which states the condition is met and a h = 1 if it is not met. For all the controllers and all of the metrics except for the time to target metric, the data were found to not be normal. As the metric data are a collection of data that describe a reach, the data that cause the trajectory smoothness, SSE, and variance to not be normal could not be removed to normalize the sets of data without affecting the time to target metric. These terms were found to be nonnormal as there were large enough outliers that influenced the data sets to be considered nonnormal. Nonparametric analysis of variance is used for these reasons to determine statistical significance between controllers for the quantitative data. The qualitative data, as they are based on rankings of preference given by test subjects, are considered to be nonparametric. The qualitative data are analyzed with the same nonparametric analysis methods used for the quantitative metrics.

#### 5.1.2.1 Friedman Test

The Friedman test is the nonparametric version of the ANOVA test but does not assume that the data are normally distributed [43]. In the case of MATLAB the Friedman test compares the variance between the columns of data and does not consider the rows and the interaction effects. There are only two conditions that are needed for the Friedman test to be used.

- The data come from continuous distribution sets
- The observations are mutually independent

Both of these conditions are met given the data collection methods and the data being compared. The Friedman methods test for the null hypothesis that the columns of data being compared are significantly different based on the column medians. It returns a p value indicating the significance between the columns. In the case of this test a p value less than 0.05 (5%) indicates there is significance difference between the compared data sets in the columns. The Friedman test tests multiple columns for significance difference, based on median values. It does not indicate where the significance between the data sets is from. For this, another test is needed which explicitly tests the significance between two data sets. This is covered in the next section.

#### 5.1.2.2 Sign Test

The sign test is a nonparametric test which can be used to compare two sets of data for significant difference, by analyzing the array computed from the subtraction of the two data sets for a zero median [44]. For example, given data set x and y, the sign test method looks at the array of x minus y to determine if it has a zero median. It returns a statistical significance value (p) rating the x minus y array on this condition. A p value less than 0.05 (5%) indicates that the data sets do not have a zero median, when they are subtracted from each other, and thus it can be concluded that the difference between the data sets is significant. In the case of this thesis when comparing controllers, if $p < 0.05$, a true difference between the controllers for a particular metric exists, indicating control improvements.

## 5.2 Results and Discussion

This section presents the results and discussion of the analyzed data from both the quantitative and qualitative metrics. The results are displayed to show the medians of the values to be consistent with the statistical methods which use the median as the measure to determine the variance between data sets. The data are split into the sections for quantitative and qualitative results. In each section the results are divided into the comparison of the full data set which is the analysis of the results across all of the test subjects at all of the targets to capture the global trends in the data. The results are also sectioned into target locations which consider the results of reaching tests for all test subjects but at specific target ranges where the humerus is at $0^o$, $45^o$, and $90^o$.

### 5.2.1 Quantitative Results

The quantitative results are first analyzed to determine the difference between the controllers across the whole target range for all of the test subjects. These data consider all four metrics of controller performance and compare them vs. the standard controller. Initial comparisons based on inspection show a drastic difference between the natural arm and any of the controllers. For this reason the statistical methods were not run between the natural arm and the prosthetic control modes as the data would always show that the natural arm across all test subjects was better performing. The median results for the combined 10 test subjects are in Table 7 for the full data set results displayed on a per target basis, Figure 55 for the time to target, Figure 56 for the trajectory smoothness, Figure 57 for the steady state error around the target, and Figure 58 for the variance around the target.

Table 7: Median Results for Ten Test Subjects Across the Six Reaching Targets

| Median Results for Ten Test Subjects | | | | |
|---|---|---|---|---|
| **Humerus 0 deg (Target 1)** | | | | |
| **Parameter** | **Nat Arm** | **Std Control** | **GC** | **GCF** |
| Time to Target (sec) | 1.51 | 5.61 | 4.50 | 5.39 |
| Trajectory Smoothness (∑Jerk Sq./sec (m^2/sec^10)) | 11070.92 | 29685.43 | 68795.57 | 13103.20 |
| Variance around Target (cm) | 0.04 | 0.62 | 0.78 | 0.41 |
| Steady State Error (cm) | 0.01 | 0.13 | 0.10 | 0.06 |
| **Humerus 0 deg (Target 2)** | | | | |
| **Parameter** | **Nat Arm** | **Std Control** | **GC** | **GCF** |
| Time to Target (sec) | 1.76 | 5.80 | 4.86 | 5.21 |
| Trajectory Smoothness (∑Jerk Sq./sec (m^2/sec^10)) | 23473.14 | 41884.90 | 49705.65 | 42398.28 |
| Variance around Target (cm) | 0.01 | 0.46 | 0.32 | 0.24 |
| Steady State Error (cm) | 0.01 | 0.21 | 0.15 | 0.11 |
| **Humerus 45 deg (Target 3)** | | | | |
| **Parameter** | **Nat Arm** | **Std Control** | **GC** | **GCF** |
| Time to Target (sec) | 1.77 | 6.10 | 5.49 | 5.77 |
| Trajectory Smoothness (∑Jerk Sq./sec (m^2/sec^10)) | 17947.57 | 115036.22 | 26505.23 | 48953.77 |
| Variance around Target (cm) | 0.05 | 1.01 | 0.24 | 0.31 |
| Steady State Error (cm) | 0.02 | 0.67 | 0.11 | 0.13 |
| **Humerus 45 deg (Target 4)** | | | | |
| **Parameter** | **Nat Arm** | **Std Control** | **GC** | **GCF** |
| Time to Target (sec) | 1.78 | 7.67 | 5.78 | 6.14 |
| Trajectory Smoothness (∑Jerk Sq./sec (m^2/sec^10)) | 45010.65 | 189526.00 | 50403.58 | 53958.32 |
| Variance around Target (cm) | 0.04 | 1.63 | 0.26 | 0.25 |
| Steady State Error (cm) | 0.02 | 0.78 | 0.10 | 0.12 |
| **Humerus 90 deg (Target 5)** | | | | |
| **Parameter** | **Nat Arm** | **Std Control** | **GC** | **GCF** |
| Time to Target (sec) | 1.86 | 8.34 | 7.54 | 6.94 |
| Trajectory Smoothness (∑Jerk Sq./sec (m^2/sec^10)) | 41514.78 | 65571.46 | 55997.48 | 199954.79 |
| Variance around Target (cm) | 0.16 | 1.13 | 0.61 | 0.83 |
| Steady State Error (cm) | 0.05 | 0.54 | 0.17 | 0.20 |
| **Humerus 90 deg (Target 6)** | | | | |
| **Parameter** | **Nat Arm** | **Std Control** | **GC** | **GCF** |
| Time to Target (sec) | 1.89 | 8.45 | 6.55 | 5.92 |
| Trajectory Smoothness (∑Jerk Sq./sec (m^2/sec^10)) | 64551.35 | 90704.38 | 120366.62 | 121751.30 |
| Variance around Target (cm) | 0.08 | 0.37 | 0.63 | 0.70 |
| Steady State Error (cm) | 0.04 | 0.25 | 0.18 | 0.24 |

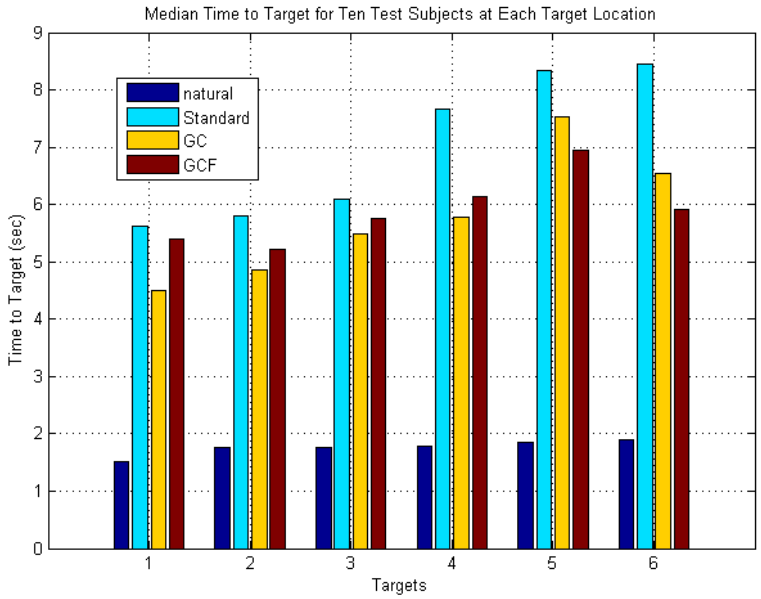


Figure 55: Median Time to Target for Ten Test Subjects at Each Target (1-6)

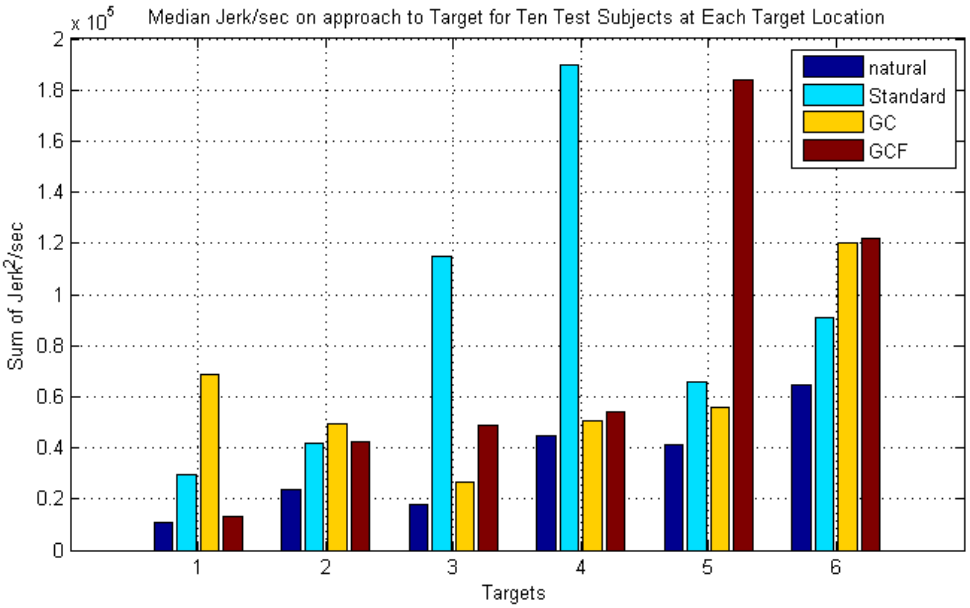


Figure 56: Median Trajectory Smoothness Measure (sum($Jerk^2$)/sec = $m^2/sec^{10}$) on Approach to the Targets for Ten Test Subjects at Each Target Location

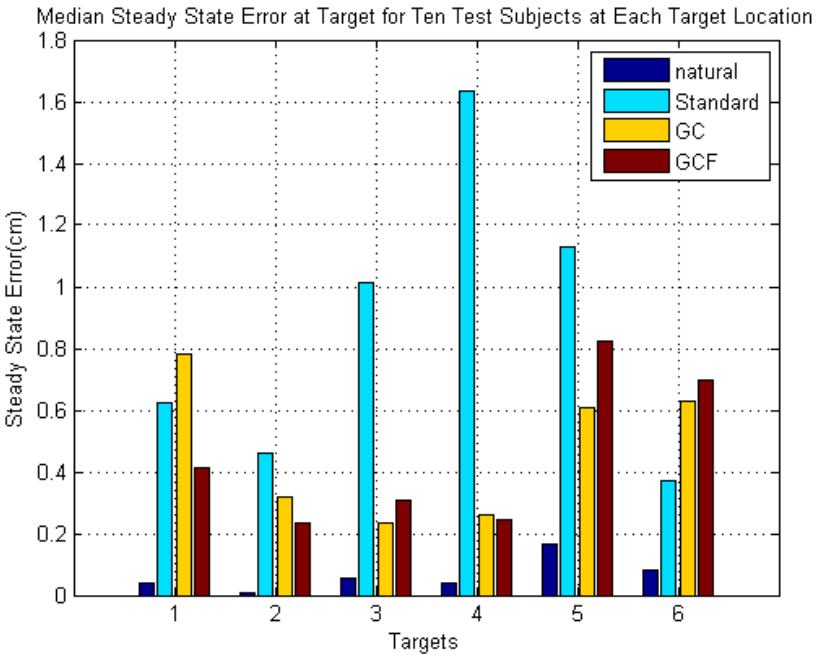


Figure 57: Median Steady State Error for Ten Test Subjects at Each Target

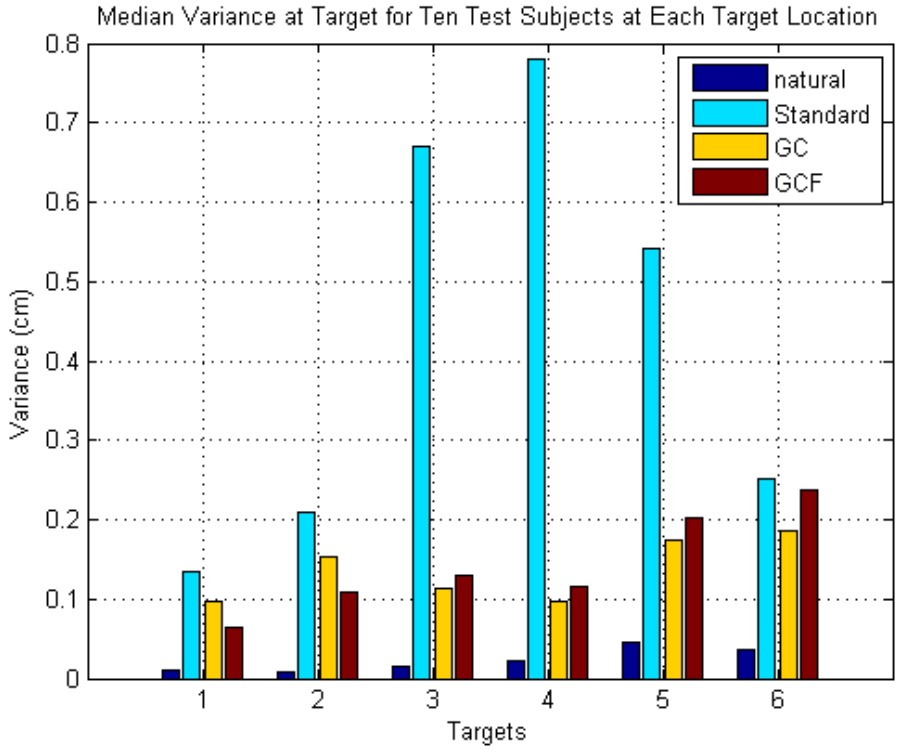


Figure 58: Median Variance for Ten Test Subjects at Each Target Location

5.2.1.1 Statistical Results for Full Data Set

The use of the Friedman test on the full quantitative data set shows that there is statistical significance for all of the quantitative metrics, except trajectory smoothness (jerk), ($p< 0.05$) when comparing the three controllers, Table 8. As there was proof of significance in the variance of the data between controllers further tests were run to better understand the true variance between the new controllers and the standard controller. The non-parametric sign test was used to test for significance, which compares two sets of data to find similarities. The significance is displayed in Table 9. In a similar finding to the Friedman test across the 6 targets for 10 test subjects, only the trajectory smoothness was not found to be significant. All of the other values were highly significant in comparison to the standard controller thus leading to the result that the newer controllers except in the area of trajectory smoothness, when looking at the full test range are better than the standard control scheme as obtained through these tests. However, comparing the quantitative data across all targets does not show a significant enough difference in any quantitative metric to state that GC is better than GCF (or vice versa) in these categories.

Table 8: Friedman Analysis of Variance Results Across All Targets

| **Friedman Test for Analysis of Variance** | |
|---|---|
| **Metric** | **p>Chi^2 (< 0.05)** |
| Time to Target | < 0.01 |
| Trajectory Smooth. | 0.0966 |
| Steady State Error | < 0.01 |
| Variance | < 0.01 |

Table 9: Comparative Sign Test Results Between Controller Types Across all Targets

| Sign Test Results for Significance (p values) for the Full Data Set | | | |
|---|---|---|---|
| **Metric** | **Standard vs. GC** | **Standard vs. GCF** | **GC vs. GCF** |
| Time to Target | < 0.01 | < 0.01 | 0.519 |
| Traj. Smoothness | 0.013 | 0.6988 | 0.519 |
| Steady State Error | < 0.01 | < 0.01 | 0.6989 |
| Variance | < 0.01 | < 0.01 | 1 |

5.2.1.2 Significance of Target Location

It was noticed that though the significance of the quantitative data as a whole for all test subjects was found, there were also trends in the data that showed that there were specific regions in the reaching ranges that performed remarkably better than the standard controller. These cases existed around targets 3, 4, and5 or the mid to upper range of the reaching zone. To better understand the effect of the controllers at the different target ranges of the reaching tasks, the reaching targets were combined into collective ranges based on the humerus angles attempted during the reaches. These ranges can be seen in Table 10. In the following histograms, Figure 59 to Figure 62, the quantitative parameters have been combined into target regions rather than individual targets for all 10 test subjects. The p-values are displayed in numerical form for each metric in Table 11. The * marks statistical significance between the standard controller and a gravity compensation controller. The (!) marks significance between the two gravity compensation controllers.

Table 10: Key for Reading Combined Bar Graphs

| Target Coding | | |
|---|---|---|
| **Humeral Position** | **Target Numbers** | **Target Location(s)** |
| Low | 1,2 | Humerus at $0^o$ (High, Low) |
| Mid | 3,4 | Humerus at $45^o$ (High, Low) |
| High | 5,6 | Humerus at $90^o$ (High, Low) |

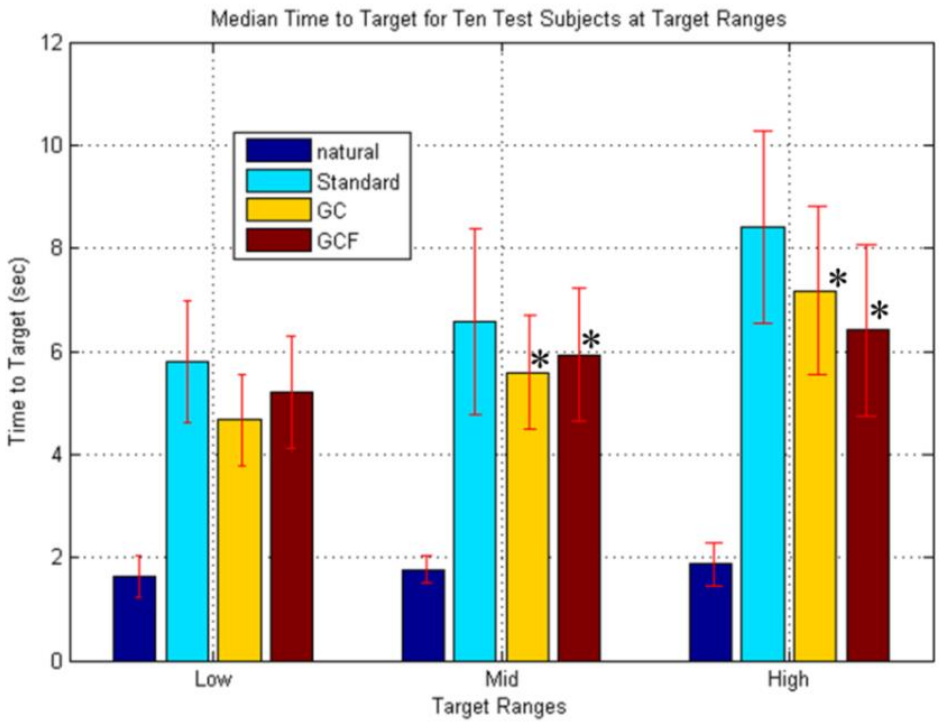


Figure 59: Combined Median Time to Target Values Over the Target Ranges (* Marks Stats. Significance Between New Contr. and Stand.)

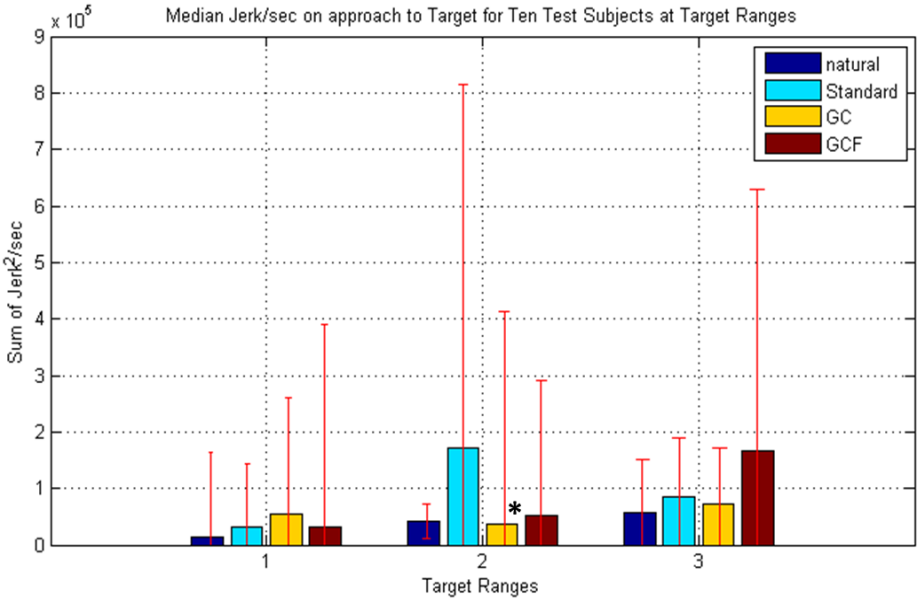


Figure 60: Combined Median Trajectory Smoothness (sum(Jerk$^2$)/sec = m$^2$/sec$^{10}$) Values Over the Target Ranges (* Marks Stats. Significance Between New Contr. and Stand.)

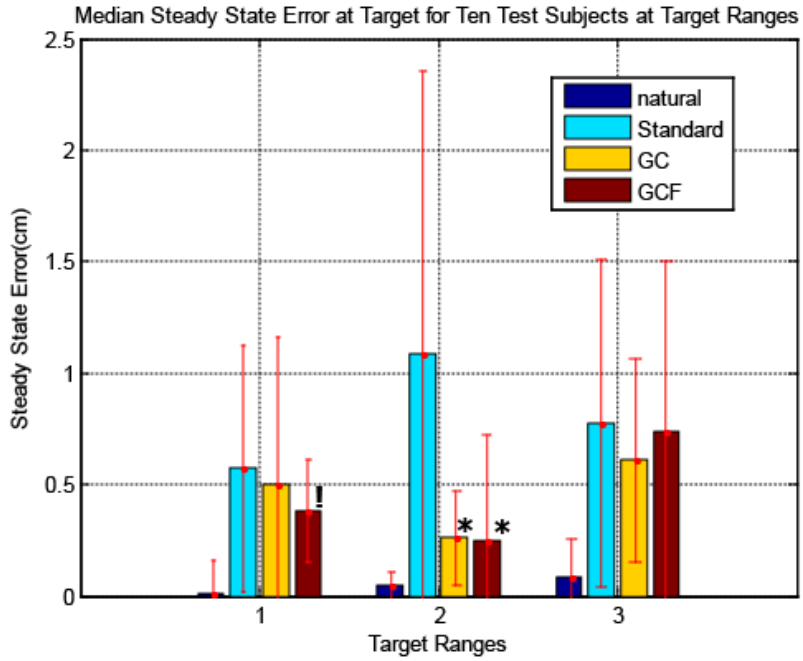


Figure 61: Combined Median Steady State Error Over the Target Ranges (* Marks Stats. Significance Between New Contr. and Stand., ! Marks Stat. Significance Between New Contr.)

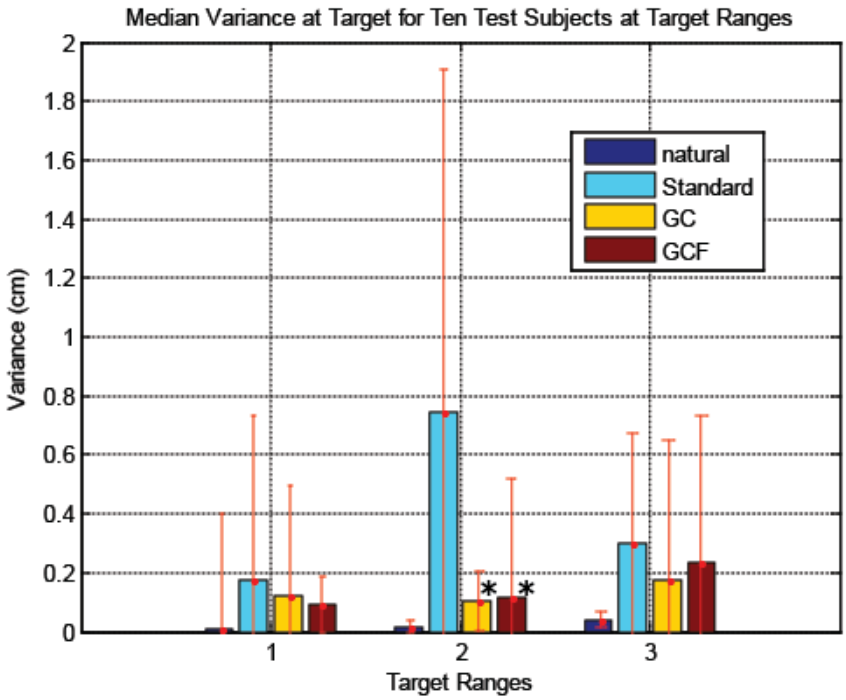


Figure 62: Combined Median Variance Over the Target Ranges (* Marks Stats. Significance Between New Contr. and Stand

Table 11: p-values from Combined Sign Test Ratings to Determine Statistical Significance Between Controllers (* Marks Stats. Significance Between New Contr. and Stand., ! Marks Stat. Significance Between New Contr)

| **Table of Statistical Significance (p values ) Using Sign Test Evaluation** | | | |
|---|---|---|---|
| **Time to Target** | | | |
| **Target Range** | **Standard vs. GC** | **Standard vs. GCF** | **GC vs. GCF** |
| Low Targets | 0.12 | 0.12 | 0.5 |
| Mid Targets | 0.012* | 0.04* | 0.82 |
| High Targets | < 0.01* | < 0.01* | 1 |
| **Jerk** | | | |
| **Target Range** | **Standard vs. GC** | **Standard vs. GCF** | **GC vs. GCF** |
| Low Targets | 1 | 0.5 | 0.5 |
| Mid Targets | 0.012* | 0.5 | 0.82 |
| High Targets | 0.115 | 0.5 | 0.115 |
| **Steady State Error** | | | |
| **Target Range** | **Standard vs. GC** | **Standard vs. GCF** | **GC vs. GCF** |
| Low Targets | 0.5 | 0.12 | 0.04 ! |
| Mid Targets | < 0.01* | < 0.01* | 0.5 |
| High Targets | 0.26 | 1 | 0.82 |
| **Variance** | | | |
| **Target Range** | **Standard vs. GC** | **Standard vs. GCF** | **GC vs. GCF** |
| Low Targets | 0.12 | 0.12 | 0.26 |
| Mid Targets | < 0.01* | < 0.01* | 1 |
| High Targets | 0.12 | 0.5 | 0.26 |

5.2.2 Qualitative Results

When considering the full range of targets across all test subjects, the user ratings showed the following median results as captured in graphic display in Figure 63 and in Table 12. In all cases the new controllers across all test subjects at each target showed that there was a preference for the newer gravity compensated controllers. As the data are based on ranking on a scale of preference the data are considered nonparametric and the Friedman test can again be used to find if there is significance across the whole range. When this test is run on the whole range of data, it shows that there is a high significance between the three controllers in considering the six targets with a p = 7.15628e-5 which is much less than 0.05. For the full data set the significance between controllers for all targets concerning user input on controllability was also tested. Across the full range the following significance ratings were found in Table 13.

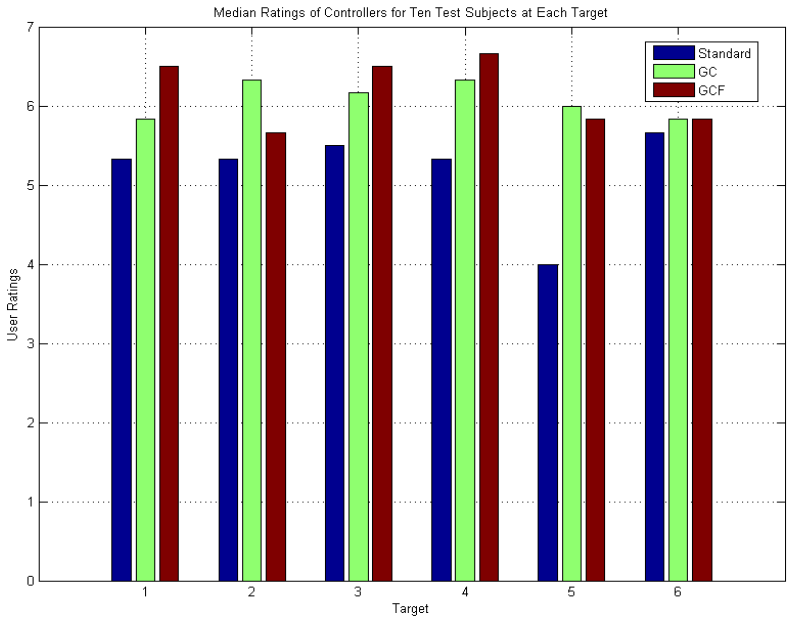


Figure 63: Median Ratings per Controller from Qual. Data (0 worst, 10 best "natural arm")

Table 12: Median Results for Ten Test Subjects from Qual. Data (0 worst, 10 Best "natural arm")

| Median Results for Ten Test Subjects (Qualitative Rating) | | | |
|---|---|---|---|
| **Humerus 0 deg (Target 1)** | | | |
| **Parameter** | **Std Control** | **G (Free Swing)** | **G (No Free Swing)** |
| Qualitative Rating | 5.33 | 5.83 | 6.5 |
| **Humerus 0 deg (Target 2)** | | | |
| **Parameter** | **Std Control** | **G (Free Swing)** | **G (No Free Swing)** |
| Qualitative Rating | 5.33 | 6.33 | 5.67 |
| **Humerus 45 deg (Target 3)** | | | |
| **Parameter** | **Std Control** | **G (Free Swing)** | **G (No Free Swing)** |
| Qualitative Rating | 5.50 | 6.17 | 6.50 |
| **Humerus 45 deg (Target 4)** | | | |
| **Parameter** | **Std Control** | **G (Free Swing)** | **G (No Free Swing)** |
| Qualitative Rating | 5.33 | 6.33 | 6.67 |
| **Humerus 90 deg (Target 5)** | | | |
| **Parameter** | **Std Control** | **G (Free Swing)** | **G (No Free Swing)** |
| Qualitative Rating | 4.00 | 6.00 | 5.83 |
| **Humerus 90 deg (Target 6)** | | | |
| **Parameter** | **Std Control** | **G (Free Swing)** | **G (No Free Swing)** |
| Qualitative Rating | 5.67 | 5.83 | 5.83 |

Table 13: Sign Test Evaluation for Qual. Data Between Controllers for Full Data Set

| Sign Test Evaluation of User Rankings of Controllers for Full Data Set | | | |
|---|---|---|---|
| **Metric** | **Standard vs. GC** | **Standard vs. GCF** | **GC vs. GCF** |
| p | < 0.01 | < 0.01 | 0.6655 |

5.2.2.1 Significance of Target Location

The combined qualitative data were also combined to show how each test subject ranked the controller when considering the same target ranges. When comparing the targets in their respective ranges of low, middle and high; it was found that the gravity compensation controllers were most significant in their effect compared to the standard when using the sign test in the middle range. The p-value results can be seen in Figure 64 and in Table 14. These results are further discussed in section 5.2.3.

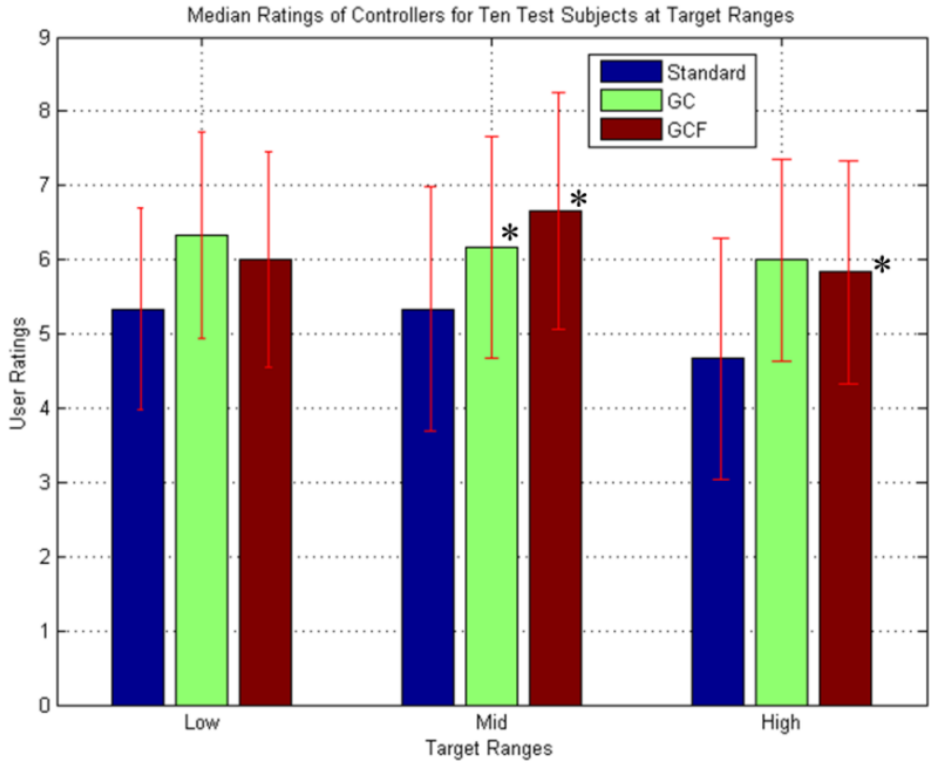


Figure 64: Median Combined Ratings of Controllers Over the Target Ranges (* Marks Stat. Significance Between New Contr. and Stand.)

Table 14: Sign Test Evaluation Results of Qual. Data for Combined Target Ranges (* Marks Stat. Significance Between New Contr. and Stand.)

| **Sign Test for Qualitative Data at Combined Target Ranges (p values)** | | |
|---|---|---|
| **Low Targets (1)** | | |
| **Standard vs. GC** | **Standard vs. GCF** | **GC vs. GCF** |
| 0.096 | 0.79 | 1 |
| **Mid Targets (2)** | | |
| **Standard vs. GC** | **Standard vs. GCF** | **GC vs. GCF** |
| 0.021* | < 0.01* | 0.42 |
| **High Targets (3)** | | |
| **Standard vs. GC** | **Standard vs. GCF** | **GC vs. GCF** |
| 0.096 | < 0.01* | 1 |

### 5.2.3 Discussion

#### 5.2.3.1 Full Target Range

The data presented in Figure 55 through Figure 57 show that the median values particularly in the holding metrics of SSE and variance are highly different between both new controllers and the standard controller. In comparing the values in Table 7, and viewing the sign test results in Table 9, the new controllers outperform the standard in all cases except for trajectory smoothness (jerk) between the GCF vs. Standard and GCF vs. GC. As seen the trajectory smoothness significance is rated to be $p = 0.013$, $p = 0.519$ and $p = 0.6989$ for the standard vs. GC, standard vs. GCF and the GC vs. GCF, respectively. It can be said then that when looking at the measurement data across the whole range of targets for all test subjects the trajectory smoothness (jerk) on approach to the target was different for the GC controller compared to the standard but not significantly different compared to the GCF. However, when viewing the values of the medians the standard outperformed the GC controller in this metric concerning all test subjects at all targets, showing that the significance was on the side of the standard controller. It can also be said that the new controllers did not improve over the standard control for trajectory smoothness as calculated from the obtained Vicon position data. However, as a whole, when considering all target ranges for the quantitative metric performance, the new controllers are better than the standard controller as they are better in the other three quantitative metrics. The difference between the GC and GCF controllers did not show any significant difference between the two in any of the metrics when considering the full data set across all targets. The difference between the two controllers is only a matter of friction compensation which is really the effective impedance level at the elbow. In considering the quantitative metrics, it does not appear

that the impedance level tested has an effect on the control improvement. However, as only one gain on the GC impedance settings was tested for all test subjects this effect might have a larger influence on the control. As discussed further in the conclusions, Chapter 6, it might be better to test more impedance levels in future work to understand the full impact as the GC controller in many cases outperformed the GCF controller when comparing the median values, as seen in Table 7 at the low and mid target ranges.

The test subject ratings of the controllers show a significant level of difference between the new controllers and the standard, considering the full range of data across all of the targets, as seen in Table 12 and Table 13. In particular, the new controllers when considering all the test subjects at the full target range have better scores than the standard with ratings greater than a point or more for all targets except for target 6. This shows a significant increase in user preference for the new controllers over the standard. Again, with test subject ratings on the controllability, there was not much difference between the two new controllers which typically rank within a few tenths of each other, as seen in Table 12. This seems to be consistent with the quantitative metrics as well, given that the performance between the GCF and GC controllers for all the physical metrics did not show a significant difference. Target location also seemed to matter which is discussed in the next section for the ranges of targets split up by humerus angle.

#### 5.2.3.2 Discussion of Target Location Significance

In viewing the data across all targets it is noticed that there was a high level of difference between the new controllers and the standard controller around the middle targets. This middle range is where the humerus is in the middle zone of operation with the humerus at around $45^{o}$ in flexion, targets 3 and 4. For this reason the data, as

previously mentioned in Section 5.2.1, were sectioned into target ranges defined by the humerus positions to determine if the obtained values were actually statistically significant in comparison to the standard controller. The sign test was used to compare the controllers between each other after combining the data sets for these ranges. It was found that for all quantitative metrics, except for the GCF control type in trajectory smoothness, the new controllers are highly different from the standard controller and given the levels of performance at each metric, substantially outperformed the standard controller. In each metric for the middle range, both the GC and GCF controllers were lower in time to target (median comparison Stand. = 6.58 sec, GC = 5.59 sec, and GCF = 5.93 sec), had less steady state error (median comparison Stand. = 1.09 cm, GC = 0.263 cm, and GCF = 0.25 cm) and variance around the target (median comparison Stand. = 0.745 cm, GC = 0.104 cm, and GCF = 0.116 cm) even in considering the standard deviation at each metric, marked by the error bars. These results show that while there is a difference between the new controllers and the standard controller overall, the new controllers are most different around the middle target region or the region where the humerus is positioned at about $45^{o}$ of flexion. The exception is for the GC controller at the midrange for trajectory smoothness, jerk, and a significant difference between the GCF and GC controllers for the steady state error marked by (!).

In concerns to the GCF and GC difference, again, as only one impedance level was tested between the GC and GCF controllers, the differences between the types for the tested impedance on the GC controller show no true difference when taking the metrics as a whole. However, the difference at the steady state error indicates that there might be impedance settings at these target locations that will a show a difference between the new control types. This is discussed further in the conclusions.

The GC controller was found to have lower jerk on approach in the middle range compared to the standard. For the rest of the metrics, in the lower target region, there is not a significant enough difference between the standard and the new controllers to say there is a control improvement in this zone. The high region where the humerus is at about $90^{o}$, the new controllers were not different enough in any physical quantitative metric to be considered better than the standard controller.

The qualitative data when comparing target ranges also support the quantitative data in that the new gravity compensation controllers were more controllable, as rated by the test subjects, in the middle target ranges as seen in Figure 64 and Table 14. In this case the new controllers scored median ratings of GC = 6.17 (std = 1.48), GCF = 6.67 (std = 1.59), and S = 5.33 (std = 1.64) for the middle targets. The qualitative data from user ratings also show that the GCF controller did have a significant difference in comparison to the standard controller at the high target ranges. For the high targets the median scores are GC = 6 (std = 1.35), GCF = 5.83 (std = 1.5), and S = 4.67 (std= 1.62). In observation of these target ranges these scores have reasonable ratings as test subjects had the most difficulty at the mid to high ranges with the standard controller to attempting to reach the targets. As with the other target range results the comparison between the new controllers for test subject controllability ratings is not significant enough so show an difference in control performance from a user perspective. These higher target ranges in general were more difficult to control than the rest of the ranges for all control types.

## 5.3 Chapter Summary

Overall the new controllers with gravity compensation show a marked improvement in the ability to reach a target over the standard controller. This is also shown to be true in

concern with the test subject ratings that are given for each control type for the overall targets. The new gravity compensation controllers are preferred over the standard controller. The new controllers over all the targets and test subjects do not show a difference in the quantitative or qualitative metrics to say that there is a difference between the two new types. When looking at where in the reaching zones the controllers are most preferred by the test subjects and performed the best, the new gravity compensation controllers did best around the midrange targets where the humerus is at about $45^{o}$ in flexion. In this area the new controllers statistically outperformed the standard controller decreasing the time to get to a target, the steady state error once on target, and the variance around the target. In looking at the performance as compared to the natural arm, while the new controllers did better than the standard and moved closer to a more natural arm performance, there is still a highly significant difference and the human arm much outperforms all controllers at all targets. Much more design research is needed both mechanically and in controllers before the prosthesis performs to the "gold standard" of the human arm in these tasks. Future work that can expand the research findings from this project, to move toward a more natural performing prosthesis and better controllers are discussed in the following chapter of conclusions, Chapter 6.

# CHAPTER 6

# CONCLUSIONS

## 6.1 Discussion

The objective of this thesis was to improve above elbow prosthetic limb end effector controllability and placement. It was identified that moving and placing the prosthesis terminal device (TD) using current clinical methods of proportional antagonistic muscle EMG control is difficult to perform. It is thought that part of the difficulty in moving the limb is the result of only using a proportional controller to overcome adverse nonlinear environmental external and internal torques present at the prosthetic elbow joint. The solution designed and tested in this thesis to combat the nonlinear environmental torques was to develop a torque feedback compensation control using predicted analytical models to remove the adverse torque at the elbow joint. The environmental torques focused on in this study was the effect of gravity and internal friction. Two new controllers were developed to compensate for these torque effects. One is called GCF and is compensates for gravity torques only. The other is called GC and compensates for the gravity torque and the friction torque by changing the impedance at the elbow to allow it to be close to frictionless. Gravity torque compensation in multilink robotic joints is a method that has been classically used in the robotics field but to the knowledge of the author, given study into previous research, is not known to have been explicitly used in above elbow

prosthetic limbs as a topic of research to show control improvement for reaching tasks, until present. The Utah Arm 2 was used as the prosthetic platform for the controls study. An inclinometer to measure the shoulder angles based on its orientation in the gravity field was integrated into the prosthesis. The onboard potentiometer and load cell, based on a strain gauge pair, in the prosthesis were repurposed to measure the elbow kinematics. Using sensor data, the human-prosthetic dynamics were developed to design controllers using the dynamic models as predictive torque feedback inputs to compensate for adverse torques, specifically, gravity and friction.

In addition, reaching tests to analyze control performance were developed to better characterize the above elbow prosthesis performance. The tests presented targets in a user's humeral and elbow flexion workspace, which represented distances to objects that can be encountered in tasks of everyday living. The motions of the reaching were record using three-dimensional motion capture cameras to analyze how each controller approached and held at a presented target. To better classify the controller performance four quantitative metrics, which are physical measures to help quantify reaching mechanics, and one qualitative metric were developed to compare the controllers with linked to the reaching task. The quantitative metrics are the measures of the time to a target, how smooth the reach to a target is (trajectory smoothness), the steady state error at a target, and the variance or shakiness at a target. The controllers were compared to each other using these metrics to determine control improvement. The qualitative metric was based on a user rating of the control, from 0 (worst) to 10 (best), on how controllable they felt the prosthesis was as referenced to their natural arm.

The results of the test performed using the testing schemes as described in Chapter 4 and displayed in Chapter 5 were analyzed in two different ways. The first was to analyze

the whole data set encompassing all test subjects across all targets and evaluating the statistical significance between control types. The second method was to analyze the statistical significance between controllers by breaking the test results into target regions to determine the control performance in certain reaching zones where the humerus was at approximately $0^o$, $45^o$, and $90^o$ in flexion.

The main finding of the performed experiments, based on the collected data, shows that both of the new gravity compensated controllers outperform the standard control type in the qualitative test subject rankings and all but trajectory smoothness in the quantitative metrics when considering the statistical significance of the collected combined data of all test subjects across all targets. The most significant performance improvement when considering target areas is where the humerus is at $45^0$ in flexion, again, except in the metric of trajectory smoothness. The trajectory smoothness metric is derived from the prosthetic end effector jerk data which is calculated during the approach to a designated reaching target. The EMG gains which dictate the prosthetic arm sensitivity to muscle signals were the same between the controllers the only difference between the standard controller and the GCF controller is the gravity compensation term. In comparing the standard controller to the GC controller the difference in between the two is the gravity term and the impendence in the elbow joint set by the torque servo gain. As seen from the results in Chapter 5, in comparing all test subjects the statistical difference between the new controllers and the standard control shows no improvement. On a more thorough inspection by looking at the specific target ranges the only significant level is at the middle range, humerus at $45^0$ for trajectory smoothness, when comparing the GC controller to the standard. This lends to the conclusion that while gravity compensation in itself does not significantly improve the approaching motion of

reach as captured by the trajectory smoothness, there is a possible significance when changing the impedance in the prosthetic elbow to remove the internal frictional forces. With the GC controller having lower impedance, there are not as high of friction forces which allows for more fluid transitions from start and stop which would affect the motion of the arm on approach. In this research, only one gain was set with the torque servo gain for the GC control loop, which controls the impedance level. As only one gain and thus one impedance level was tested, not enough data are available to fully understand the impedance impact on the prosthetic controllers. Further testing to determine the effect of variable impedance levels influencing the reaching approach to a target, as measured by trajectory smoothness, is suggested as future research. This is expanded upon in section 6.2.

Other conclusions can be drawn from the collected data as concerns the other target ranges in the low and high regions. In the lower target region where the humerus is at $0^o$ at targets 1 and 2, there is not a significant enough difference between the standard and the new controllers to say there is a control improvement in this zone. This is likely due to the four-bar linkage already being designed to fight the arm weight in this configuration, where the humerus is at $0^o$ flexion and the elbow angle is around $90^o$. In this zone, due to the crossed four-bar linkage any additional gravity compensation methods for the Utah Arm 2 are probably not needed. In the high region where the humerus is at about $90^o$, targets 5 and 6, the new controllers were not different enough in any physical quantitative metric, except for the time to target. The lower time to target significance could likely be due to the gravity compensation controllers aiding in the lifting of the arm on approach causing it to reach the target in less time than the standard. It was originally hypothesized that, particularly in this range, the same gravity

compensation effect would also aid in the steady state error and variance as the new controllers, as designed, appear to be more stable. However, this was found not to be the case to a statistically different degree. This result is likely due to two reasons. Firstly, this range is difficult to reach in and it is hard to position even the natural arm for sustained holding in these positions, as can be seen by the natural arm having increased values for both targets 5 and 6 for all metrics as compared to the lower ranges. Secondly, with the test subjects tested, the bypass socket at this range caused a heavier moment on the shoulder joints than is naturally present. Currently this zone for nonamputees does not show a significant difference in control; however, with more experienced amputees this might prove to be different and can be a focus in future work.

The other key finding from the performed research experiments with gravity compensation controllers shows that there is not a significant difference between the GC and GCF controllers when considering the data collected across the full range of targets, either in user rankings of control effort or in the quantitative metrics. However, there is a slight difference that arises in the qualitative and quantitative metrics when analyzing the data by target ranges. When comparing the GC and GCF controllers to one another in the lower range, the GC controller would have a tendency to overshoot the target at this lower range and the TD would come to rest at slightly further distances (a few mm), in comparison to the GCF controller, from the target, SSE difference. The comparison between the GC and GCF controllers do not seem to be significantly different from each other in any other metric. The difference between the control types is the impedance levels. Other than the middle range, the high range for the GCF controller showed a significant difference as compared to the standard in user ratings of controllability. The preference could be due to the sensitivity aspect of the arm at these upper positions and

users noticing this effect. The GC controller was not designed to have thresholds on the EMG inputs. Smaller EMG signals, if large enough to produce a motor torque to overcome the lower impeded elbow joint, would move the forearm more freely, and thus be harder to "control" at this position. In future designs it is suggested that the GC controller have a slight EMG limit so as to have a signal threshold level to overcome such that smaller unintentional muscle contractions are rejected.

In conclusion, the new gravity compensated controllers outperform the standard controller in the areas of time to target, steady state error, variance at the target, and in test user ratings when considering the results of the combined data of all the targets for all of the test subject trials. The new gravity compensation controllers in comparison to the standard perform the best in the middle range (humerus = $45^{o}$ in flexion). It was also found that the new gravity compensation control types (GC vs. GCF) are not different enough between each other to say that one did better than the other. It can also be concluded that the smoothness at which someone is able to control the new controllers as compared to the standard control on the reaching approach to a target, as captured by the trajectory smoothness, is not significantly changed by the addition of gravity compensation. This metric is predicted to be more influenced by the impedance level in the prosthetic elbow joint and further studies into how impedance effects the smoothness of the reaching approach should be studied in future work. Considering these findings, as found in the experiments using the Utah Arm 2 architecture, using gravity compensation in the prosthetic control scheme for above elbow prosthetic joints can be said to improve the control over the standard EMG proportional control, both in physical performance as captured in the majority of the physical metrics and in the user preferences as captured by the using ratings. It is suggested that further tests with the gravity compensated

controllers be conducted on a next set of test subjects using amputees to better understand their performance aspects and feasibility in clinical applications. Other suggestions of concentrated research to build upon these successes are suggested in the next section, 6.2.

## 6.2 Future Work

Based on the experience and results obtained from the research performed in this thesis, several suggestions may be made for future research.

1. As mentioned in the previous section the new controllers performed best in the middle target range where the humerus is approximately at $45^{o}$ of flexion. It is suggested that this range with these control types be further analyzed with more targets. In addition it is suggested that the controllers only be active, in this range. As seen in Chapter 5, the results do not show much of a need of the controllers in the lower range of motion where the humerus is at the side of the test subject, $0^{o}$ in flexion. In is suggested that a study designated to fully understand this reaching zone be done.
2. The two new controllers as discussed in Chapter 3 are called GC (gravity compensation with a torque feedback free-swing affect) and GCF (with only gravity compensation active and no torque feedback for impedance changes). In the results there was not much of a difference between the controllers in any of the physical metrics or test subject's controllability preferences. However, only one gain for impedance was used in the entire control scheme for the GC controller. It is suggested that the tests be run to determine what the impedance effects are explicitly to determine if there is a true difference between control types at any target range. It is also suggested that the GC controller be designed to

have an EMG limit set on the controllers such that slight EMG signals do not affect the prosthetic forearms performance.

3. Only gravity and internal stiction was considered in the design of the new controllers. There are other adverse external torques induced by the inertia and angular velocity terms. In post analysis tests using the Vicon position data it was found that given the estimate of inertia and mass of the arm in Chapter 3, the inertia term could peak to as high as 2.8Nm and the velocity terms in plane peaked at 0.44Nm in magnitude when considering multiple tests across all test subjects. These are significant in comparison to the max values of gravity torque 1.55Nm and stiction torque 1.22Nm. These dynamics have been developed and it is suggested that these be included in the overall control design to determine if their affect changes physical performance of the prosthesis and controllability.
4. In these tests only the flexion plane was tested, as mentioned in Chapter 4. The shoulder motion in amputees typically includes the ability to include abduction. The sensors in the develop inclinometer are capable of sensing this angle. The dynamics to include this angle (DOF) in the gravity, inertia, Coriolis, and centripetal terms have been developed. Further tests in this area would help in understanding how the controllers work over a full range of motion; these are suggested to be done.
5. In this thesis as a preliminary test set only nonamputees were tested. It is suggested to test a set of amputees with the same controllers developed to determine the control performance with the target end user population.
6. Future work in integrating the inclinometer sensor into the prosthesis or the socket and shrinking its size are suggested as well. It is also suggested that the sensor be

made wireless such that it can be made more manageable in testing as well as be moved to an actual clinical design.

7. It is also suggested that the target robot arm be equipped with a touch sensor at the end of the target. This touch sensor would be used to indicate when the pointer marker has actually come into contact with the target in a more accurate way. It could also be used as an input switch to the Vicon system to trigger recording times or create a time stamp in the data to better verify where contact was made. The current method of the data inspection of where contact is made works, but there can be effects of human error in selecting the correct points and a more automated triggering system could fix this issue. In addition, if the touch sensor was a form of a pressure sensor it could also be used to determine the force the point marker contacted the target with. This is another critical piece of data in the reach that was not considered in this research.

# APPENDIX A

## CROSSED FOUR-BAR LINKAGE ANALYSIS

The following derivation covers the input and output mechanics of the four-bar linkage present in the Utah Arm 2 prosthetic limb used in testing. The prosthetic forearm image of the arm with the identified four-bar linkage can be seen in Chapter 2 Section 2.2.2.3. The primary equation of use is the law of cosines in analyzing the linkage. $\theta_P$ is the angle of the pot which is variable depending upon arm position but is known by the calibration in Chapter 2.

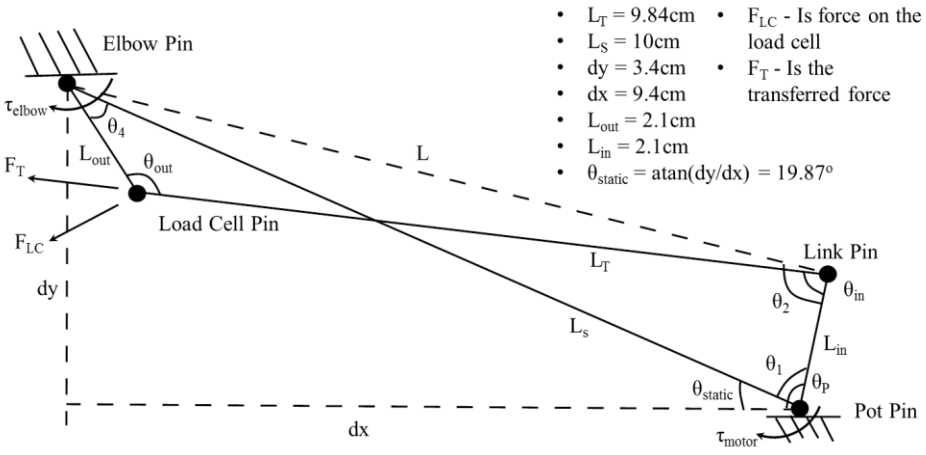


$$\theta_1 = \theta_P - \theta_{static}$$

$$L = \sqrt{L_S^2 + L_{in}^2 - 2(L_{in})(L_S)\cos(\theta_1)}$$

$$L^2 = L_T^2 + L_{out}^2 - 2(L_T)(L_{out})\cos(\theta_{out})$$

$$\cos(\theta_{out}) = \frac{L^2 - L_T^2 - L_{out}^2}{-2(L_T)(L_{out})}$$

$$\theta_{out} = 2atan\left(\sqrt{\frac{(1-\cos(\theta_{out}))}{(1+\cos(\theta_{out}))}}\right)$$

$$\cos(\theta_2) = \frac{L_S^2 - L^2 - L_{in}^2}{-2(L)(L_{in})}$$

$$\theta_2 = 2atan\left(\sqrt{\frac{(1-\cos(\theta_2))}{(1+\cos(\theta_2))}}\right)$$

$$\cos(\theta_{S2}) = \frac{L_{out}^2 - L^2 - L_T^2}{-2(L)(L_T)}$$

$$\theta_{S2} = 2atan\left(\sqrt{\frac{(1-\cos(\theta_{S2}))}{(1+\cos(\theta_{S2}))}}\right)$$

$$\theta_{in} = \theta_2 - \theta_{S2}$$

The corresponding force and torque transfers (given the predicted torque at the elbow from external) are:

$$F_T = \tau_{elbow}/(L_{out}\sin(\theta_{out}))$$

$$F_{LC} = F_T\cos(\frac{\pi}{2} - \theta_{out})$$

$$\tau_{motor} = (F_T\cos\left(\frac{\pi}{2} - \theta_{in}\right))/L_{in}$$

$$\tau_{motor}\left(\frac{L_{out}\sin(\theta_{out})}{L_{in}\cos\left(\frac{\pi}{2} - \theta_{in}\right)}\right) = \tau_{elbow}$$

APPENDIX B

# DERIVATION OF THEORETICAL INERTIAL AND VELOCITY INDUCED TORQUES ABOUT THE ELBOW JOINT

The overall torque about the elbow concerning the motion induced torque is the dot product of the z-axis for the third frame or the frame attached to the elbow and the inertia and cross product induced torques. The derivation starts below.

$$\tau_{elbow} = z_3.(n_4 + \vec{r}_{14} x f_{12})$$

$$n_4 = I\vec{\omega}_{14} + \vec{\omega}_{14} x\, I\vec{\omega}_{14}$$

$$I = \begin{bmatrix} I_x & 0 & 0 \\ 0 & I_y & 0 \\ 0 & 0 & I_z \end{bmatrix}^4$$

$$n_4 = \begin{bmatrix} (\ddot{\theta}_1 S_{23} + \dot{\theta}_1(\dot{\theta}_2 + \dot{\theta}_3)C_{23})I_x \\ (\ddot{\theta}_1 C_{23} - \dot{\theta}_1(\dot{\theta}_2 + \dot{\theta}_3)S_{23})I_y \\ (\ddot{\theta}_2 + \ddot{\theta}_3)I_z \end{bmatrix}^4 + \begin{bmatrix} \dot{\theta}_1 S_{23} \\ \dot{\theta}_1 C_{23} \\ \dot{\theta}_2 + \dot{\theta}_3 \end{bmatrix}^4 x \begin{bmatrix} I_x & 0 & 0 \\ 0 & I_y & 0 \\ 0 & 0 & I_z \end{bmatrix}^4 \begin{bmatrix} \dot{\theta}_1 S_{23} \\ \dot{\theta}_1 C_{23} \\ \dot{\theta}_2 + \dot{\theta}_3 \end{bmatrix}^4$$

$$n_4.z_3 = \left(\ddot{\theta}_2 + \ddot{\theta}_3\right)I_z + \left(\dot{\theta}_1^2 C_{23} S_{23} I_y - \dot{\theta}_1^2 C_{23} S_{23} I_x\right)$$

The cross product term of the motion torque yields the following:

$$f_{12} = m\ddot{\vec{r}}_{14}$$

$$\vec{r}_{14} = l_{COM\,X} x_4 + l_{COM\,Y} y_4 + l_{hx} x_3 + l_{hy} y_3$$

$$\vec{\omega}_{14} = \dot{\theta}_1 y_2 + (\dot{\theta}_2 + \dot{\theta}_3) z_4$$

$$\ddot{\vec{r}}_{14} = t_1 z_2 + t_2 y_4 + t_3 y_3 + t_4 x_4 + t_5 x_3 + t_6 x_2$$

$$t_2 = \left[ (\ddot{\theta}_2 + \ddot{\theta}_3) l_{COM\,X} + ((\dot{\theta}_2 + \dot{\theta}_3)^2 l_{COM\,Y} + \dot{\theta}_1 (\dot{\theta}_2 + \dot{\theta}_3) l_{hx}) \right]$$

$$t_3 = \ddot{\theta}_2 l_{hx}$$

$$t_4 = \left[ \left( (\ddot{\theta}_2 + \ddot{\theta}_3) l_{COM\,Y} + \ddot{\theta}_2 l_{hy} \right) - (\dot{\theta}_2 + \dot{\theta}_3)^2 l_{COM\,X} \right]$$

$$t_5 = \dot{\theta}_1^2 l_{hx}$$

$$t_6 = \dot{\theta}_1^2 (-C_{23} l_{COM\,X} + S_{23} l_{COM\,Y} - C_2 l_{hx} + S_2 l_{hy})$$

Put everything in terms of frame 4 (forearm frame):

$$x_3 = \cos(\theta_3)\, x_4 - \sin(\theta_3) y_4$$

$$y_3 = \sin(\theta_3)\, x_4 + \cos(\theta_3) y_4$$

$$x_2 = \cos(\theta_2 + \theta_3)\, x_4 - \sin(\theta_2 + \theta_3) y_4$$

$$\vec{r}_{14} = \left( l_{comx} + l_{hx} \cos(\theta_3) + l_{hy} \sin(\theta_3) \right) x_4 + (l_{comy} - l_{hx} \sin(\theta_3) + l_{hy} \cos(\theta_3)) y_4$$

$$\ddot{\vec{r}}_{14} = t_1 z_2 + (t_4 - t_5 \cos(\theta_3) + t_3 \sin(\theta_3) + t_6 \cos(\theta_2 + \theta_3))\, x_4 + (t_2 + t_3 \cos(\theta_3) + t_3 \sin(\theta_3) - t_6 \sin(\theta_2 + \theta_3)) y_4$$

$$\vec{r}_{14}\, x\, m\ddot{\vec{r}}_{14} = \begin{bmatrix} x_4 & y_4 & z_4 \\ A & B & 0 \\ D & F & C \end{bmatrix} = (BCx_4 - ACy_4 + (AF - BD) z_4) m_2$$

$$z_3 . (BCx_4 - ACy_4 + (AF - BD) z_4) m_2 = (AF - BD) m_2$$

$$A = (l_{COM\,X} + l_{hx} C_3 + l_{hy} S_3)$$

$$B = (l_{COM\,Y} - l_{hx} S_3 + l_{hy} C_3)$$

$$C = t_2 + t_3 C_3 + t_3 S_3 - t_6 S_{23})$$

$$D = (t_4 - t_5 C_3 + t_3 S_3 + t_6 C_{23})$$

$$\boldsymbol{\tau_{elbow}} = \left(\boldsymbol{\ddot{\theta}_2} + \boldsymbol{\ddot{\theta}_3}\right)\boldsymbol{I_z} + \left(\boldsymbol{\dot{\theta}_1^2 C_{23} S_{23} I_y} - \boldsymbol{\dot{\theta}_1^2 C_{23} S_{23} I_x}\right) + \boldsymbol{m_{forearm}}(\boldsymbol{AC} - \boldsymbol{BD})$$

This equation can be further simplified if the abduction is not included or considered not active. $\theta_1 = 0$.

APPENDIX C

IRB TEST SUBJECT CONSENT FORM

University of Utah
Institutional Review Board
Approved 5/15/2014
Expires 5/14/2016
IRB_00066441

# Consent Document

*For Minimal Risk Research*

**BACKGROUND**

This is a quantitative research study with the purpose of improving the control of prosthetic arms. Current prosthetic control methods use signals from the user's muscles (called myoelectric or EMG signals). These signals are used to control the prosthesis in a very simple manner: the stronger the difference in the signals of antagonist muscles (such as biceps and triceps), the faster the prosthesis motion. There is no sensing of the environment such as other motions of the body or accelerations such as when riding in a vehicle. This lack of sensing the environment can cause difficulties in controlling the prosthesis when reaching upward or other motions of the user. We will investigate control methods that include the sensing of the shoulder and body motions. These methods will be compared with the current methods and any improvement will be evaluated.

**STUDY PROCEDURE**

The arm motions of the subject will be tracking by an optical tracking system (Vicon). It has the capability of tracking motions in 3 dimensions over the entire workspace of the arm.

The experiment will be to reach to a target using both your unconstrained arm and hand and then repeat the tasks while wearing an EMG controlled artificial arm. The target will be provided by a small robot with a Vicon tracking ball at the end of the arm. You will hold another track ball and reach to the target and hold for a few seconds.

You will be given time to use the prosthesis and adjust the signals so you become familiar and comfortable with the system. The testing will begin when you say that you are ready.

The target locations will be randomly presented and the entire tracking experiment should last one hour to an hour and a half.

Video and still photographs may be made that will be shown at scientific meetings with your consent. You do not need to consent to participate in the study. We will not record any video or photographs in this case.

**RISKS**
The risks of this study are minimal. The intention of this study is to gather information about the response of normally functioning persons in normal conditions. Because of this you should not feel any discomfort or pain during or after the experiment. There may be some fatigue due to the repetitive nature of the task. However, if at any time you feel discomfort please let the researcher know and the experiment will be terminated.

**BENEFITS**
There is no direct benefit for taking part in this study. We hope that the information gathered will help to validate work currently being done to advance prosthetic development.

**CONFIDENTIALITY**
No personal identification information will be collected from you. You will be assigned a unique number which will connect their biometric data with the data collected from the experiment. All biometric data can be used in the publication of this study along with the data collected during the experiments.

**PERSON TO CONTACT**
If you have any questions or concerns or complaints regarding this study please contact Sanford Meek at 801-581-8562 or by email at meek@mech.utah.edu or Jim Dotterweich at 720-985-6198or by email atjames.dotterweich@utah.edu. If you feel you have been injured as a result of your participation please contact Jim Dotterweich at 720-985-6198 available 24 hour a day.

**Institutional Review Board:** Contact the Institutional Review Board (IRB) if you have questions regarding your rights as a research participant. Also, contact the IRB if you have questions, complaints or concerns which you do not feel you can discuss with the investigator. The University of Utah IRB may be reached by phone at (801) 581-3655 or by e-mail at irb@hsc.utah.edu.

**Research Participant Advocate:** You may also contact the Research Participant Advocate (RPA) by phone at (801) 581-3803 or by email at participant.advocate@hsc.utah.edu.

**VOLUNTARY PARTICIPATION**
Participation in these experiments is completely voluntary. If you do not desire to participate or wish to terminate your participation at any time during the experiment there will be no penalty or loss of benefits.

**COSTS ANDCOMPENSATION TO PARTICIPANTS**
There is no cost nor compensation for participation in this study.

**CONSENT:**

By signing this consent form, I confirm I have read the information in this consent form and have had the opportunity to ask questions. I will be given a signed copy of this consent form. I voluntarily agree to take part in this study.

_____
Participant's Name

_____ _____
Participant's Signature Date

_____
Name of Person Obtaining Consent

_____ _____
Signature of Person Obtaining Consent Date

REFERENCES


[1] D. S. Childress and R. F. Weir, "Control of Limb Prostheses," in *Atlas of Amputations and Limb Deficiencies*, Smith DG, Michael JW, and Bowker JH, Eds., 3rd ed. Rosemont: American Academy of Orthopedic Surgeons, 2003.

[2] E. A. Biddiss and T. T. Chau, "Upper limb prosthesis use and abandonment: A survey of the last 25 years," in *Prosthetics and Orthotics International*, 2007, vol. 31, pp. 236-257.

[3] T. Doyon, "Bio-Robotics: The DEKA Luke Prosthetic Arm," in *NHJES Conference*, 2012

[4] *Myoelectric Arm Prosthesis*, Otto Bock HealthCare GmbH, Duderstadt, Germany, 2009

[5] S. C. Jacobsen, D. F. Knutti, T. R. Johnson, and H. H. Sears, "Development of the Utah Artificial Arm," in *IEEE TRANSACTIONS On Biomedical Engineering*, 1982, vol. BME-29, no. 4, pp. 249 – 269.

[6] H. Sears, E. Inverson, S. Archer, and T. Jacobs, "Evolution of the Utah Arm to Improve User Function," in *MyoElectric Controls/Powered Prosthetics Symposium*, August 2008.

[7] A. Muzumdar Ed., "Powered Upper Limb Prostheses," in *Powered Upper Limb Prostheses*, Berlin, Germany: Springer, 2004

[8] R. F. Weir, "The Great Divide - The Human-Machine Interface, Issues in the Control of Prosthesis, Manipulators, and other Human Machine Systems," in *IEEE 29th Annual Proceedings of The Bioengineering Conference*, 2003

[9] E. Scheme and K. Englehart, "Electromyogram pattern recognition for control of powered upper-limb prostheses: State of the art and challenges for clinical use," in *Journal of Rehabilitation Research and Development*, 2011, vol. 48, no. 6, pp. 643-660.

[10] T. A. Kuiken et al., "Targeted Muscle Reinnervation for Real-time Myoelectric Control of Multifunction Artificial Arms," in *JAMA*, 2009, vol. 301, no.6, pp. 619-628.

[11] J. Panero and M. Zelnik, "Human Dimensions and Interior Space a Source Book of Design Reference Standard*,"* New York: Whitney Library of Design, 1979.

[12] N. Diffrient, A.R. Tilley, and D. Harman, "Human Scale a Project of Henrey Dreyfuss Associate*,"* Cambridge: The MIT Press, 1981.

[13] T. Flash and N. Hogan. "The coordination of arm movements: an experimentally confirmed mathematical model," in *The Journal of Neuroscience*, 1985, vol. 5, no. 7.

[14] N. Yang, M. Zhang, C. Huang, and D. Jin, "Synergic analysis of upper limb target-reaching movements," in *Journal of Biomechanics*, 2002,vol. 35 pp. 739-746.

[15] F. Lacquaniti and J. F. Soechting, "Coordination of Arm and Wrist Motion During a Reaching Task," in *The Journal of Neuroscience*, 1981, vol. 2, no. 4 pp. 399-408.

[16] V. Mathiowetz, G. Volland , N. Kashman, and K. Weber, "Adult Norms for the Box and Block Test of Manual Dexterity," in *The American Journal of Occupational Therapy*, 1985, vol. 39, no. 6, pp. 386-391.

[17] M. C. Carrozza, G. Cappiello, S. Micera, B. B. Edin, L. Beccai, and C. Cipriani, "Design of a cybernetic hand for perception and action," in *Biol Cybern*, 2006, vol. 95, no. 6, pp. 629-644.

[18] C. M. Light, P. H. Chappell, and J. P. Kyberd, "Establishing a Standardized Clinical Assessment Tool of Pathologic and Prosthetic Hand Function: Normative Data, Reliability, and Validity," in *Arch. Physical Medicine and Rehabilitation*, 2002, vol. 83

[19] J. P. Kyberd, A. Murgia, M. Gasson, T. Tjerks, C. Metcalf, P. H. Chappell, K. Warwick, S. E. Lawson, and T. Barnhill, "Case studies to demonstrate the range of applications of the Southampton Hand Assessment Procedure," in *British Journal of Occupational Therapy*, 2009, vol. 72 no. 5.

[20] D. J. Bennett, J. M. Hollerbach, Y. Xu, and I. W. Hunter, "Time-varying stiffness of human elbow joint during cyclic voluntary movement," in *Experimental Brain Research*, 1992, vol. 88, pp. 433-442.

[21] K. P. Tee, E. Burdet, C. M. Chew, and T. E. Milner, "A model of force and impedance in human arm movements," in *Biological Cybernetics*, 2004, vol. 90, pp.368-375.

[22] F. Guenzkofer, F. Engstler, H. Bubb, and K. Bengler, "Isometric elbow flexion and extension joint torque measurements considering biomechanical aspects," in *First International Symposium on Digital Human Modeling*, 2011, pp. 14-15.

[23] S. G. Meek, J. E. Wood, and S. C. Jacobsen. "Model-based, multi-muscle EMG control of upper-extremity prostheses," in *Multiple Muscle Systems*, Springer: New York, 1990, pp. 360-376.

[24] R. R. Fullmer, S. G. Meek, and S. C. Jacobsen, "Generation of the 7 Degree of Freedom Controller Equations for a Prosthetic Arm," in *Conf. on Applied Motion Control,* Minneapolis, MN, 1985.

[25] M. M. Bridges, M. P. Para, and J. M. Masher, "Control System Architecture for the Modular Prosthetic Limb," in *Johns Hopkins APL Technical Digest*, 2011, vol. 30, No. 3.

[26] A. Blank, A. M. Okamura, and L. L. Whitcomb, "Task-Dependent Impedance Improves User Performance with a Virtual Prosthetic Arm," in *ICRA*, 2011

[27] J. W. Sensinger and R. F. Weir, "User-Modulated Impedance Control of a Prosthetic Elbow in Unconstrained, Perturbed Motion," in *IEEE Transactions on Biomedical Engineering*, 2008,vol. 55 No. 3.

[28] A. D. Dragan and S. S. Srinivasa, "A policy-blending formalism for shared control," in *The International Journal of Robotics Research*, vol. 32, pp. 790 – 805

[29] J. J. Craig, "Introduction to Robotics Mechanics and Control", Reading: Addison-Wesley, 1986

[30] A. Petruska and S. Meek, "Non-Drifting Limb Angle Measurement Relative to the Gravitational Vector During Dynamic Motions Using Accelerometers and Rate Gyros," in *International Conference on Intelligent Robots and Systems*, San Francisco, CA, USA, September 25-30, 2011

[31] J. S. Hebert and J. Lewicke, "Case report of modified box and blocks test with motion capture to measure prosthetic function," in *Journal of Rehabilitation Research and Development*, 2012, vol. 49, no. 8, pp. 1163-1174.

[32] H. Bouwsema, C. K. van der Sluis, and R. M. Bongers, "Movement characteristics of upper extremity prosthesis during goal-directed tasks," in *Clinical Biomechanics*, 2010, vol. 25 pp. 523-529.

[33] S. L. Carey, M. J. Highsmith, M. E. Maitland, and R. V. Dubey, "Compensatory movements of transradial prosthesis users during common tasks," in *Clinical Biomechanics*, 2008, vol. 23 pp. 1128-1135.

[34] S. L. Carey, R. V. Dubey, G. S. Bauer, and M. J. Highsmith, "Kinematic Comparison of Myoelectric and Body Powered Prosthesis While Performing Common Activities," in *Prosthetics and Orthotics International*, 2009, vol. 33, pp. 179-186.

[35] J. A. Doeringer and N. Hogan, "Performance of Above Elbow Body-Powered Prosthesis in Visually Guided Unconstrained Motion Tasks," in *IEEE Transactions on Biomedical Engineering*, 1995, vol. 42 no. 6 pp. 621-631.

[36] *Hardware Installation and Configuration: DS1104 R and D Controller Board Manual*, 4.1 ed., dSpace, Paderborn, Germany, 2004.

[37] *U3 Instruction Manual: For prosthetists trained to fit the Utah Arm*, Doc No. 1910024-Rev.B, Motion Control Inc., Salt Lake City, UT, 2006.

[38] *Quanser Rotary Servo User Manual: SRV02*, Quanser Inc., Markham, ON Canada, 2011

[39] G. A. Wood, "Data Smoothing and Differentiation Procedures in Biomechanics," in *Exercise Sport Science Rev, 1982*, vol. 10, pp. 308-362.

[40] C. Reinsch, "Smoothing by spline functions", in *Numer. Math*, 1962, vol. 10, pp. 177–183.

[41] *MATLAB Product Manual: Curve Fitting Toolbox: spaps*, Mathworks Inc., Natick, MA, 2011.

[42] C. M. Jarque and A. K. Bera. "A test for normality of observations and regression residuals," in *International Statistical Review*, 1987, vol. 55, no. 2, pp. 163–172.

[43] M. Hollander, and D. A. Wolfe, "Nonparametric Statistical Methods," Hoboken: John Wiley and Sons, Inc., 1999.

[44] J. D. Gibbons, "Nonparametric Statistical Inference," New York: Marcel Dekker, 1985.